



ELSEVIER

Available online at www.sciencedirect.com

SCIENCE @ DIRECT®

Journal of Non-Crystalline Solids xxx (2006) xxx–xxx

JOURNAL OF
NON-CRYSTALLINE SOLIDSwww.elsevier.com/locate/jnoncrsol

Review

Homogeneous crystal nucleation in silicate glasses: A 40 years perspective

Vladimir M. Fokina ^{a,*}, Edgar D. Zanotto ^b, Nikolay S. Yuritsyn ^c,
Jörn W.P. Schmelzer ^d

^a Vavilov State Optical Institute, ul. Babushkina 36-1, 193171 St. Petersburg, Russia

^b LaMaV – Vitreous Materials Laboratory, Federal University of São Carlos, 13565-905 São Carlos, SP, Brazil

^c Grebenshchikov Institute of Silicate Chemistry, Russian Academy of Sciences, ul. Odoevskogo 24-2, 199155 St. Petersburg, Russia

^d Institut für Physik, Universität Rostock, 18051 Rostock, Germany

Received 18 June 2005; received in revised form 27 January 2006

13 Abstract

14 We review a plethora of relevant experimental results on internal homogeneous crystal nucleation in silicate glasses obtained in the
15 last four decades, and their analyses in the framework of the classical nucleation theory (CNT). The basic assumptions and equations of
16 CNT are outlined. Particular attention is devoted to the analysis of the properties of the critical nuclei, which, to a large extent, govern
17 nucleation kinetics. The main methods employed to measure nucleation rates are described and the possible errors in the determination
18 of the crystal number density (and, correspondingly, in nucleation rates) are discussed. The basic regularities of both time and temper-
19 ature dependencies of nucleation rates are illustrated by numerous experimental data. Experimental evidence for a correlation between
20 maximum nucleation rates and reduced glass transition temperatures is presented and theoretically justified. Special attention is given to
21 serious problems that arise in the quantitative description of nucleation rates when using the CNT, for instance: the dramatic discrepancy
22 between calculated and measured nucleation rates; the high value of the crystal nuclei/melt surface energy, σ_{cm} , if compared to the
23 expected value estimated via Stefan's rule; the increase of σ_{cm} with increasing temperature; and the discrepancies between the values
24 of the surface energy and the time-lag for nucleation when independently estimated from nucleation and growth kinetics. The analysis
25 of the above mentioned problems leads to the following conclusion: in contrast to Gibbs' description of heterogeneous systems under-
26 lying CNT, the bulk thermodynamic properties of the critical nuclei generally differ from those of the corresponding macro-phase result-
27 ing simultaneously in significant differences of the surface properties as compared with the respective parameters of the planar interfaces.
28 In particular, direct experimental evidence is presented for compositional changes of the crystal nuclei during formation of the critical
29 nuclei and their growth from critical to macro-sizes. In addition, detailed examinations of crystal nucleation and growth kinetics show a
30 decrease of both the thermodynamic driving force for nucleation and of the critical nuclei/liquid interfacial energy, as compared with the
31 respective properties of the macro-phase. However, despite significant progress in understanding crystal nucleation in glasses in the past
32 four decades, many problems still exist and this is likely to remain a highly interesting subject for both fundamental and applied research
33 for a long time.

34 © 2006 Published by Elsevier B.V.

35 **Keywords:** Crystallization; Glass ceramics; Nucleation; Crystals; Glass transition; Oxide glasses; Silicates; Thermodynamics

1. Introduction

Glasses can be defined as non-crystalline solids that
undergo a *glass transition* in the course of their prepara-
tion. One of the most important and traditional (but not
the only) method of vitrification consists in supercooling

* Corresponding author. Address: ul. Nalichnay 21, ap.7, 199406 St. Petersburg, Russia. Tel.: +7 812 355 30 38.

E-mail address: vfokin@pisem.net (V.M. Fokina).

42 a liquid escaping crystallization. Thus, when a liquid is
 43 cooled down at sufficiently high rates, crystallization can
 44 occur to a limited degree or can be completely arrested
 45 down to temperatures corresponding to very high viscosi-
 46 ties, in the range $\eta \geq 10^{13} - 10^{12}$ Pa s $\approx \eta(T_g)$, where T_g is
 47 the glass transition temperature. Below this temperature,
 48 the viscosity is so high that large-scale atomic rearrange-
 49 ments of the system are no longer possible within the
 50 time-scale of typical experiments, and the structure
 51 freezes-in, i.e., the structural rearrangements required to
 52 keep the liquid in the appropriate metastable equilibrium
 53 state cannot follow any more the change of temperature.
 54 This process of freezing-in the structure of an undercooled
 55 liquid transforming it into a glass is commonly denoted as
 56 *glass transition*. Typical glass-forming liquids, such as sili-
 57 cate melts, are usually characterized by: (i) relatively high
 58 viscosities ($\eta > 100$ Pa s) at the melting point or liquidus
 59 and (ii) a steep increase of the viscosity with decreasing
 60 temperature. These properties favor vitrification. The
 61 mechanism above sketched leads to the conclusion that
 62 the glass structure must be similar to that of the parent
 63 undercooled liquid at temperatures near T_g and, indeed,
 64 this similarity has been experimentally observed.

65 Glass is thermodynamically unstable with respect to the
 66 undercooled liquid, i.e., there is no energy barrier between
 67 the glass and its corresponding undercooled (metastable)
 68 liquid. At a first glance, the high stability of the glassy state
 69 reflects only a relaxation problem; the system cannot
 70 evolve to a metastable state due to the kinetic inhibition
 71 of this process at low temperatures. On heating, relaxation
 72 of the glass structure may occur to reach first a metastable
 73 liquid state corresponding to the given temperature and
 74 then, eventually, go over into the crystalline state. The lat-
 75 ter evolution process, as will be shown below, involves
 76 overcoming of a thermodynamic potential barrier. At
 77 room temperature glasses can exist for extremely long peri-
 78 ods of time because their high viscosity inhibits structural
 79 rearrangements required for crystal nucleation and growth.
 80 However, when a glass is heat-treated for a sufficiently long
 81 time at temperatures within or above the glass transition
 82 range, devitrification readily starts, as a rule, from the sur-
 83 face and sometimes in the bulk via heterogeneous or homo-
 84 geneous nucleation (see below).

85 Nucleation, or the process of formation of the precur-
 86 sors of the crystalline phases, may occur by different mech-
 87 anisms. Commonly one divides these processes into
 88 homogeneous and heterogeneous nucleation. Homoge-
 89 neous nucleation is a stochastic process occurring with
 90 the same probability in any given volume (or surface) ele-
 91 ment. Alternatively, nucleation occurring on preferred
 92 nucleation sites, e.g., such as pre-existing interfaces, previ-
 93 ously nucleated phases, and surface defects, is denoted as
 94 heterogeneous nucleation. Depending on the location
 95 where nucleation takes places, volume (bulk) and surface
 96 crystallization can be distinguished.

97 Glass-forming melts are interesting models for studies of
 98 nucleation, growth and overall crystallization phenomena.

Their high viscosities result in relatively low (measurable) 99
 rates of crystallization, which may permit detailed studies 100
 of nucleation and growth kinetics. Homogeneous nucle- 101
 ation can sometimes be observed at deep undercoolings 102
 ($T/T_m < 0.6$) because glass-forming melts are excellent sol- 103
 vents for solid impurities that thus only exist as ionic spe- 104
 cies when the liquid is vitrified. In addition, the rapid 105
 increase of viscosity with decreasing temperature makes it 106
 possible to ‘freeze-in’ different states of the crystallization 107
 process by quenching previously heat-treated specimens 108
 to room temperature. Hence, as it was figuratively said in 109
 Ref. [1], ‘glasses did and may serve as the Drosophila of 110
 nucleation theory in order to test different approaches’. 111
 Moreover, silicate glass is one of the oldest materials pro- 112
 duced by mankind, having its origin about 6000 years 113
 ago in ancient Mesopotamia [2], but are still gaining tech- 114
 nological importance. 115

116 It is evident from the above discussion that crystalliza- 116
 tion and glass formation are competitive processes. In this 117
 way, in order to avoid uncontrolled crystallization of glassy 118
 articles one needs to know the main factors that govern 119
 crystal nucleation and growth. On the other hand, con- 120
 trolled nucleation and crystallization of glasses underlay 121
 the production of glass-ceramics invented in the mid- 122
 1950s [3], which are widely used in both domestic and 123
 high-technology applications. By the foregoing reasons, 124
 the investigation of glass crystallization kinetics is of great 125
 interest from both practical and theoretical points of view. 126
 Since, in many respects, the nucleation stage determines the 127
 pathways of overall crystallization, in this review we will 128
 focus our attention on nucleation, with particular emphasis 129
 on the analysis of relevant experimental results in the 130
 framework of the classical nucleation theory (CNT). 131
 Hereby we will restrict ourselves to selected data for homo- 132
 geneous nucleation obtained mainly with silicate glasses. 133

134 The present paper is organized as follows: In Section 2, 134
 the basic equations of CNT are briefly summarized, which 135
 are then employed for nucleation data analysis. Section 3 136
 presents the main methods that may be employed to exper- 137
 imentally determine nucleation rates. Section 4 is devoted 138
 to experimental findings concerning transient and steady- 139
 state crystal nucleation in glasses. In particular, evidence 140
 for a strong correlation between nucleation rates and 141
 reduced glass transition temperature is given. An analysis 142
 of the problems arising in the application of CNT to exper- 143
 imentally observed nucleation rate data is performed in 144
 Section 5. The paper is completed by concluding remarks. 145

2. Basic assumptions and equations of classical nucleation 146 theory (CNT) 147

2.1. Historical notes 148

149 In its original form, classical nucleation theory is based 149
 on the thermodynamic description of heterogeneous sys- 150
 tems developed by Gibbs [4]. Following Gibbs, a real inho- 151
 mogeneous system is replaced by a model system consisting 152

153 of two homogeneous phases divided by a mathematical
154 surface of zero thickness. While the properties of the ambi-
155 ent phase are known, the bulk properties of the critical
156 clusters are determined via Gibbs' equilibrium conditions.
157 A detailed analysis shows that the cluster bulk properties
158 determined in such way are widely identical to the proper-
159 ties of the newly evolving macroscopic phase coexisting in
160 stable equilibrium with the ambient phase at a planar inter-
161 face. The free energy of the heterogeneous system – consist-
162 ing of a cluster of the newly evolving phase in the ambient
163 phase – is expressed as the sum of the bulk contributions of
164 the nucleus and the ambient phase. These bulk terms are
165 supplemented by interfacial contributions, the main one
166 is given by the product of the interfacial area and specific
167 surface energy.

168 When applying the theory to cluster formation, these
169 surface terms initially result in an increase of the character-
170 istic thermodynamic potential, which leads to the existence
171 of a critical cluster size. Only clusters with sizes larger than
172 the critical size are capable to grow up to macroscopic
173 dimensions in a deterministic way. The change of the char-
174 acteristic thermodynamic potential resulting from the for-
175 mation of clusters of critical size is commonly denoted as
176 the work of critical cluster formation. This quantity reflects
177 the thermodynamic aspects in the description of nucleation.

178 In addition to thermodynamic aspects of nucleation, the
179 dynamics of cluster formation and growth must be appro-

180 priately incorporated into the theory. Different approaches
181 have been employed depending on the particular problem
182 being analyzed. The application of CNT to the formation
183 of crystals originates from the work of Kaischew and
184 Stranski [5]. These authors investigated this problem for
185 the case of crystal formation from supersaturated vapor
186 employing the approach developed by Volmer and Weber
187 [6] for vapor condensation. Further advances in CNT
188 including nucleation in the condensed systems, which are
189 the focus of the present review, were connected with the
190 work of Becker and Döring [7], Volmer [8], Frenkel [9],
191 Turnbull and Fisher [10], Reiss [11] and others. Photo-
192 graphs of some of these pioneers of nucleation theory are
193 shown in Fig. 1.

194 According to CNT, the description of homogeneous and
195 heterogeneous nucleation can be basically performed by
196 the same methods. We will present first the results for
197 homogeneous nucleation and afterwards will introduce
198 the modifications required to account for the effect of insol-
199 soluble solid impurities and interfaces that may lead to heter-
200 ogeneous nucleation.

2.2. Homogeneous nucleation

201
202 As we already discussed, homogeneous nucleation sup-
203 poses the same probability of critical nucleus formation
204 in any given volume or surface element of the system under



Fig. 1. From top left to right bottom: J.W. Gibbs, G. Tammann, M. Volmer, R. Kaischew, J. Frenkel, and D. Turnbull.

205 study. According to CNT (see, e.g., Refs. [12,13]), the
206 steady-state homogeneous volume nucleation rate can be
207 written as
208

$$I_{st} = I_o \exp \left[-\frac{W_* + \Delta G_D}{k_B T} \right], \quad (1)$$

$$I_o = 2N_1 \frac{k_B T}{h} \left(\frac{a^2 \sigma_{cm}}{k_B T} \right)^{1/2}.$$

211 This equation determines the so-called steady-state nucle-
212 ation rate, I_{st} , i.e., the number of supercritical clusters
213 formed per unit time in a unit volume of the system. The
214 pre-exponential term, I_o , depends only weakly on tempera-
215 ture (if compared to the exponential function) and varies
216 between 10^{41} and $10^{43} \text{ m}^{-3} \text{ s}^{-1}$ for different condensed sys-
217 tems [14]. In Eq. (1) k_B and h are the Boltzmann and
218 Planck constants, respectively; $N_1 \sim 1/a^3$ is the number of
219 structural (formula) units, with a mean size a , per unit vol-
220 ume of melt; σ_{cm} is specific surface free energy of the crit-
221 ical nucleus-melt interface; ΔG_D is the activation free
222 energy for transfer of a ‘structural unit’ from the melt to
223 a nucleus (kinetic barrier). To a first approximation, the ki-
224 netic barrier for glass-forming liquids is often replaced by
225 the activation free energy for viscous flow, ΔG_η . W_* is the
226 thermodynamic barrier for nucleation, i.e., the increase in
227 the free energy of a system due to the formation of a nu-
228 cleus with critical size, r_* . The critical nucleus size can be
229 determined from the condition

$$\frac{\partial W}{\partial r} = 0, \quad W = c_1 r^2 \sigma_{cm} - c_2 r^3 \Delta G_V, \quad (2)$$

232 where $\Delta G_V = G_l - G_c$ is the difference between the free
233 energies of liquid and crystal per unit volume of the crystal
234 (i.e., the thermodynamic driving force for crystallization)
235 and c_1 and c_2 are shape factors. In the case of a spherical
236 nucleus, we obtain the expressions
237

$$r_* = \frac{2\sigma_{cm}}{\Delta G_V} \quad (3)$$

240 and

$$W_* = \frac{16\pi}{3} \frac{\sigma_{cm}^3}{\Delta G_V^2}. \quad (4)$$

244 The thermodynamic driving force for crystallization is
245 given by
246

$$\Delta G_V V_m = \frac{\Delta H_m}{T_m} (T_m - T) + \int_T^{T_m} \Delta C_p dT' - T \int_T^{T_m} \frac{\Delta C_p}{T'} dT', \quad (5)$$

249 where V_m is the molar volume, ΔH_m and T_m are the molar
250 heat of melting and the melting temperature of the crystal,
251 respectively, and $\Delta C_p = C_p^l - C_p^c$ is the difference between
252 the molar heat capacities of liquid and crystal at constant
253 pressure. The experimental values of ΔG_V are normally
254 bounded by the approximations usually assigned to Turn-
255 bull (Eq. (6)) and Hoffman (Eq. (7)) that assume $\Delta C_p = 0$
256 and $\Delta C_p = \text{constant}$, respectively [13],

$$\Delta G_V(T) = \Delta H_V \left(1 - \frac{T}{T_m} \right), \quad (6)$$

$$\Delta G_V(T) = \Delta H_V \left(1 - \frac{T}{T_m} \right) \frac{T}{T_m}. \quad (7) \quad 259$$

Here ΔH_V is the melting enthalpy per unit volume of the
260 crystal. One should note, however, that Eq. (6) was first
261 employed by Thomson and Volmer (cf. Ref. [8]).
262

Eq. (1) describes the time-independent steady-state
263 nucleation. Such nucleation regime occurs if a stationary
264 size distribution of the newly evolving subcritical ($r < r_*$)
265 and critical ($r = r_*$) nuclei is established in the system.
266 The cooling rates typically employed for glass formation
267 from the melt, and the heating rates of small glass speci-
268 mens to any given temperature T under investigation are
269 commonly too high to maintain a steady-state distribution
270 of nuclei in the system. Hence, some time period is needed
271 for a reconstruction of the initial nuclei distribution
272 towards the time-independent distribution corresponding
273 to the temperature of study. During this period the nucle-
274 ation rate varies and approaches a steady-state value given
275 by Eq. (1).
276

The time required to establish steady-state nucleation in
277 a system is commonly denoted as the time-lag for nucle-
278 ation, τ . It characterizes the duration for the onset of the
279 steady-state distribution, and hence the evolution of the
280 nucleation rate, $I(t)$, towards a steady-state value, I_{st} . In
281 the cases when the initial concentration of critical and
282 sub-critical nuclei may be neglected, τ and $I(t)$ can be
283 expressed by Eqs. (8) and (9), respectively [15,16],
284
285

$$\tau = \frac{16h}{\pi} \frac{\sigma_{cm}}{\Delta G_V^2 a^4} \exp \left(\frac{\Delta G_D}{k_B T} \right), \quad (8)$$

$$I(t) = I_{st} \left[1 + 2 \sum_{m=1}^{\infty} (-1)^m \exp \left(-m^2 \frac{t}{\tau} \right) \right]. \quad (9) \quad 287$$

Integration of Eq. (9) results in the following expression for
288 the time-dependence of the number of super-critical nuclei
289 per unit volume of the system, N_V ,
290
291

$$\frac{N_V(t)}{I_{st} \tau} = \left[\frac{t}{\tau} - \frac{\pi^2}{6} - 2 \sum_{m=1}^{\infty} \frac{(-1)^m}{m^2} \exp \left(-m^2 \frac{t}{\tau} \right) \right]. \quad (10) \quad 293$$

For sufficiently long times, t , as compared with τ this
294 expression can be approximated by
295
296

$$N_V(t) = I_{st} \left(t - \frac{\pi^2}{6} \tau \right). \quad (11) \quad 298$$

For the experimental estimation of τ , it is convenient to
299 use the induction period, t_{ind} , defined via Eq. (12) as
300
301

$$\tau = \frac{6}{\pi^2} t_{ind}. \quad (12) \quad 303$$

The induction period, t_{ind} , is easily determined as the inter-
304 section of the asymptote (Eq. (11)) with the time-axis. An-
305 other more correct way to estimate I_{st} and τ is by fitting the
306 experimental values of $N(t)$ to Eq. (10).
307

308 2.3. Heterogeneous nucleation

309 The existence of foreign solid particles and phase
310 boundaries may favor nucleation. This effect is due mainly
311 to the diminished thermodynamic barrier as compared to
312 that for homogeneous nucleation, owing to a decrease of
313 the contribution of the effective surface energy to the work
314 of critical cluster formation. For example, the thermody-
315 namic barrier for nucleation in the case of condensation
316 on planar interfaces is given by [12]

$$318 W_*^{\text{het}} = W_* \Phi, \quad \Phi = \frac{1}{2} - \frac{3}{4} \cos \theta + \frac{1}{4} \cos^3 \theta. \quad (13)$$

319 Depending on the value of the wetting angle, θ , the param-
320 eter Φ varies from zero to unity. The value of Φ depends on
321 the mechanism of nucleation catalysis.

322 In order to adapt the expression for the steady-state
323 nucleation rate, Eq. (1), to the description of heterogeneous
324 nucleation, the number of ‘structural’ units per unit vol-
325 ume, N_1 , which appears in the pre-exponential term of
326 Eq. (1), must be replaced by the number, N^S , of ‘structural
327 units’ in contact with the catalyzing surface per unit vol-
328 ume. Hence, in the case of heterogeneous nucleation, the
329 following equation can be written for the steady-state
330 nucleation rate:

$$332 I_{\text{st}}^{\text{het}} \cong N^S \frac{k_B T}{h} \exp \left[-\frac{W_* \Phi + \Delta G_D}{k_B T} \right]. \quad (14)$$

333 Catalyzing surfaces may be represented, for instance, by
334 dispersed solid particles that act as nucleation sites. In this
335 case, their curvature and number may strongly affect the
336 nucleation kinetics [14,17]. The exhaustion of available
337 nucleation sites due to crystal nucleation leads to satur-
338 ation of the kinetic curve N versus t . If, however, for some
339 reason such saturation is not achieved, the knowledge of
340 the $N(t)$ -dependence is not sufficient to conclude what type
341 of nucleation took place.

342 3. Experimental methods to estimate nucleation rates

343 3.1. General problem

344 At high undercoolings corresponding to the range of
345 measurable homogeneous (volume) nucleation rates in typ-
346 ical glass-forming liquids, the critical nuclei are undetect-
347 able by common experimental techniques, hence they
348 must first be developed to a visible size to allow one to
349 determine (e.g., using a microscope) their number density,
350 N , as a function of time, allowing then to estimate the
351 nucleation rate as $I = dN/dt$. In order to perform such
352 task, different methods have been developed.

353 3.2. Double-stage (‘development’) method

354 If the overlapping of the nucleation and growth rate
355 curves is weak (i.e., the crystal growth rates are very low
356 at temperatures corresponding to high nucleation rates),
357 the observation of the nucleated crystals and the estimation

of the crystal number density is a quite difficult task. For
these cases, about a hundred years ago, Gustav Tammann
(who was studying crystallization of organic liquids) pro-
posed the following procedure, which is now known as
the Tammann or ‘development’ method [18]. Crystals
nucleated at a low temperature, T_n , are grown up to micro-
scopic sizes at a higher temperature, $T_d > T_n$. The develop-
ment temperature T_d has to meet the following conditions
for nucleation (I) and growth (U) rates: $I(T_d) \ll I(T_n)$ and
 $U(T_d) \gg U(T_n)$. After a lapse of seventy years, Ito et al.
[19] and Filipovich and Kalinina [20] independently applied
Tammann’s method to the study of crystal nucleation
kinetics in lithium disilicate glasses. Since then, this method
has been widely employed for glass crystallization studies.
Some problem inherent in this method and connected with
the possible dissolution of some part of the originally
formed (at the nucleation temperature) nuclei at the devel-
opment temperature will be discussed later.

358 3.3. Single-stage methods

359 3.3.1. The direct method

When there is considerable overlap of the $I(T)$ and $U(T)$ -
curves, the number density of crystals can be measured
directly after single-stage heat treatments at T_n . Then, the
obtained $N(T_n, t)$ -curve will be shifted (relatively to the true
one) to higher times by a time $t_o = (r_{\text{res}} - r_*)/U(T_n) \cong r_{\text{res}}/$
 $U(T_n)$ that is needed to grow the crystals up to the micro-
scope resolution limit, $\varepsilon = 2r_{\text{res}}$ [21]. Finally, one must cor-
rect the number densities to account for stereological
errors. This procedure will be described in Section 3.4.

360 3.3.2. Crystal size distribution analysis

Continuous nucleation and growth normally result in a
broad distribution of crystal sizes, i.e., the first nucleated
crystal has the largest size and so forth. If the crystal
growth rate is known, one can calculate the ‘birth dates’
of crystals belonging to different size groups and then plot
a $N(t)$ -curve. Toshev and Gutzow derived the basic form-
ulas relating the size distribution of spherical isolated
particles embedded in a continuous matrix with that of
their circular intersections on a sample cross-section for
both steady-state and transient volume nucleation [22].
For surface crystallization the size distribution is easily
constructed from direct measurements. This method,
known as Köster’s method, also works in the case of heter-
ogeneous nucleation from a finite number of active centers
when the latter are depleted in a relative short time, and
further advancement of crystallization only occurs via crys-
tal growth. It has been systematically employed to study
the surface nucleation rates in metallic [23] and silicate
glasses [24].

361 3.4. Stereological corrections

The use of reflected light microscopy can lead to large
errors in the determination of the number of crystals per

410 unit volume due to the stereological methods employed to
 411 calculate volume properties (size distributions, numbers,
 412 etc.) based on statistical evaluations performed on cross-
 413 sections through the specimens. Thus a significant fraction
 414 of the cut crystals (in the cross-sections) can be smaller
 415 than the resolution limit of the microscope used, which
 416 may lead to an underestimation of the crystal numbers
 417 and, consequently, of the determined values of nucleation
 418 rates. In Refs. [25,26], equations were derived for the frac-
 419 tional underestimation, f , of the number of spherical parti-
 420 cles per unit volume and of the nucleation rates, as
 421 obtained from stereological techniques for reflected light
 422 microscopy or SEM, for typical cases of crystal nucleation
 423 in glasses. The following two cases bound the most com-
 424 mon experimental situations: (i) a monodisperse system
 425 of spherical particles that can result from instantaneous
 426 heterogeneous nucleation; (ii) a uniform size distribution
 427 of spherical particles from the critical size to D_M , where
 428 D_M is the largest diameter of the clusters in the distribu-
 429 tion. Such distribution is typical for simultaneous nucle-
 430 ation and growth with constant rates in a single-stage
 431 heat treatment. The equations for these cases are:

432 *Case (i). Monodisperse systems:*

$$434 \quad f = \frac{2}{\pi} \arcsin(\sigma_1), \quad (15)$$

435 *Case (ii). Uniform size distribution from the critical size to*
 436 *D_M :*

$$438 \quad f = 1 - \left\{ \frac{2}{\pi} [\cos \theta_1 [1 - \ln(1 + \sin \theta_1)] + \theta_1 + \sigma_1 \ln \sigma_1 - \sigma_1] \right\}. \quad (16)$$

439 In above equations, $\theta_1 = \arccos \sigma_1$, $\sigma_1 \equiv \varepsilon/D_M$, and ε is the
 440 resolution limit of the microscope used. Comparison with
 441 experimental nucleation data for two silicate glasses dem-
 442 onstrated that these equations predict well the observed
 443 underestimations of the number of spherical particles.
 444 Fig. 2 shows the function f for cases (i) and (ii).

445 To minimize these errors employing reflected light opti-
 446 cal microscopy methods, one should use high magnification
 447 objective lenses or SEM. Alternatively, transmission meth-
 448 ods could be used because they lead to much smaller errors
 449 than reflection techniques.

450 Similar underestimates occur when one tries to deter-
 451 mine volume fractions crystallized, and these may be sub-
 452 jected to significant errors when the largest grain size of
 453 the distribution is close to the microscope resolution limit
 454 [26]. For transformations occurring from a fixed number
 455 of nuclei, the systematic errors are smaller than those
 456 observed in the continuous nucleation case, but can still
 457 be significant when reflected light microscopy is used.
 458 Transmission methods are more time-consuming, but lead
 459 to much smaller errors than reflection techniques.

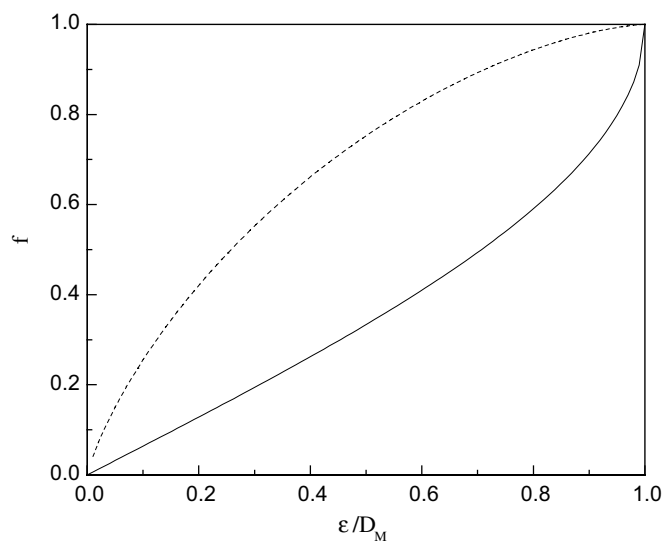


Fig. 2. Fractional underestimation of the number of spherical particles versus the ratio between the microscope resolution limit and the largest particle diameter. Solid and dashed curves refer to cases (i) and (ii), respectively.

3.5. Probabilistic approach for the analysis of the nucleation process

462 For the sake of completeness we should briefly mention
 463 a method based on the stochastic nature of nucleation [27].
 464 The appearance of critical nuclei is a stochastic event that
 465 can be characterized by an average waiting period, $\bar{\tau}$,
 466

$$468 \quad \bar{\tau} = \frac{1}{IV}, \quad (17)$$

469 where I is the nucleation rate and V is the volume of the
 470 system under study.

471 Since the probability of critical nucleus formation due to
 472 a successful series of attachment and separation reactions is
 473 very low, nucleation can be treated as a Poissonian process.
 474 Hence the probability of appearance of one critical nucleus
 475 in a time period τ^1 is
 476

$$478 \quad P_1(\tau^1) = \lambda \tau^1 \exp(-\lambda \tau^1), \quad (18)$$

479 where $\lambda = 1/\bar{\tau}$.

480 In cases of high nucleation rates, their measurement is
 481 normally limited to relatively low undercoolings that corre-
 482 spond to high values of the crystal growth rate. Thus, the first
 483 few super-critical nuclei trigger crystallization of the whole
 484 sample. Fitting the experimental distribution of waiting times
 485 of the first nucleus, τ^1 , to Eq. (18) one can estimate an aver-
 486 age waiting period, $\bar{\tau}$, and then the nucleation rate from Eq.
 487 (17). Such analysis has been employed, e.g., for metals dis-
 488 persed in the form of small drops when the use of other meth-
 489 ods is connected with difficulties (see, e.g., [13,28]).

3.6. Overall crystallization kinetics

490
 491 Crystal nucleation followed by subsequent growth
 492 results in the overall crystallization of the sample. This

493 process can be described by determining the volume frac- 535
 494 tion of the transformed phase, $\alpha(t)$. The formal theory of 536
 495 overall-crystallization kinetics under isothermal conditions 537
 496 was developed in the late 1930s by Kolmogorov [29], John- 538
 497 son and Mehl [30], and Avrami [31], and is well-known as 539
 498 the JMAK theory. According to this theory, the volume 540
 499 fraction of the new phase is given by

502
$$\alpha(t) = 1 - \exp \left[-g \int_0^t I(t') \left[\int_{t'}^t U(t'') dt'' \right]^3 dt' \right], \quad (19)$$

503 where g is a shape factor, which is equal to $4\pi/3$ for spher- 547
 504 ical crystals. If the nucleation (I) and growth (U) rates are 548
 505 constant throughout the transformation (e.g., steady-state 549
 506 homogeneous stoichiometric nucleation), Eq. (19) can be 550
 507 rewritten as

510
$$\alpha(t) = 1 - \exp \left[-\frac{gIU^3 t^4}{4} \right]. \quad (20)$$

511 When the number of growing crystals, N_0 , does not 547
 512 change with time (as it is typical for fast heterogeneous 548
 513 nucleation on a finite number of active sites), Eq. (19) 549
 514 transforms to

517
$$\alpha(t) = 1 - \exp[-gN_0U^3t^3]. \quad (21)$$

518 Avrami proposed that, in general, the following relation 559
 519 should be used:

522
$$\alpha(t) = 1 - \exp(-Kt^n). \quad (22)$$

523 In typical applications, Eq. (22) is employed in the form

526
$$\ln(-\ln(1 - \alpha)) = \ln K + n \ln t. \quad (23)$$

527 The values of K and n can be estimated then by fitting the 563
 528 experimental data of $\alpha(t)$ to Eq. (23). Thus the coefficient K 564
 529 includes I and U , or N_0 and U . The Avrami coefficient, n , 565
 530 depends on both nucleation and growth mechanisms, and 566
 531 can be written for the case of three-dimensional growth as 567
 532

534
$$n = k + 3m, \quad (24)$$

where k and m are taken from the formulas $N \sim t^k$ and 535
 $r \sim t^m$ describing the variation of crystal number (N) and 536
 crystal size (r) with time. 537

The knowledge of the Avrami coefficient, n , is helpful to 538
 understand the mechanism of phase transformation at a 539
 given temperature. When it is possible to independently 540
 measure the crystal growth rate, one can then calculate 541
 the nucleation rate from the coefficient K . This method is 542
 not as precise as direct measurements, but can give useful 543
 information about nucleation in advanced stages of crystal- 544
 lization, when the application of other methods is hindered 545
 (see Section 5). 546

For the simplest cases of constant nucleation rate (or 547
 constant number of crystals) and linear growth, Eqs. (20) 548
 and (21) have been tested by using I_{st} , U , and N_0 data inde- 549
 pendently measured by optical microscopy in glasses of 550
 stoichiometric compositions $2Na_2O \cdot CaO \cdot 3SiO_2$ [32] and 551
 $Na_2O \cdot 2CaO \cdot 3SiO_2$ [33]. Good agreement was obtained 552
 between the values of gIU^3 (or gN_0U^3), calculated from fit- 553
 ting the $\alpha(t)$ -data to the JMAK equation, and directly mea- 554
 sured values. Recently, the JMAK-equation was also 555
 successfully employed, together with measured crystal 556
 growth rates, to estimate extremely high nucleation rates 557
 in a stoichiometric glass of fresnoite composition [34]. 558

4. Interpretation of nucleation experiments by the classical 559
 nucleation theory 560

4.1. Non-steady state (transient) nucleation 561

4.1.1. Estimation of the time-lag in nucleation 562

Typical $N(T_n, T_d, t)$ -curves obtained by the ‘develop- 563
 ment’ method are shown in Fig. 3. As we already men- 564
 tioned, only the nuclei that achieve the critical size, 565
 $r_*(T_d)$, during heat treatment at T_n can grow at the devel- 566
 opment temperature T_d . The other nuclei have a high prob- 567
 ability to dissolve at T_d . As the result, the number of 568
 crystals nucleated at given conditions and developed at 569
 T_d has, strictly speaking, to decrease with increasing T_d 570

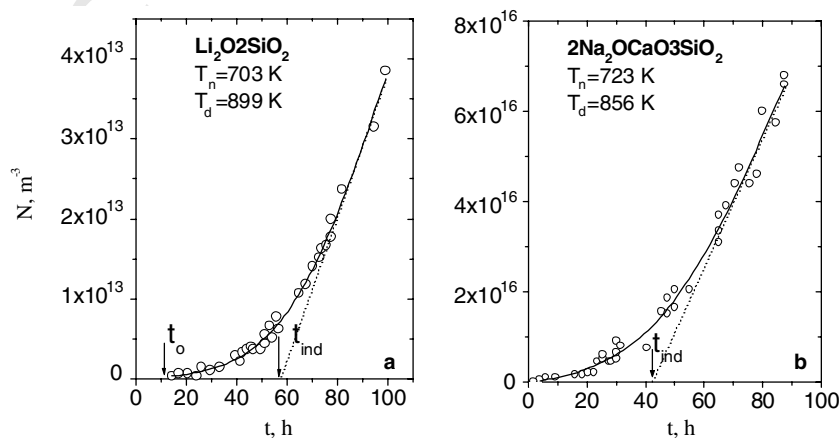


Fig. 3. Typical curves of the number density of $Li_2O \cdot 2SiO_2$ (a) and $2Na_2O \cdot CaO \cdot 3SiO_2$ (b) crystals in glasses of respective stoichiometric compositions versus time of nucleation obtained by the ‘development’ method [35,36].

(see Figs. 4 and 5). The total number of supercritical crystals, N , nucleated at a temperature, T_n , in a time, t , is given by

$$N(T_n, r_*(T_n), t) = \int_0^t I(T_n, t') dt'. \quad (25)$$

The number of crystals nucleated in the same conditions, but having sizes larger than the critical size, $r_*(T_d)$, and which are, consequently, capable to grow at T_d , is given by

$$N(T_n, r_*(T_d), t) = \int_0^{t-t_0} I(T_n, t') dt', \quad (26)$$

where t_0 is the period of time that critical nuclei of size $r_*(T_n)$ need in their growth to reach the size $r_*(T_d)$. This time interval is determined by

$$t_0(T_n, T_d) = \int_{r_*(T_n)}^{r_*(T_d)} \frac{dr}{U(T_n, r)}. \quad (27)$$

Eqs. (25) and (26) yield

$$N(T_n, r_*(T_n), t) = N(T_n, r_*(T_d), t + t_0). \quad (28)$$

Hence, $N(T_n, r_*(T_n), t)$ plots are similar to $N(T_n, r_*(T_d), t)$ -plots with the difference that the latter is shifted along the time-axis by a time t_0 . Thus, the development method can provide the correct value of the steady-state nucleation rate, but overestimates the induction time for nucleation by t_0 .

The period during which heat treatment at the nucleation temperature T_n does not influence crystallization at T_d can be identified with t_0 (given by Eq. (27); here we neglect the time of the first critical nucleus formation). This time is indicated by an arrow in Fig. 3(a). According to Eq. (27), the higher the growth rate U at the nucleation temperature, T_n , and the closer is T_d to T_n ($r_*(T_n)$ is correspondingly closer to $r_*(T_d)$), the lower is t_0 . Hence, for a strong overlap of the nucleation and growth rate curves, the value of t_0 is not very high and can often be neglected. Fig. 3(b) confirms this assumption for a $2\text{Na}_2\text{O} \cdot \text{CaO} \cdot 3\text{SiO}_2$ glass. On the other hand, when the overlap of the nucleation and growth rate curves is weak, as observed for lithium disilicate glass, one has to reduce the measured value of $t_{\text{ind}}(T_n, T_d)$ by a time $t_0(T_n, T_d)$ (see Fig. 3(a)) to estimate $t_{\text{ind}}(T_n)$. The value of $t_{\text{ind}}(T_n)$ can be roughly estimated via extrapolation of the $t_{\text{ind}}(T_n, T_d)$ -values for the $N(T_n, T_d, t)$ -curves, obtained at different T_d , to t_{ind} corresponding to $T_d = T_n$. Fig. 5(a) presents examples of such $N(T_n, T_d, t)$ -curves for lithium disilicate glass. Fig. 5(b) shows the values of t_{ind} , taken from these curves, versus development temperature. When T_d approaches $T_n = 453^\circ\text{C}$, t_{ind} is about 1.9 h (the average value of the linear and quadratic polynomial extrapolations). Hence, one can approximately estimate t_0 as $t_0(T_d, T_n) = t_{\text{ind}}(T_n, T_d) - t_{\text{ind}}(T_n)$, e.g., for $T_d = 530^\circ\text{C}$ and $T_n = 453^\circ\text{C}$ t_0 is about 0.9 h. A similar value is obtained by extrapolating the initial section of the $N(t)$ -curve 1 (see also curve 5) to $N = 0$. Thus, according to Eq. (12), one can assume that Eq. (29) holds, i.e.,

$$\tau(T_n) = \frac{6}{\pi^2} (t_{\text{ind}}(T_n, T_d) - t_0(T_n, T_d)). \quad (29)$$

Kinetic $N(t)$ -curves, such as those presented by Fig. 3, can be plotted in dimensionless coordinates $(N(T, t - t_0)/I_{\text{st}}(T)\tau(T))$ versus $(t - t_0)/\tau(T)$. Fig. 6(a) shows that these coordinates allow one the combination of data for different glasses and different temperatures in the same plot. The experimental points are quite close to the theoretical master curve calculated with Eq. (10). This curve corresponds to increasingly higher nucleation rates towards the steady-state value, I_{st} . The evolution of the nucleation rate calculated by Eq. (9) is shown in Fig. 6(b).

As we already mentioned in Section 3.3, if one employs the single-stage method, the induction periods obtained from experimental $N(T_n, t)$ -curves must be reduced by a period of time $t_0 \approx r_{\text{res}}/U(T_n)$. An example of such curve, obtained for Au-catalyzed nucleation in NaPO_3 glass, is

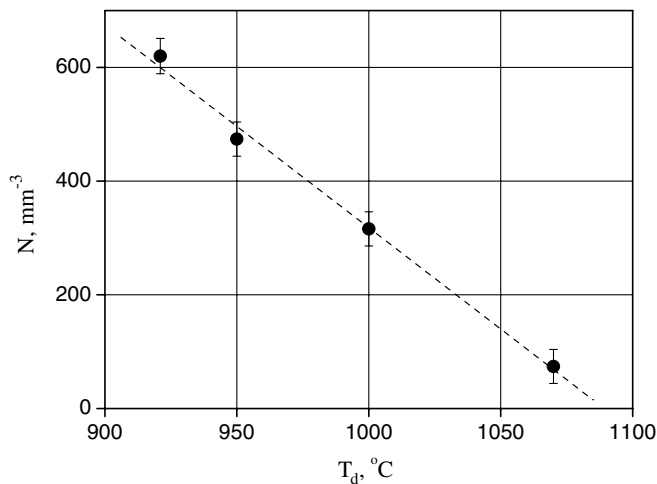


Fig. 4. Number density of crystals versus development temperature in a lithium aluminum silicate glass subjected to nucleation treatment for 5 min at $T_n = 785^\circ\text{C}$ [37].

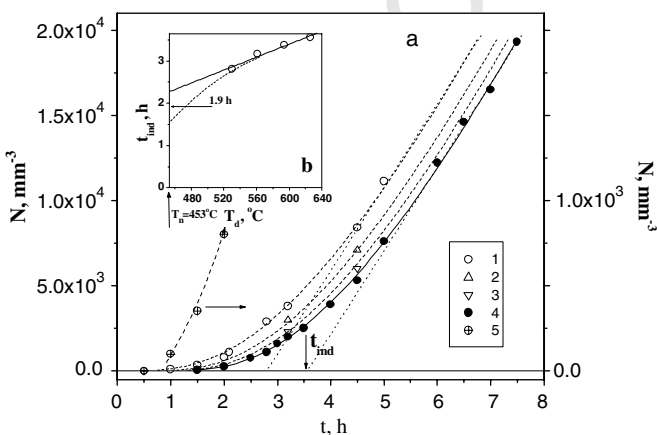


Fig. 5. (a) Number density of $\text{Li}_2\text{O} \cdot 2\text{SiO}_2$ crystals developed at $T_d = 530^\circ\text{C}$ (curves 1 and 5), 560°C (curve 2), 594°C (curve 3), and 626°C (curve 4) as a function of nucleation time at $T_n = 453^\circ\text{C}$ [38]. (b) Induction time versus development temperature.

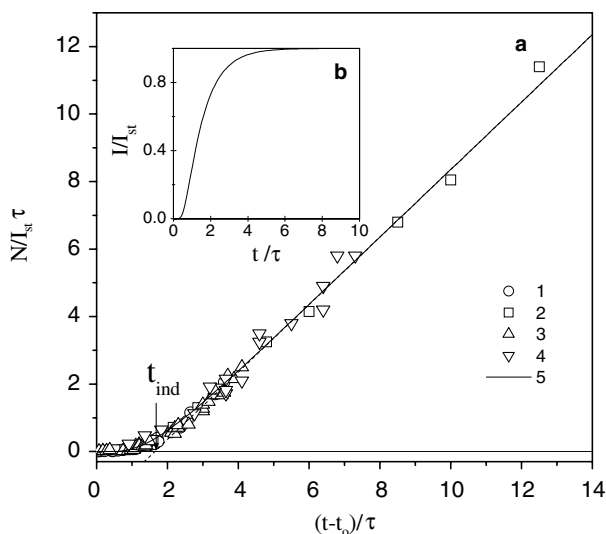


Fig. 6. (a) $N/I_{st}\tau$ versus reduced time for glasses $\text{Li}_2\text{O}\cdot 2\text{SiO}_2$ (curves 1 and 2), and $2\text{Na}_2\text{O}\cdot \text{CaO}\cdot 3\text{SiO}_2$ (curves 3 and 4) [35] for $T = 430^\circ\text{C}$ (curve 1), 465°C (curve 2), 465°C (curve 3) and 470°C (curve 4). Curve 5 was calculated from Eq. (10). (b) Reduced nucleation rate versus reduced time calculated from Eq. (9).

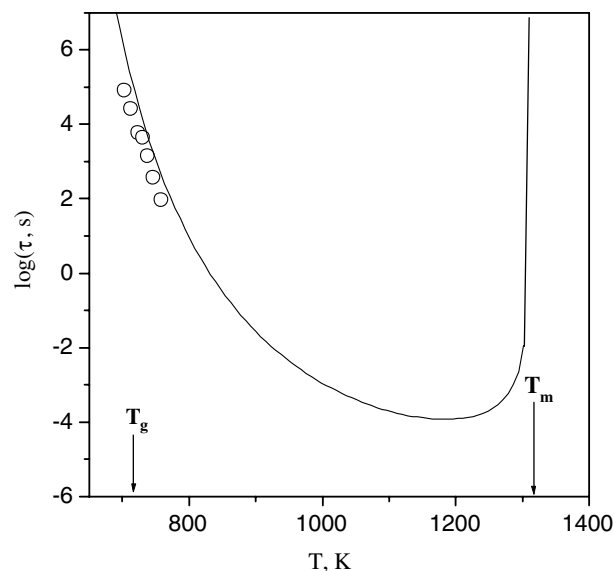


Fig. 8. Temperature dependence of the time-lag for nucleation. Circles refer to experimental data for $\text{Li}_2\text{O}\cdot 2\text{SiO}_2$ glass [41]. The full line was calculated by Eq. (8).

646 shown in Fig. 7. The dashed line indicates the case of
647 steady-state nucleation where the shift, t_0 , is taken into
648 account. The comparison of this line with experimental
649 data gives clear evidence for the transient character of the
650 $N(t)$ -curves. It should be emphasized that one of the first
651 experimental demonstrations of transient nucleation in
652 glasses was presented in Ref. [39].

653 4.1.2. Temperature dependence of the time-lag for nucleation

654 According to Eq. (8), when the degree of undercooling
655 increases, the time-lag τ passes through a minimum. This
656 behavior is due to the interplay between the decrease of

657 $1/\Delta G_V^2$ and the increase of the exponential term. This mini-
658 mum is located at a low undercooling. Since, in the case of
659 glass-forming silicate melts, detectable (internal) homoge-
660 neous nucleation rates are observed only at very deep
661 undercoolings, $\Delta T/T_m \geq 0.4$ [40], at these undercoolings
662 only an increase of the time-lag with increasing undercool-
663 ing is observed. Fig. 8 illustrates this trend for lithium disil-
664 icate glass. The circles refer to experimental data. The solid
665 line is determined according to Eq. (8) with $\sigma_{cm} = 0.2 \text{ J/m}^2$
666 assuming that the activation free energy ΔG_D is equal to
667 that for viscous flow, ΔG_η . For deep undercoolings the
668 validity of this last assumption has been a subject of contro-
669 versial discussion, however, it is commonly assumed to
670 be valid for $T > 1.2T_g$ (see, e.g., [42]).

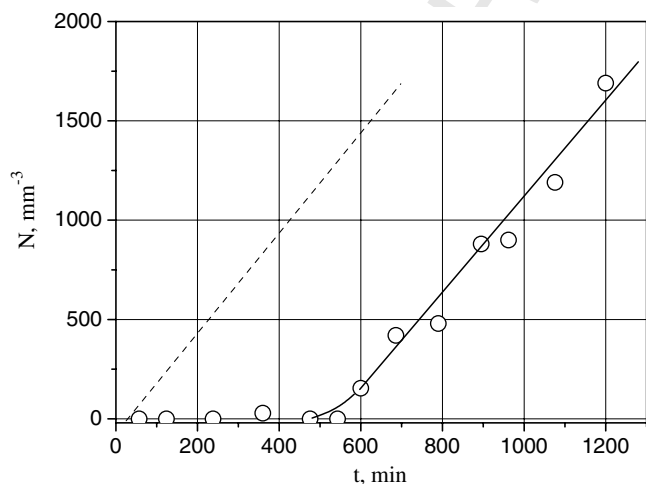


Fig. 7. Number density of crystals in NaPO_3 glass doped with 0.45% Au versus time of heat treatment at $T = 332^\circ\text{C}$ obtained by a single-stage method [39]. The dashed line refers to the steady-state nucleation rate. The shift due to the time required to grow the crystals to visible sizes is taken into account.

671 4.1.3. Transient nucleation with a pre-existing nucleus 672 size distribution

673 So far we discussed transient nucleation assuming the
674 absence of an appreciable number of pre-existing nuclei.
675 This assumption is quite reasonable for interpreting time-
676 lag phenomena for glasses obtained via fast quenching of
677 the melt. In contrast, preliminary annealing of a glass at
678 some temperature, T_1 , for sufficiently long times, $t \geq \tau(T_1)$,
679 results in the formation of a cluster distribution that acts as
680 an initial distribution at the temperature T_2 . Then this dis-
681 tribution evolves towards a steady-state distribution corre-
682 sponding to the temperature T_2 , complicating the time-
683 dependence of the nucleation rate.

684 For example, for lithium disilicate glass annealed at T_1 ,
685 the nucleation rate at $T_2 > T_1$ passes through a maximum
686 before reaching the steady-state value. Fig. 9 shows the
687 $N(t)$ -curves at $T_2 = 465^\circ\text{C}$ for a rapidly quenched parent
688 glass (curve 1) and for glasses that had been previously
689 annealed at $T_1 = 430^\circ\text{C}$ (curves 2 and 3). All curves were

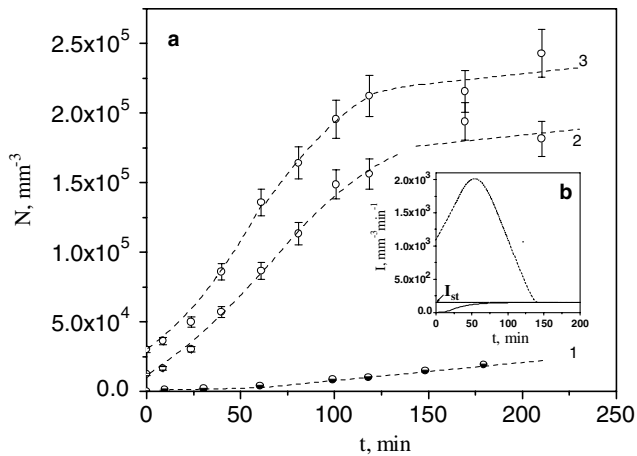


Fig. 9. (a) Number density of $\text{Li}_2\text{O}\cdot 2\text{SiO}_2$ crystals obtained via the ‘development’ method ($T_d = 626^\circ\text{C}$) versus time of nucleation at $T_n = 465^\circ\text{C}$. Curve 1 refers to the quenched glass. Curves 2 and 3 refer to glasses subjected to preliminary treatment at $T = 430^\circ\text{C}$ for 65 h (curve 2) and 89 h (curve 3) [43]. (b) Nucleation rate versus time. Solid and dashed lines correspond to curves 1 and 3 from (a), respectively.

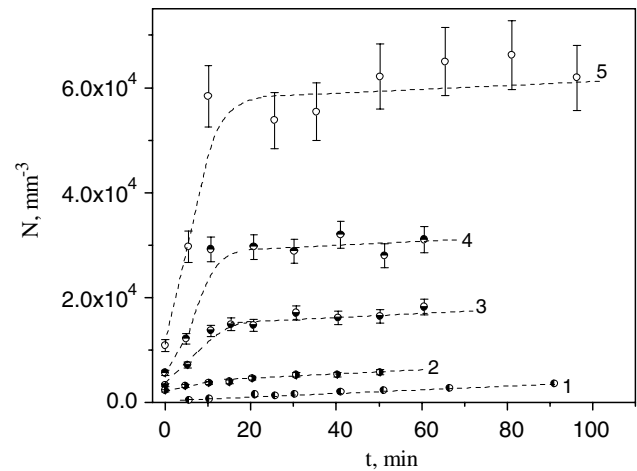


Fig. 10. Number density of $\text{Li}_2\text{O}\cdot 2\text{SiO}_2$ crystals obtained via the ‘development’ method ($T_d = 626^\circ\text{C}$) versus time of nucleation at $T_n = 485^\circ\text{C}$. Curve 1 quenched glass, curves 2–5 glasses subjected to preliminary treatment at $T = 473^\circ\text{C}$ (curve 2), 451°C (curve 3), 440°C (curve 4), and 430°C (curve 5) for the following times: $t = 0.75$ h (curve 2), 4.5 h (curve 3), 18 h (curve 4), and 65 h (curve 5) which exceed the time-lags at T [43].

690 obtained by the ‘development’ method at $T_d = 626^\circ\text{C}$.
 691 Curves 2 and 3 demonstrate, as compared with curve 1, a
 692 strong increase in the number of crystals, and only for
 693 times higher than about 120 min the nucleation rate
 694 reaches steady-state conditions corresponding to the tem-
 695 perature T_2 . The evolution of the nucleation rate corre-
 696 sponding to curve 3 is shown in Fig. 9(b).

697 Such unusual behavior of the nucleation kinetics is
 698 caused by the transition of an initial distribution formed
 699 at T_1 for sizes less than $r_*(T_d)$ into the steady state cluster
 700 size distribution corresponding to T_2 . Since the number of
 701 nuclei having sizes $r \geq r_*(T)$ increases with decreasing tem-
 702 perature, down to $T = T_m/3$, a strengthening of the effect of
 703 the preliminary heat treatment with decrease of T_1 should
 704 be expected. This is indeed the case as shown in Fig. 10.
 705 The presented effects of the multistage heat treatments were
 706 well-described by the numerical modeling of the cluster
 707 evolution performed in the framework of the classical
 708 nucleation theory [44–46] with the exception of the heat
 709 treatments involving the temperature $T_1 = 430^\circ\text{C}$ [45].
 710 Since the values of the parameters needed for the simula-
 711 tions were estimated via a fitting procedure this disagree-
 712 ment could be caused by the error in the $I_{st}(430^\circ\text{C})$
 713 estimation or viscosity data taken from other authors. Nev-
 714 ertheless, the simulations clearly show that the nucleation
 715 kinetics is governed by the evolution of the nuclei
 716 distribution.

717 4.2. Steady-state nucleation

718 4.2.1. Temperature dependence of steady-state nucleation 719 rates

720 Some examples of steady-state nucleation rates, I_{st} , mea-
 721 sured from the slope of the linear part of the $N(t)$ -plots,
 722 such as those shown in Fig. 3, are presented in Fig. 11 as
 723 a function of reduced temperature. The values of $I_{st}(T)$ pass

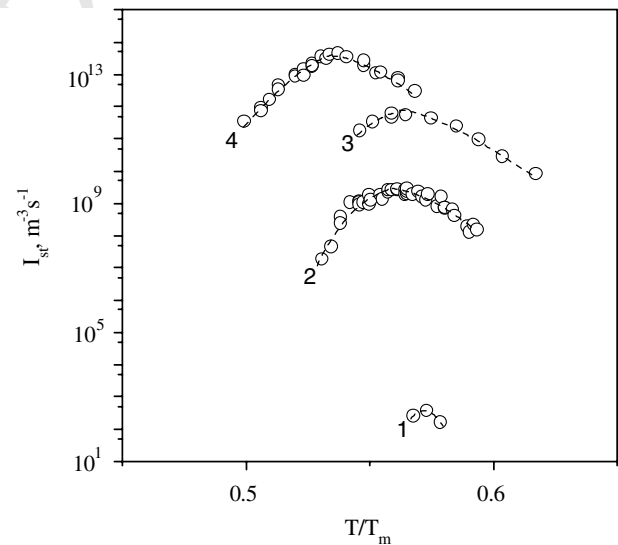


Fig. 11. Steady-state nucleation rate versus reduced temperature for some stoichiometric glasses: (curve 1) $3\text{MgO}\cdot\text{Al}_2\text{O}_3\cdot 3\text{SiO}_2$ [47]; (curve 2) $\text{Li}_2\text{O}\cdot 2\text{SiO}_2$ [35]; (curve 3) $\text{Na}_2\text{O}\cdot 2\text{CaO}\cdot 3\text{SiO}_2$ [48]; (curve 4) $2\text{Na}_2\text{O}\cdot\text{CaO}\cdot 3\text{SiO}_2$ [36].

724 through a maximum at a temperature T_{max} . The
 725 magnitudes of $I_{st}(T_{\text{max}}) \equiv I_{\text{max}}$ vary from 5×10^{13} to $3 \times$
 726 $10^2 \text{ m}^{-3} \text{ s}^{-1}$ and cover practically the whole range of avail-
 727 able measurements of nucleation rates in silicate glasses
 728 with stoichiometric compositions.

729 The reason for the existence of the nucleation rate maxi-
 730 mum follows from a simple analysis of Eq. (1). Since the
 731 pre-exponential term, I_0 , depends only weakly on tempera-
 732 ture, the temperature dependence of the nucleation rate is
 733 determined mainly by the thermodynamic and kinetic bar-
 734 riers for nucleation. A temperature decrease produces two

735 effects: a decrease of the thermodynamic barrier due to an
 736 increase in the thermodynamic driving force for crystalliza-
 737 tion, leading to a higher nucleation rate, and an increase of
 738 the kinetic barrier, leading to a lower nucleation rate (the
 739 kinetic barrier is, as mentioned earlier, often replaced by
 740 the activation free energy for viscous flow). As a result of
 741 these two opposite tendencies, one finds a maximum of
 742 the steady-state nucleation rate at a temperature T_{\max} ,
 743 which is located well below T_m .

744 Eq. (4) for the thermodynamic barrier can be rewritten
 745 as

$$746 \frac{W_*}{k_B T} = C_1 \frac{1}{T_r(1 - T_r)^2}, \quad C_1 = \frac{16\pi}{3} \frac{\alpha_{ST}^3 \Delta H_m}{RT_m}, \quad T_r \equiv \frac{T}{T_m}. \quad (30)$$

749 Here we used the linear approximation for the thermody-
 750 namic driving force, Eq. (6), and the following semi-empir-
 751 ical equation:

$$754 \sigma_{cm} = \alpha_{ST} \frac{\Delta H_m}{V_m^{2/3} N_A^{1/3}} \quad (31)$$

755 for the specific surface energy of the nucleus/melt interface
 756 proposed by Skapski and Turnbull [49,50]. In Eq. (31),
 757 ΔH_m is the melting enthalpy per mole, V_m is the molar vol-
 758 ume, N_A is Avogadro's number, and α_{ST} is an empirical
 759 dimensionless coefficient, smaller than unity, reflecting the
 760 fact that surface atoms have less neighbors than bulk
 761 atoms. Assuming that ΔG_D is of the same order of magni-
 762 tude as the activation free energy for viscous flow, ΔG_η , one
 763 can write the kinetic barrier as

$$764 \frac{\Delta G_D(T)}{k_B T} = \frac{C_2}{T_r - T_{or}}, \quad C_2 \equiv \frac{2.30B}{T_m} \cong 30(T_{gr} - T_{or}),$$

$$766 T_{or} \equiv \frac{T_o}{T_m}, \quad T_{gr} \equiv \frac{T_g}{T_m}, \quad (32)$$

767 where T_o and B are the empirical coefficients of the Vogel–
 768 Fulcher–Tammann (VFT) equation and T_g is the glass
 769 transition temperature. The application of the VFT-rela-
 770 tion implies the assumption of a temperature-dependent
 771 activation free energy, ΔG_η . In the definition of C_2 we took
 772 into account the fact that $\Delta G_\eta/(k_B T) \cong 30$ at $T = T_g$.

773 Fig. 12 shows $I_{st}(T_r)$ -curves calculated with Eqs. (1),
 774 (30), and (32), reasonable estimates of the pre-exponential
 775 term and values of the parameters C_1 and C_2 , as indicated
 776 in the figure caption. One can see that the decrease in the
 777 kinetic barrier, caused by a decrease in C_2 at a fixed value
 778 of C_1 , results in a shift of the nucleation rate maximum to
 779 lower temperatures (cf. curves 1–4). The reduced tempera-
 780 ture $T_r \equiv T/T_m = 1/3$ is a lower limit to $T_r^{\max} \equiv T_{\max}/T_m$
 781 obtained when the kinetic barrier tends to zero (cf. curve
 782 5). This shift is accompanied by a strong increase in the
 783 magnitude of $I(T_{\max}) \equiv I_{\max}$. When the thermodynamic
 784 barrier is diminished, at fixed values of C_2 , by decreasing
 785 the parameter C_1 (which is proportional to α_{ST} and the
 786 reduced melting enthalpy $\Delta H'_m = \Delta H_m/RT_m$), the value

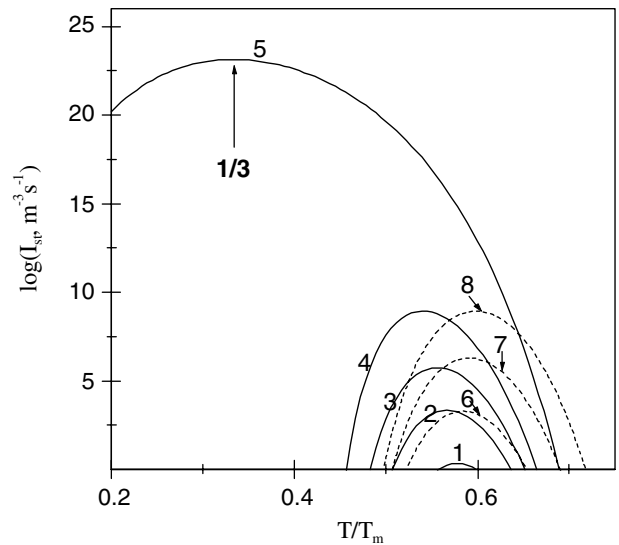


Fig. 12. Temperature dependence of homogeneous nucleation rates. The curves were calculated with Eqs. (1), (30), and (32) with a pre-exponential term $I_o = 10^{42} \text{ m}^{-3} \text{ s}^{-1}$ and following values of the parameters characterizing the temperature independent parts of the thermodynamic (C_1) and kinetic (C_2) barriers: $C_1 = 6.5$ (curves 1–5), 5.8 (curve 6), 5.1 (curve 7), 4.5 (curve 8); $C_2 = 6$ (curves 1 and 6–8), 4.8 (curve 2), 3.9 (curve 3), 2.8 (curve 4), 0 (curve 5).

of I_{\max} also increases (curves 1 and 6–8), but the value of T_{\max} shifts to higher temperatures.

The effect of variation of the kinetic barrier on the nucleation rate can be qualitatively illustrated for lithium disilicate [51] and sodium metasilicate [52] glasses with different H_2O content (a few percent of water often result in a significant decrease of viscosity) as shown in Fig. 13. A decrease in the thermodynamic barrier can be also caused by a decrease in the effective crystal/melt interfacial energy as in the case of heterogeneous nucleation. As a result, as was shown in Ref. [53], the temperature T_{\max} for heterogeneous surface nucleation is displaced to higher values as compared with homogeneous nucleation.

4.3. Correlation between nucleation rate and glass transition temperature

The methods discussed in Section 3 to measure nucleation kinetics are both difficult to perform and time consuming. Also, owing to several restrictions, they cannot always be employed. Hence, the knowledge of any correlation between nucleation rate and easily measurable properties of glasses is highly desirable. As one example, well before the development of nucleation theory for condensed systems, Tammann called attention to the following tendency: the higher the melt viscosity at the melting temperature, the lower is its crystallizability [54].

Almost eighty years after Tammann's pioneering research work, James [55] and Zanotto [56], based on numerous experimental nucleation rate data for several silicate glasses, concluded that glasses having a reduced glass transition temperature, $T_{gr} \equiv T_g/T_m$, higher than ~ 0.58 –

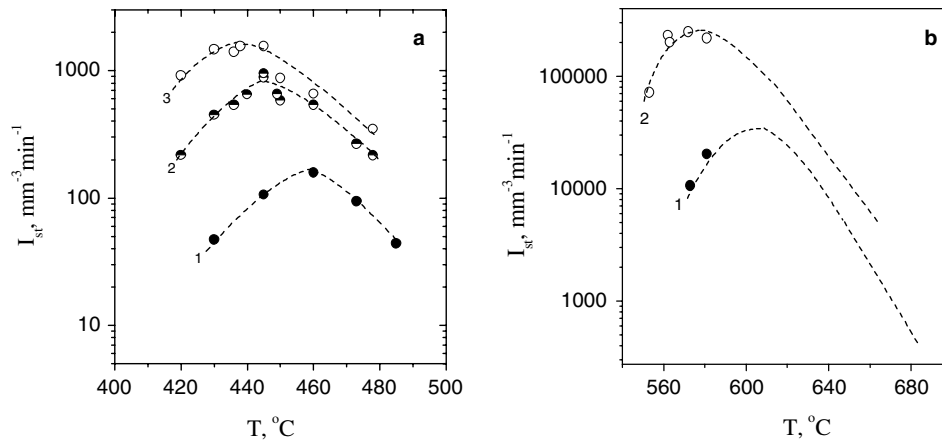


Fig. 13. Temperature dependencies of the steady-state nucleation rates in $\text{Li}_2\text{O} \cdot 2\text{SiO}_2$ [51] (a) and $\text{Na}_2\text{O} \cdot 2\text{CaO} \cdot 3\text{SiO}_2$ [52] (b) glasses containing different amounts of H_2O : (a) 0.05 mol% (curve 1), 0.12 mol% (curve 2), and 0.20 mol% (curve 3); (b) 0.01 mol% (curve 1), 0.2 mol% (curve 2).

817 0.60, display only surface (mostly heterogeneous) crystalliza-
 818 tion; while glasses showing volume (homogeneous) nucleation
 819 have values $T_{gr} < 0.58$ –0.60. Since at temperatures $T < T_m$
 820 the nucleation rate is always positive, the absence of vol-
 821 ume nucleation for glasses having $T_{gr} > 0.60$ merely indi-
 822 cates undetectable nucleation on laboratory time/size
 823 scales. Hence, an increase in the nucleation rate with
 824 decreasing T_{gr} could be expected. Indeed, a drastic increase
 825 of the magnitude of I_{max} with decreasing T_{gr} has been dem-
 826 onstrated by Deubener [57]. Fig. 14 presents a plot of the
 827 $I_{max}(T_{gr})$ -dependence, which has been extended in Ref.
 828 [58] and in the present work. In a relatively narrow range
 829 of T_{gr} (from 0.47 to 0.58) shown by 55 glasses of stoichiomet-
 830 ric and non-stoichiometric compositions, belonging to
 831 eight different silicate systems, the nucleation rates drop by
 832 about 17 orders of magnitude! When T_{gr} increases, the

kinetic inhibition of nucleation proceeds at higher temper- 833
 atures and at higher values of the thermodynamic barrier 834
 due to lower values of the thermodynamic driving force. 835
 As a consequence, nucleation becomes practically unde- 836
 tectable at $T_{gr} > 0.58$. This result confirms the findings of 837
 James [55] and Zanotto [56]. The lines in Fig. 14 are calcu- 838
 lated from CNT (Eqs. (1), (30), and (32)) with reasonable 839
 values of the parameters C_1 and C_2 indicated in the figure 840
 caption. Remember that C_1 and C_2 characterize the temper- 841
 ature independent parts of the thermodynamic and kinetic 842
 barriers for nucleation, respectively. Since Eq. (32) 843
 contains two independent parameters C_2 and T_{or} , the vis- 844
 cosity and, correspondingly, T_{gr} , was varied in two differ- 845
 ent ways, by keeping either C_2 (solid line) or T_{or} (dashed line) 846
 fixed. In the most interesting temperature range 847
 ($0.5 < T_r < 0.6$) these different ways of varying T_{gr} lead 848
 to similar results. The lines reflect correctly the experimentally 849
 observed general trend. However, in applying the men- 850
 tioned rule to particular systems one has to act with some 851
 precaution since a substantial variation of the thermody- 852
 namic barrier can result in a considerable variation of I_{max} 853
 for glasses having similar values of T_{gr} . For instance, fres- 854
 noite ($2\text{BaO} \cdot \text{TiO}_2 \cdot 2\text{SiO}_2$) and wollastonite ($\text{CaO} \cdot \text{SiO}_2$) 855
 glasses have T_{gr} about 0.57, while the values of the param- 856
 eter α_{ST} are 0.4 and 0.6, respectively. The latter fact leads to 857
 a strong difference in the values of the thermodynamic bar- 858
 riers and correspondingly to a strong difference in I_{max} . 859
 Also nucleation of metastable phases, such as $\text{BaO} \cdot 2\text{SiO}_2$, 860
 is possible as shown in Ref. [59]. 861

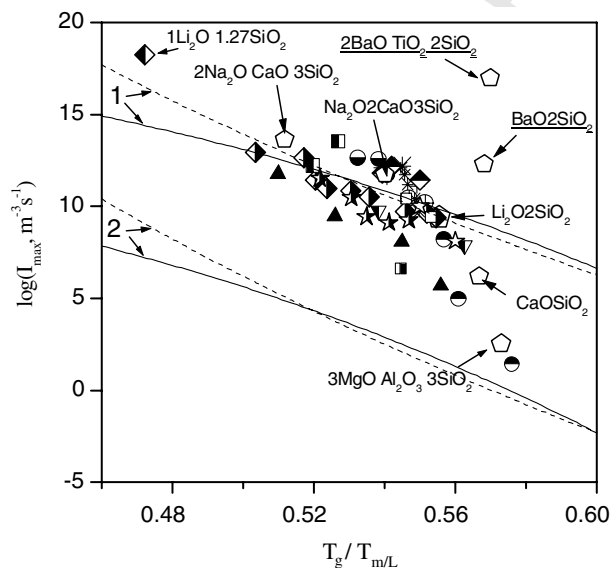


Fig. 14. Maximum nucleation rate as a function of reduced glass transition temperature for 55 silicate glasses. The lines are calculated from CNT with $C_1 = 4.5$ (curve 1) and 6.5 (curve 2). Solid lines refer to $C_2 = 4.5$ and $T_{or} = T_{gr} - C_2/30$; dashed lines to $T_{or} = 0.4$ [58].

An important parameter is the location of T_{max} . It is 862
 commonly accepted that T_{max} is close to T_g . However, it 863
 was shown in Ref. [58] that the ratio T_{max}/T_g depends on 864
 T_{gr} . T_{max}/T_g is higher than one (i.e., T_{max} exceeds T_g) at 865
 low T_{gr} , approaches one at about $T_{gr} \sim 0.55$, and then 866
 becomes smaller than one. This trend results in an addi- 867
 tional increase of the kinetic barrier at T_{max} with increasing 868
 T_{gr} caused by the increase of $\eta(T_{max})$. 869

Computations of $I_{st}(T)$ temperature dependencies simi- 870
 lar to those published in Ref. [58] and presented here were 871

872 performed by Turnbull in the 1960s (see, e.g., Ref. [60]).
 873 However, at that time, with the exception of the measure-
 874 ments of Tammann [61] and Mikhnevich [62] for organic
 875 liquids, nucleation rate data were not available in wide
 876 temperature ranges including T_{\max} . In order to verify the
 877 existence of a correlation between I_{\max} and T_{gr} , as pro-
 878 posed here, an abundance of experimental points must be
 879 available. This is now the case (cf. Fig. 14).

880 5. Nucleation rate data and CNT: some serious problems

881 5.1. Different approaches for the interpretation of 882 experimental data by CNT

883 As shown in the previous sections, in its original form
 884 CNT provides a good qualitative description of nucleation
 885 rate data for silicate glasses, however, serious problems
 886 arise when one tries to employ this theory for a quantita-
 887 tive interpretation of experimental data.

888 If one uses the Stokes–Einstein equation to connect the
 889 kinetic barrier of nucleation with the glass viscosity one can
 890 rewrite Eq. (1) for the steady-state nucleation rate as
 891

$$893 I_{\text{st}} = K_{\eta} \frac{1}{\eta} \exp\left(-\frac{W^*}{k_B T}\right), \quad K_{\eta} = I_o \frac{h}{4l^3}, \quad (33)$$

894 where the size parameter l has the order of the Si–O bond
 895 length. Hereby, the diffusivity across the crystal/liquid
 896 interface is replaced by the volume diffusivity.

897 The use of the Stokes–Einstein equation in Eq. (33) can
 898 be avoided if one estimates the kinetic barrier from the
 899 nucleation time-lag. In this case, Eq. (1) takes the following
 900 form:
 901

$$903 I_{\text{st}} = K_{\tau} \frac{1}{\Delta G_V^2 t_{\text{ind}}} \exp\left(-\frac{W^*}{k_B T}\right), \quad K_{\tau} = I_o \frac{8h\sigma_{\text{cm}}}{3a^4}. \quad (34)$$

904 In the analysis of crystallization kinetics in glass-forming
 905 systems, it is commonly accepted – in accordance with
 906 CNT and Gibbs' classical description of heterogeneous sys-
 907 tems – to use the properties of the newly evolving macro-
 908 phase as reference states for the description of the bulk
 909 properties of the critical nucleus. Additionally one has to
 910 properly specify the value of the specific interfacial energy,
 911 σ_{cm} . Since measurements of the interfacial energy of the
 912 crystals in their own melt are confronted with serious diffi-
 913 culties, one usually employs the easily measurable thermo-
 914 dynamic driving force for crystallization of the macro-
 915 phase for the determination of the work of critical cluster
 916 formation. Hereby, σ_{cm} is commonly taken as a fit param-
 917 eter and is treated, to a first approximation, as a size-inde-
 918 pendent (capillarity approximation) and temperature
 919 independent quantity. The respective values of σ_{cm} are de-
 920 noted in Tables 1 and 2 as σ_{cm}^* . These approximations allow
 921 one to estimate both the magnitude of the pre-exponential
 922 term, I_o , in Eq. (1) and the value of crystal-melt surface en-
 923 ergy, σ_{cm} , from a fit of experimental data (I_{st} , η , or t_{ind}).
 924 According to Eqs. (33), (34), and (4), $\ln(I_{\text{st}}\eta)$ and

Table 1

Ratio of experimental and theoretical pre-exponential, and surface energy values calculated by CNT for different glasses [40]

Glass	$\Delta C_p = 0$		$\Delta C_p = f(T)$	
	$\log(I_o^{\text{exp}}/I_o^{\text{theo}})$	σ_{cm}^*	$\log(I_o^{\text{exp}}/I_o^{\text{theo}})$	σ_{cm}^*
$\text{Li}_2\text{O} \cdot 2\text{SiO}_2$	15	0.19	19	0.20
$\text{Na}_2\text{O} \cdot 2\text{CaO} \cdot 3\text{SiO}_2$	18	0.17	72	0.19
$2\text{Na}_2\text{O} \cdot \text{CaO} \cdot 3\text{SiO}_2$	27	0.15	139	0.17

The specific interfacial energy is given in J m^{-2} .

Table 2

Liquid–crystal surface energies (in J m^{-2}) calculated from nucleation and growth data [69]

Glass	σ_{cm}	σ_{cm}^*	σ_{cm}^{**}	K	σ_{cm}^r
$\text{Li}_2\text{O} \cdot 2\text{SiO}_2$	1.4	0.20	0.152–0.156 (450 °C < T < 485 °C)	0.19–0.23	0.050–0.060
$\text{Na}_2\text{O} \cdot 2\text{CaO} \cdot 3\text{SiO}_2$	1.5	0.18	0.099–0.110 (580 °C < T < 685 °C)	0.13	0.026

925 $\ln(I_{\text{st}} t_{\text{ind}} \Delta G_V^2)$ versus $1/(T \Delta G_V^2)$ plots should yield straight
 926 lines. Their intercepts and slopes can be employed to evalu-
 927 ate I_o and σ_{cm}^* , respectively. However, these approxima-
 928 tions lead to the following problems:

- (i) The use of Eq. (33) [55,63] and Eq. (34) [64] leads to
 929 drastic discrepancies between the experimental, I_o^{exp} ,
 930 and theoretical, I_o^{theo} , values of the pre-exponential
 931 factor. This discrepancy was first observed for crystal
 932 nucleation in undercooled Ga [65] and Hg [66]. In
 933 order to illustrate this issue, Table 1 shows the
 934 $(I_o^{\text{exp}}/I_o^{\text{theo}})$ -ratio, and surface energy values for some
 935 stoichiometric silicate glasses calculated from
 936 $\ln(I_{\text{st}} t_{\text{ind}} \Delta G_V^2)$ versus $1/(T \Delta G_V^2)$ plots for temperatures
 937 above the glass transition range. To trace these plots,
 938 both the linear (Turnbull) approximation (Eq. (6))
 939 and the experimental values (Eq. (5)) of the thermo-
 940 dynamic driving force for crystallization of the stable
 941 macro-phases were used. The discrepancy between
 942 theory and experiment is strongly affected by the
 943 choice of ΔG_V (see also Appendix A, where an anal-
 944 ysis similar to that given in Ref. [13] is performed).
 945 The experimental values of ΔG_V are close to Turn-
 946 bull's approximation in the case of $\text{Li}_2\text{O} \cdot 2\text{SiO}_2$ glass,
 947 and to Hoffman's approximation in the case of
 948 $2\text{Na}_2\text{O} \cdot 1\text{CaO} \cdot 3\text{SiO}_2$ glass. These equations normally
 949 bound the experimental values of ΔG_V [13], and the
 950 $(I_o^{\text{exp}}/I_o^{\text{theo}})$ -ratio increases as one passes from Turn-
 951 bull's to Hoffman's approximation. However, inde-
 952 pendently of the particular choice of the expression
 953 of the thermodynamic driving force, i.e., with any
 954 reasonable approximation or with experimental val-
 955 ues of ΔG_V , the mentioned discrepancy remains quite
 956 large.
 957

(ii) The values of the surface energy, σ_{cm} , calculated as described above (in the deeply undercooled regime close to T_g), are lower than the melt–vapor surface energy, σ_{mv} , which can be measured directly [67,68] (above the equilibrium melting point) by a factor of about 0.5–0.6. These values must then be corrected since σ_{cm} refers to nuclei of critical size, r_* , while σ_{mv} refers to planar melt/vapor interfaces. In the case of lithium disilicate glass, for instance, corrections made with the Tolman equation, Eq. (35), for the size effect, increase this factor to 0.8 [69]. Such high values of σ_{cm} , as compared with σ_{mv} , strongly overestimate its real magnitude. Indeed, according to Stefan’s rule [70], one would expect the ratio $\sigma_{\text{cm}}/\sigma_{\text{mv}}$ to be approximately equal to $\sigma_{\text{cm}}/\sigma_{\text{mv}} \cong \Delta H_{\text{cm}}/\Delta H_{\text{mv}} \ll 1$, where $\Delta H_{\text{cm}} \equiv \Delta H_m$ and ΔH_{mv} are the melting enthalpy of the crystalline phase and enthalpy of evaporation, respectively.

It follows that the widespread believe – the driving force of critical cluster formation can be determined correctly via the classical Gibbs’ approach and all necessary corrections have to be incorporated into the theoretical description via the introduction of appropriate values of the specific interfacial energy – is challenged by above given analysis and has to be reconsidered. In the following sections, possible reasons for the failure of CNT in application to a quantitative description of nucleation experiments will be analyzed in detail.

5.2. Temperature and size-dependence of the nucleus/liquid specific surface energy

The discrepancy between experimental and theoretical values of I_0 can be avoided if one calculates σ_{cm} from nucleation data (I_{st} and t_{ind} or η) employing the theoretical expression for I_0 . This procedure slightly decreases the values of σ_{cm} and leads to a weak increase of σ_{cm} with increasing temperature [71] ($d\sigma/dT \sim (0.06\text{--}0.16) \times 10^{-3} \text{ J/m}^2 \text{ K}$) regardless of the way of estimating the kinetic barrier. As far as we know, Turnbull [66] was the first to draw attention to this fact. At a first sight such kind of temperature dependence of σ_{cm} (i.e., an increase of the surface tension with increasing temperature obtained via the mentioned treatment of nucleation experiments) is in conflict with the theoretical expectations of most, but not all, authors (see the discussion below). Commonly the opinion is favored that, from a thermodynamic point of view, a decrease of σ_{cm} (for planar interfaces (σ_∞)) with temperature should be expected [72–74], at least, in the temperature range where crystallization processes may occur [74]. It follows that we are confronted here with a contradiction between the discussed interpretation of experimental results and general theoretical expectations.

As will be shown now this contradiction can be partly removed by taking into account a possible curvature (or nucleus size) dependence of the surface energy. Recall that

the specific surface energy estimated from nucleation rate data refers to nuclei of critical size. Curvature corrections are expected to reduce the effective value of the surface energy. When the critical nucleus size increases with increasing temperature, the effect of curvature corrections decreases (see Eq. (35)), leading to higher effective values of the surface energy.

To a first approximation, Tolman’s equation (that was originally derived for a liquid drop in equilibrium with its vapor) can be used to decouple these size and temperature effects. The Tolman equation reads

$$\sigma(r_*) = \frac{\sigma_\infty}{\left(1 + \frac{2\delta}{r_*}\right)}, \quad (35)$$

where the Tolman parameter δ is a measure of the (unknown) width of the interfacial region between the coexisting phases.

Employing this relation, the work of formation of a spherical critical nucleus may be written as

$$W_* = \frac{16\pi}{3} \frac{\sigma_\infty^3}{\left(1 + \frac{2\delta}{r_*}\right)^3 \Delta G_V^2}, \quad (36)$$

where

$$r_* = \frac{2\sigma_\infty}{\Delta G_V} - 2\delta \quad (37)$$

holds.

Fig. 15 shows the average values of $(d\sigma_\infty/dT)$ at $T \geq T_g$ versus the Tolman parameter. Using experimental nucleation data for $\text{Li}_2\text{O} \cdot 2\text{SiO}_2$ glass, fits of σ_∞ have been performed for different values of δ employing Eq. (34). For this glass, as δ increases $(d\sigma_\infty/dT)$ progressively decreases and becomes negative for $\delta > 2.4 \times 10^{-10} \text{ m}$. Thus, reasonable values of the Tolman parameter may be chosen such that σ_∞ decreases with increasing temperature, in line with

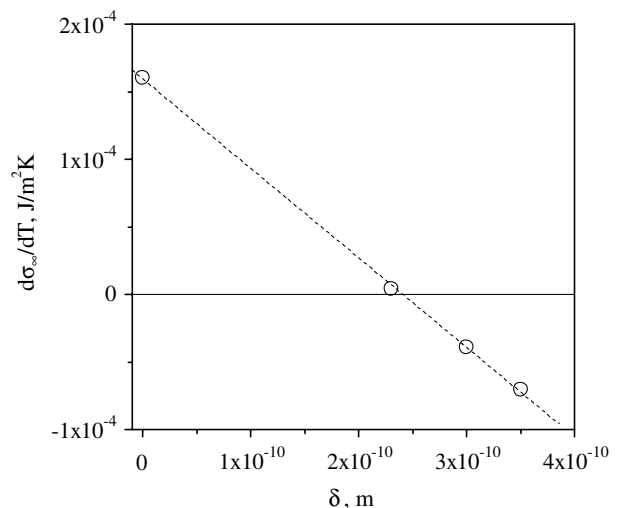


Fig. 15. $(d\sigma_\infty/dT)$ versus Tolman’s parameter for $\text{Li}_2\text{O} \cdot 2\text{SiO}_2$ crystals in a glass of the same composition. The kinetic barrier for nucleation was estimated from the nucleation time-lag.

1046 the theoretical predictions of Refs. [72,73]. Similar results
1047 were obtained for a $\text{Na}_2\text{O}\cdot 2\text{CaO}\cdot 3\text{SiO}_2$ glass [71].

1048 For completeness of the discussion, we would like to
1049 mention also another interpretation of the increase of σ_{cm}
1050 with increasing temperature widely discussed in Ref. [75].
1051 The argumentation is based on model considerations sup-
1052 posing an increased ordering of the liquid near the crystal.
1053 These ideas were expressed first by Turnbull [66] and result
1054 in an entropy decrease. Employing some plausible assump-
1055 tions, the positive temperature coefficient of σ_{cm} can be
1056 accounted for then by the mentioned entropy loss. Run-
1057 ning ahead we could also suppose that the temperature
1058 dependence of σ_{cm} is the result of a possible change of
1059 the critical nucleus composition and/or structure with its
1060 size.

1061 However, regardless of the above possible interpretations
1062 the values of the specific surface energy estimated from
1063 nucleation rate data in the framework of the classical Gibbs'
1064 approach remain too high when compared with the respective
1065 melt–vapor surface energies. Consequently, the problem
1066 posed at the end of the preceding section remains unsolved
1067 by these considerations.

1068 5.3. Estimation of crystalliquid specific surface energies 1069 via dissolution of subcritical nuclei

1070 Essentially all known methods to determine the nucleus-
1071 undercooled liquid surface energy are based on nucleation
1072 experiments involving certain additional assumptions.
1073 However, in order to test the classical nucleation theory
1074 or to make theoretical predictions, independent estimates
1075 of the specific surface energy are required. Such an inde-
1076 pendent method of estimating σ_{cm} for clusters of near-crit-
1077 ical sizes has been developed recently [69]. The results are
1078 summarized below.

1079 The new method is based on the dissolution phenome-
1080 non (discussed in Sections 3 and 4) of subcritical nuclei
1081 with an increase in temperature. As we already have
1082 shown, an $N(T_n, r_*(T_n), t)$ -plot coincides with the
1083 $N(T_n, r_*(T_d), t)$ -plot, with the only difference that the latter
1084 is shifted along the time-axis by a time t_o (Eq. (27)). Then,
1085 kinetic $N(T_n, t)$ -curves obtained with different development
1086 temperatures T_{d1} and $T_{d2} > T_{d1}$ should be shifted with
1087 respect to each other by a time $\Delta t_o = t_{o2} - t_{o1}$. Fig. 5 shows
1088 an example of such kinetic curves. The following equation:
1089

$$1091 \Delta t_o = \int_{r_*(T_{d1})}^{r_*(T_{d2})} \frac{dr}{U(T_n, r)} = \frac{1}{U(T_n, \infty)} [r_*(T_{d2}) - r_*(T_{d1}) + r_*(T_n) \ln \left(\frac{r_*(T_{d2}) - r_*(T_n)}{r_*(T_{d1}) - r_*(T_n)} \right)] \quad (38)$$

1092 was derived in Ref. [38] to estimate this shift. In the deriva-
1093 tion of Eq. (38) a size-dependent crystal growth velocity
1094 [76] was used of the form

$$1095 U(T, r) = U(T, \infty) \left[1 - \frac{r_*(T)}{r} \right]. \quad (39)$$

Employing Eq. (3) for the critical nucleus size and assum-
ing that σ_{cm} depends only slightly on temperature, Eq.
(38) can be rewritten as

$$1100 \sigma_{\text{cm}} = \frac{1}{2} \frac{\Delta t_o U(T_n, \infty)}{\left[\frac{1}{\Delta G_V(T_{d2})} - \frac{1}{\Delta G_V(T_{d1})} + \frac{1}{\Delta G_V(T_n)} \ln \left[\frac{\frac{\Delta G_V(T_{d2})}{\Delta G_V(T_{d1})} \frac{\Delta G_V(T_n)}{\Delta G_V(T_n)}}{\frac{\Delta G_V(T_{d1})}{\Delta G_V(T_n)}} \right] \right]}. \quad (40) \quad 1103$$

1104 Hence, it is possible to calculate the average value of σ_{cm} in
1105 the temperature range $T_n - T_{d2}$ from experimental values of
1106 Δt_o , $U(T_n, \infty)$ and ΔG_V . Note that in doing so neither nucle-
1107 ation rate nor time-lag data are required. The values of σ_{cm}
1108 calculated by this method for $\text{Li}_2\text{O}\cdot 2\text{SiO}_2$ and $\text{Na}_2\text{O}\cdot 2\text{-}$
1109 $\text{CaO}\cdot 3\text{SiO}_2$ glasses are collected in Table 2, which also
1110 shows values estimated with the assumption of a size and
1111 temperature independent specific surface energy, σ_{cm}^* (see
1112 also Table 1) and σ_{cm}^{**} employing the theoretical values of
1113 I_o . The values of σ_{cm} calculated via Eq. (40) significantly
1114 exceed the corresponding values calculated from a fit of
1115 nucleation rate data to CNT (σ_{cm}^* , σ_{cm}^{**}). According to
1116 CNT such high values of σ_{cm} lead to vanishing nucleation
1117 rates. However, nucleation processes do occur and are in-
1118 deed observed in deeply undercooled glasses!

1119 In order to find out the origin of this discrepancy, one
1120 should realize that the methods discussed above do not
1121 provide us with the surface energy directly, but instead only
1122 give its combination with the thermodynamic driving force.
1123 In particular, σ_{cm} is calculated from the measured values of
1124 Δt_o and $U(T_n, \infty)$ via (see Eq. (40))

$$1125 \Delta t_o = \frac{2}{U} \sigma_{\text{cm}} f \left(\frac{1}{\Delta G_V} \right) \quad (41) \quad 1127$$

and σ_{cm}^{**} (as well as σ_{cm}^*) from the thermodynamic barrier
for nucleation

$$1128 W_* \sim \frac{(\sigma_{\text{cm}}^{**})^3}{\Delta G_V^2}. \quad (42) \quad 1130$$

1131 One should recall again that, in line with Gibbs' thermo-
1132 dynamic description of heterogeneous systems, the thermo-
1133 dynamic driving force for crystallization of macro-crystals
1134 has been used to estimate the surface energy of critical and
1135 near-critical nuclei. Provided, this assumption is correct
1136 then we obtain correct values of the specific interfacial
1137 energy. However, if this assumption occurs to be incorrect
1138 then also the estimates of the surface energy are not cor-
1139 rect. In such case, in order to arrive at correct values of
1140 the work of critical cluster formation for nucleation, the
1141 value of the surface energy has to be chosen appropriately
1142 becoming merely a fit parameter. Hence, the above dis-
1143 crepancy may result from the difference between
1144 the macroscopic values of the thermodynamic driving
1145 force, ΔG_∞ , employed and the correct driving force of crit-
1146 ical cluster formation and growth, ΔG_V , which is deter-
1147 mined by the real physical state of the critical and near-
1148 critical clusters. Since the identity of the driving force of
1149 critical cluster formation with the respective macroscopic
1150

values is the only assumption employed in the analysis it has to be removed in order to solve the discussed in this and earlier sections discrepancies. Then we have to admit that the bulk properties of critical and near-critical clusters do not coincide with the properties of the respective macroscopic phases and are not determined correctly employing Gibbs' classical thermodynamic approach. As a direct consequence from this assumption, it follows that both surface energy and thermodynamic driving force must be considered as unknown quantities.

Let us analyze now the above mentioned results introducing a coefficient $K(r)$ that connects the (supposed) real thermodynamic driving force, ΔG_V , with the respective value for the macro-phase, ΔG_∞ , as

$$\Delta G_V = K(r)\Delta G_\infty. \quad (43)$$

The coefficient $K(r)$ reflects the fact that the thermodynamic driving force for critical nuclei may differ from that of the corresponding macro-phase. If one denotes by σ_{cm}^r the true value of the surface energy estimated with account of Eq. (43) and takes into consideration that $U \sim \Delta G_V$, the following equations connecting σ_{cm}^r with σ_{cm} and σ_{cm}^{**} are obtained from Eqs. (41) and (42)

$$\sigma_{cm}^r = K(r)^2 \sigma_{cm}, \quad \sigma_{cm}^r = K(r)^{2/3} \sigma_{cm}^{**}. \quad (44)$$

Eq. (44) yield

$$K = \left(\frac{\sigma_{cm}^{**}}{\sigma_{cm}} \right)^{2/3}. \quad (45)$$

Thus, both methods provide the same value of crystal/melt surface energy if the reduced thermodynamic driving force, $\Delta G_V = K(r)\Delta G_\infty$, is employed. The values of K presented in Table 2 show a considerable reduction of the thermodynamic driving force for nucleation and growth of critical and near-critical nuclei as compared with that for the macro-crystal growth ($K < 1$). Employing this self-consistently determined value of the driving force, different estimates for the specific surface energy are obtained as compared with the case when the classical Gibbs' approach for the determination of the driving force is used. It should be emphasized that the value of σ_{cm}^r (see Table 2) is smaller than that of σ_{cm}^* and σ_{cm}^{**} . Hence, in this way, the decrease of the thermodynamic driving force results in values of the interfacial energy that are significantly more reasonable (taking Stefan's rule into account). We can conclude, consequently, that the discussed so far grave problems in the theoretical interpretation of crystallization can be removed if one assumes that the state of critical and near-critical clusters is different from the state of the newly evolving macro-phase. That is the classical Gibbs' approach does not give, consequently, in general a correct description of the bulk properties of critical and near-critical clusters.

Arriving at such conclusion, two classes of problems arise: First, one has to discuss whether there exist alternative theoretical concepts favoring this point of view or not

and whether it is possible to generalize eventually Gibbs' approach in order to remove mentioned defect in Gibbs' classical treatment. Second, one has to search for the physical origin of such differences in the state of the critical clusters as compared with the respective bulk phases and for additional arguments and experimental results confirming such point of view. Such analysis will be performed in the subsequent sections.

5.4. Bulk properties of critical clusters and properties of the newly evolving macroscopic phase: some results of theoretical analyses

5.4.1. Gibbs' theory of heterogeneous systems: basic postulates, advantages and shortcomings

In the theoretical interpretation of experimental results on the dynamics of first-order phase transitions starting from metastable initial states, up to now the classical nucleation theory has been predominantly employed treating the respective process in terms of cluster formation and growth and employing Gibbs' theory of capillarity. This preference is due to the advantage of Gibbs' approach to the description of thermodynamically heterogeneous systems allowing one to determine the parameters of the critical clusters and the work of critical cluster formation in the nucleation rate expression in a relatively simple way which is based on the knowledge of macroscopic bulk and surface properties of the ambient and newly evolving phases.

In his classical analysis [4], Gibbs describes heterogeneous systems (in application to the problems under consideration, we discuss a cluster of a newly evolving phase in the ambient phase) via an idealized model system. In this model, the real system is described as consisting of two homogeneous phases divided by a mathematically sharp interface. The thermodynamic characteristics of the system are represented as the sum of the contributions of both homogeneous phases and correction terms, the so-called superficial quantities, which are assigned to the interface. They reflect the diffuseness of the interface in the framework of Gibbs' model approach. In contrast to alternative statements [77,78] we believe that such approach is theoretically well-founded and correct provided one is able to determine the superficial quantities in an appropriate way for any real system.

In order to further develop the theoretical concept attempting to solve this task, Gibbs formulated a fundamental equation for the superficial (or interfacial) thermodynamic parameters (specified by the subscript σ) which is widely similar to the fundamental equation for homogeneous bulk phases. For spherical interfaces we restrict our considerations to, it reads [4]

$$dU_\sigma = T_\sigma dS_\sigma + \sum \mu_{i\sigma} dn_{i\sigma} + \sigma dA + C dc, \quad (46)$$

where U is the internal energy, S the entropy, T the temperature, μ_i the chemical potential, n_i the number of particles or moles of the different components ($i = 1, 2, \dots, k$), σ the surface or interfacial tension, A the surface area, and

1263 $c = (1/R)$ the curvature of the considered surface element,
 1264 while C is a thermodynamic parameter determining the
 1265 magnitude of changes of the internal energy with variations
 1266 of the curvature of the considered surface element. R is the
 1267 radius of curvature of the considered surface element.

1268 An integration of this equation results in

$$1271 U_{\sigma} = T_{\sigma} S_{\sigma} + \sum \mu_{i\sigma} n_{i\sigma} + \sigma A. \quad (47)$$

1272 A combination of both equations yield the Gibbs adsorp-
 1273 tion equation in the general form

$$1276 S_{\sigma} dT_{\sigma} + \sum n_{i\sigma} d\mu_{i\sigma} + A d\sigma = C dc. \quad (48)$$

1277 In order to assign well-defined values to the superficial
 1278 quantities and cluster size, as an essential requirement of
 1279 Gibbs' theory the location of the dividing surface has to
 1280 be specified. In application to nucleation processes, usually
 1281 the surface of tension is employed. It is defined, utilizing
 1282 Gibbs' fundamental equation for the superficial quantities,
 1283 via the equation $C = 0$. For this particular dividing surface,
 1284 the surface tension does not depend explicitly on the curva-
 1285 ture. Moreover, it follows that in the classical Gibbs'
 1286 approach the surface tension depends on $(k + 1)$ indepen-
 1287 dent state variables.

1288 With Eq. (47) and the well-known expressions for the
 1289 internal energy of homogeneous bulk phases, we get the
 1290 following expression for the internal energy of the whole
 1291 system (e.g., [79–81])

$$1294 U = T_{\alpha} S_{\alpha} - p_{\alpha} V_{\alpha} + \sum \mu_{i\alpha} n_{i\alpha} + T_{\beta} S_{\beta} - p_{\beta} V_{\beta} \\ + \sum \mu_{i\beta} n_{i\beta} + T_{\sigma} S_{\sigma} + \sum \mu_{i\sigma} n_{i\sigma} + \sigma A. \quad (49)$$

1295 Here p is the pressure, V the volume, the subscript α spec-
 1296 ifies the parameters of the cluster phase, the subscript β re-
 1297 fers to the parameters of the ambient phase.

1298 In application to nucleation, the state of the ambient
 1299 phase is known. In this way, in order to employ Gibbs' the-
 1300 ory, the bulk state of the cluster phase has to be specified.
 1301 This procedure is performed in Gibbs' classical treatment
 1302 for *equilibrium states of heterogeneous substances*, exclu-
 1303 sively (the title of his paper, Ref. [4], is 'On the equilibrium
 1304 of heterogeneous substances'), a cluster of critical size in
 1305 the ambient phase being a particular realization of a ther-
 1306 modynamic equilibrium state. By employing the general
 1307 conditions for thermodynamic equilibrium [4], two of the
 1308 three basic sets of the equilibrium conditions are obtained

$$1311 T_{\alpha} = T_{\beta} = T_{\sigma}, \quad \mu_{i\alpha} = \mu_{i\beta} = \mu_{i\sigma}, \quad i = 1, 2, \dots, k, \quad (50)$$

1312 allowing one to uniquely determine the state parameters of
 1313 the cluster phase from the knowledge of the state of the
 1314 ambient phase.

1315 The bulk properties of the critical clusters of the newly
 1316 evolving phase are determined, consequently, in Gibbs'
 1317 approach uniquely via the equilibrium conditions Eq.
 1318 (50) for temperature and chemical potentials of the differ-
 1319 ent components in the two coexisting bulk phases. Hereby
 1320 the question is not posed whether or not these state param-
 1321 eters represent a correct description of the bulk state

parameters of the cluster. It is commonly believed that this
 is the case. However, Gibbs himself made a comment that,
 in general, the properties of the critical clusters may differ
 from the predictions obtained in his approach. It follows
 further from the Gibbs method that, for the critical clus-
 ters, the interfacial tension referred to the surface of ten-
 sion is uniquely determined by the state parameters of
 either the ambient or the cluster phase (cf. Eqs. (48) and
 (50)). Consequently, once the parameters of the ambient
 phase are given, the surface tension does not depend –
 according to Gibbs' classical method – on the state param-
 eters of the cluster phase. Moreover, the superficial temper-
 ature and chemical potentials are determined by the
 respective parameters of the bulk phases as well.

As it turns out [80–82], Gibbs' method leads to state
 parameters of the critical cluster's bulk phase which are
 widely identical, at least, in application to phase formation
 in condensed phases, to the properties of the newly evol-
 ving macroscopic phases. Modifications of these properties,
 due to differences in the pressure of small clusters as com-
 pared with the equilibrium coexistence of both phases at
 planar interfaces, as given by the Young–Laplace equation
 (the third equilibrium condition),

$$p_{\alpha} - p_{\beta} = \frac{2\sigma}{r_*} \quad (51)$$

is commonly of minor importance here although the pres-
 sure differences may be large. With the numerical estimates
 $p_{\beta} = p_{\text{at}} \sim 10^5 \text{ N/m}^2$, $\sigma \sim 0.1 \text{ J/m}^2$, $r_* \sim 10^{-9} \text{ m}$ (at high
 under-cooling), we get $\Delta p \sim 2 \times 10^8 \text{ Pa}$ or $2000 p_{\text{at}}$. How-
 ever, the effect of pressure on the density is small due to
 the low compressibility of the cluster bulk phase. This re-
 sult – the wide similarity of the properties of the critical
 cluster with the properties of the evolving macroscopic
 phases – is an essential general feature of Gibbs' classical
 theory not only in application to crystallization. It leads
 – as discussed in detail here above – to contradictions in
 the interpretation of experimental results and as we will
 see below to contradictions with the results of computer
 simulations and density functional computations of the
 properties of critical clusters showing a quite different
 behavior, in particular, for higher supersaturations. So,
 why Gibbs' theory can be applied at all to nucleation?
 The following answer can be given.

In application to nucleation, not the knowledge of the
 properties of the critical clusters is commonly of major
 interest but instead the value of the work of critical cluster
 formation, W_* . This quantity is determined in Gibbs'
 description generally via $W_* \propto \sigma^3 / (p_{\alpha} - p_{\beta})^2$ [4] or in a fre-
 quently good approximation via $W_* \propto \sigma^3 / (\Delta G_V)^2$ (cf. Eq.
 (4)). For any state of the ambient phase, the driving force
 of critical cluster formation, which can be considered to
 be proportional to either $(p_{\alpha} - p_{\beta})$ or ΔG_V , is determined
 uniquely via the equilibrium conditions Eq. (50). In this
 way, as far as the process proceeds via nucleation with a
 well-defined value of the work of critical cluster formation,
 one can always find a value of the interfacial tension lead-

ing to the correct result for W_* . Such possibility exists independently on whether the driving force is determined in an appropriate way corresponding to the real situation. In general, the interfacial tension (or the specific interfacial energy in application to formation of crystalline critical nuclei) is different from its macroscopic value. This deviation from the macroscopic value is connected then with the idea of a curvature (or supersaturation) dependence of the surface tension. But in such approach, σ loses its meaning of a physical quantity. As we previously mentioned it becomes a fit parameter that compensates the inappropriate choice of the bulk reference states for the description of the critical clusters.

The failure of Gibbs' classical approach for the determination of the bulk properties of the critical clusters is connected with another disadvantage that has seldom been noticed. This classical approach is in deep conflict with the conventional method of determination of saddle points or extremums of hyper-surfaces of any dimension. In order to find these singular points of such surfaces, following the standard methods, one has to first formulate the respective equations for any arbitrary state of the system and then to apply the extremum conditions. In application to cluster formation, we would have first to formulate the thermodynamic potentials for any well-defined thermodynamic (including non-equilibrium) states of a cluster or ensembles of clusters in the ambient phase and then to search for saddle points. This is the general procedure, which is also employed in any density functional computations of the work of critical cluster formation (see the subsequent discussion).

However, Gibbs never tried in his fundamental paper [4] even to formulate the problem of the determination of the thermodynamic potential of a cluster or ensembles of clusters of non-critical sizes in the otherwise homogeneous ambient phase. His method is, consequently, in conflict with the standard theoretical procedure. It follows as another consequence that Gibbs' original treatment cannot supply one with a recipe to determine the state of sub- and supercritical clusters in a well-founded theoretical way. Any description of cluster growth processes, which is based on Gibbs' theory, involves additional assumptions, which may or may not be appropriate. Consequently, a problem arises whether it is possible to develop a generalisation of Gibbs' thermodynamic treatment allowing one to describe critical cluster formation in a theoretically more founded way and supplying one simultaneously with a regular method of theoretical determination of the properties of sub- and supercritical clusters. However, before developing the respective generalization, we briefly summarize some alternative methods of theoretical description and their results concerning the problems under consideration.

5.4.2. Continuum's approaches to the determination of the properties of heterogeneous systems: van der Waals' and modern density functional approaches

About two decades after the formulation of Gibbs' theory, van der Waals [83,84] developed an alternative contin-

uum's approach to the description of heterogeneous systems. In this approach, the interface is characterized by a continuous change of the intensive thermodynamic state parameters from the respective values in one to those characterizing the other of the coexisting phases. The van der Waals method of description of heterogeneous systems was reinvented about 60 years later by Cahn and Hilliard [85] and applied for the description of the properties of critical clusters in nucleation and for the development of the basic ideas of the classical theory of spinodal decomposition.

In the van der Waals and Cahn–Hilliard approach, the Gibbs free energy of a heterogeneous system is given in the simplest version as

$$G(p, T, x) = \int \left[g(p, T, x(\vec{r})) + \kappa(\nabla x(\vec{r}))^2 \right] dV. \quad (52)$$

For any given concentration profile, the value of the Gibbs free energy can then be found by integrating the volume density, g , of the Gibbs free energy supplemented by the surface term, $\kappa(\nabla x(\vec{r}))^2$, over the whole volume, V , of the system, i.e., any well-defined function, $x(r)$, results in some definite value of the Gibbs free energy. Critical clusters refer to saddle points of the thermodynamic potentials. Consequently, in order to determine the change of the Gibbs free energy in critical cluster formation, one has to search for such concentration or density profiles, for which the respective conditions for a saddle point of the thermodynamic potential G are fulfilled. From a mathematical point of view, the thermodynamic potential is determined, consequently, as a functional of the density or concentration profile giving the name to the method of computation of the work of critical cluster formation (density functional methods; i.e., saddle points are determined via the search for an extremum of the respective functional).

In application to nucleation-growth processes (phase transformations originating from metastable initial states), Cahn and Hilliard came to the conclusion that the bulk state parameters of the critical clusters may deviate considerably from the respective values of the evolving macrophases and, consequently, from the predictions of Gibbs' theory. These results of the van der Waals and Cahn–Hilliard-approach were reconfirmed later-on by more advanced density functional computations (cf., e.g., Refs. [86–88]) allowing one to determine the thermodynamic potential by choosing some well-defined interaction potentials between the particles of the system under consideration. Similar to the van der Waals and Cahn–Hilliard approach, the spatial distribution of the order parameter field is computed and it is assumed that the different phases and their states can be described by varying the value of the order parameters.

As an example, the composition of a critical cluster in phase formation in a binary solution is shown in Fig. 16 [80]. The supersaturation is changed by varying the molar fraction, x , of one of the components in the ambient phase inside the range from the binodal to the spinodal curves,

1434
1435
1436
1437
1438
1439
1440
1441
1442
1443
1444
1445
1446
1447
1448
1449
1450
1451
1452
1453
1454
1455
1456
1457
1458
1459
1460
1461
1462
1463
1464
1465
1466
1467
1468
1469
1470
1471
1472
1473
1474
1475
1476
1477
1478
1479
1480
1481
1482
1483
1484
1485
1486
1487
1488
1489
1490

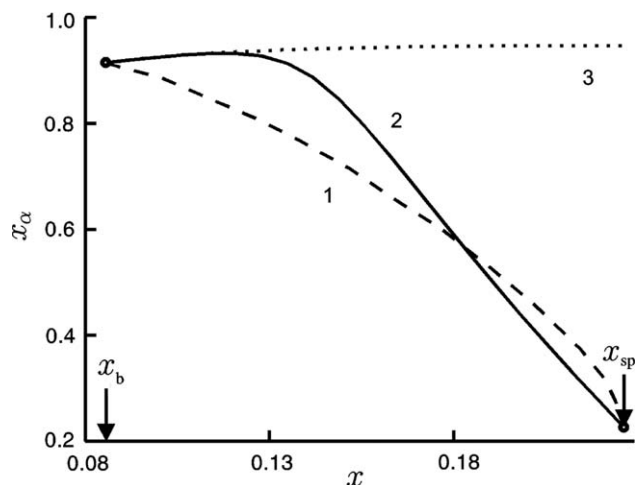


Fig. 16. Composition of the critical cluster, x_{α} , as a function of the supersaturation for segregation processes in solutions [80]. The molar fraction, x , of the segregating component in the ambient solution can be considered as a measure of supersaturation, which varies in the range between the binodal (x_b) and spinodal (x_{sp}) curves. The dotted curve (curve 3) refers to results of computations of the critical cluster parameters obtained via Gibbs' classical method; the dashed curve (curve 1) to the newly developed generalized Gibbs approach and the full curve (curve 2) to results of density functional calculations of the density in the center of the critical cluster obtained via the van der Waals square gradient method.

1491 i.e., for metastable initial states of the ambient phase. The
 1492 results of the classical Gibbs approach to the determination
 1493 of the properties of the critical clusters are given by a dot-
 1494 ted curve (curve 3). It is evident that the composition of the
 1495 critical clusters – determined in such a way – practically
 1496 does not depend on supersaturation and is widely equal
 1497 to the value in the newly evolving macroscopic phase.
 1498 The full curve (curve 2) shows the results for the cluster
 1499 composition in the center of the critical cluster as obtained
 1500 via the van der Waals and Cahn–Hilliard square gradient
 1501 approximation as described by Eq. (52). It is evident that
 1502 both approaches lead, in general, to very different results.
 1503 Qualitatively similar results are obtained when the van
 1504 der Waals and Cahn–Hilliard approach or more advanced
 1505 density functional computations are applied to the descrip-
 1506 tion of crystallization [77,89,90], i.e., the state of the critical
 1507 cluster differs, in general, from the state of the newly evol-
 1508 ving macroscopic phase.

1509 Both Gibbs' and the van der Waals or more advanced
 1510 density functional methods of description of thermody-
 1511 namically heterogeneous systems are considered commonly
 1512 as well-established theories. Nevertheless, only one of them
 1513 (if any) can be correct in the prediction of the properties of
 1514 the critical clusters. Moreover, the Gibbs and van der
 1515 Waals approaches lead to contradicting each other results
 1516 in the description of the behavior of phase separating sys-
 1517 tems in the vicinity of the classical spinodal curve (cf. Ref.
 1518 [91]). In this way, one is confronted here with internal con-
 1519 tradictions in two well-established theories, which must be,
 1520 hopefully, resolved.

1521 The question which of both mentioned theories
 1522 describes more correctly the properties of the critical clus-

1523 ters can be answered from a theoretical point of view based
 1524 on the analysis of the results of computer simulation meth-
 1525 ods of phase formation processes in model systems [92–96].
 1526 The respective analyses show that critical clusters do have
 1527 properties, in general, significantly different from the prop-
 1528 erties of the newly evolving macroscopic phases (although
 1529 in some particular cases also results are obtained which
 1530 are in agreement with the classical Gibbs approach). In this
 1531 way, computer simulation methods support, in general, the
 1532 van der Waals or alternative density functional approaches
 1533 for the description of heterogeneous systems.

1534 Consequently, we can conclude that the majority of exist-
 1535 ing theoretical approaches for the determination of the work
 1536 of critical cluster formation gives strong support to the point
 1537 of view that the state of the critical clusters may significantly
 1538 differ from the state of the newly evolving macroscopic
 1539 phases. Consequently, in order to obtain correct expressions
 1540 for the work of critical cluster formation in the interpreta-
 1541 tion of experimental results one has to account for a cluster
 1542 size dependence not only of the surface properties of the crit-
 1543 ical clusters but also of their bulk properties.

1544 5.4.3. A generalization of Gibbs' classical theory

1545 Having reached such conclusion, immediately the ques-
 1546 tion arises whether it is necessary to abandon the classical
 1547 Gibbs approach at all or whether it is possible to modify it
 1548 in such a way that it retains its advantages (use of macro-
 1549 scopic properties of the phases of interest for a determination
 1550 of the work of critical cluster formation) but overcomes its
 1551 shortcomings (incorrect determination of the bulk proper-
 1552 ties of the critical clusters) discussed above. As it turns out
 1553 such generalization of Gibbs' thermodynamic theory can
 1554 be really performed. It was initiated several years ago based
 1555 initially on a generalization of Ostwald's rule of stages in
 1556 application to nucleation. This generalization of Ostwald's
 1557 rule was formulated as follows [97]: 'Those classes of critical
 1558 clusters determine the process of the transformation, which
 1559 correspond to a minimum work of critical cluster formation
 1560 (as compared with all other possible alternative structures
 1561 and compositions, which may be formed at the given thermo-
 1562 dynamic constraints)'. This concept was then employed in
 1563 order to develop a new approach for the determination of
 1564 the work of critical cluster formation and the determination
 1565 of critical cluster properties based on a generalization of
 1566 Gibbs' classical approach [79,98].

1567 In such a generalization of Gibbs' theory, we followed
 1568 again Gibbs' method of dividing surfaces but started with
 1569 the analysis of the question how to formulate a thermody-
 1570 namic description of heterogeneous systems (clusters or
 1571 ensembles of clusters in the otherwise homogeneous ambi-
 1572 ent phase) for well-defined non-equilibrium states, when
 1573 both the clusters and the ambient phase are in an internal
 1574 thermodynamic equilibrium but the system as a whole is
 1575 not. Having a look at Eq. (49), immediately the question
 1576 arises then, how to determine the values of the superficial
 1577 temperature and chemical potentials for any well-defined
 1578 non-equilibrium states of the heterogeneous systems under

consideration. Since these parameters cannot be determined independently of the parameters of the coexisting bulk phases, we postulated long ago [99] that generally the conditions

$$T_\beta = T_\sigma, \quad \mu_{i\beta} = \mu_{i\sigma}, \quad i = 1, 2, \dots, k, \quad (53)$$

must hold. In other words, it is assumed that the superficial temperature and chemical potentials are determined widely by the properties of the ambient phase (with known properties). *Note that the bulk state parameters of the cluster phase may vary independently and may have so far arbitrary values.* Employing such condition and the fundamental equation for the superficial quantities Eq. (46) as formulated by Gibbs, the interfacial tension (referred to the surface of tension) becomes then a function of the state parameters of the ambient phase exclusively. However, for non-equilibrium states the interfacial tension has to depend, in general, not only on the properties of the ambient but also on all intensive state parameters of the cluster phase. This set of intensive state parameters of the cluster phase we denote here as $\{\varphi_{ix}\}$. In order to be able to describe such additional dependence, Gibbs' fundamental equation Eq. (46) has to be generalized resulting in (see also [79,82] for further details)

$$dU_\sigma = T_\sigma dS_\sigma + \sum \mu_{i\sigma} dn_{i\sigma} + \sigma dA + C dc + \sum \phi_{ix} d\varphi_{ix}, \quad (54)$$

where ϕ_{ix} are parameters determining the magnitude of variations of the superficial internal energy with respect to variations of the bulk state of the cluster phase.

Since all parameters φ_{ix} of the cluster phase, entering Eq. (54), are intensive quantities, the expression for the superficial internal energy Eq. (47) and also for the thermodynamic potentials are formally not changed as compared with Gibbs' original approach. In contrast, the generalized Gibbs' adsorption equation reads now

$$S_\sigma dT_\beta + \sum n_{i\sigma} d\mu_{i\beta} + A d\sigma = C dc + \sum \phi_{ix} d\varphi_{ix}. \quad (55)$$

In the generalization of Gibbs' approach, the interfacial tension can and must be considered consequently as a function both of the intensive state variables of the ambient and the cluster phases and curvature. For the surface of tension (defined also in the generalized Gibbs approach via $C = 0$) an explicit curvature dependence of the surface tension does not occur, again.

Having at ones disposal the thermodynamic potentials for the respective non-equilibrium states, the equilibrium conditions are obtained by known procedures employed already by Gibbs in his classical model approach [4]. They differ from the equilibrium conditions derived by Gibbs and read, in general,

$$r_* = 2\sigma / \left[p_\alpha - p_\beta - \sum \rho_{ix} (\mu_{ix} - \mu_{i\beta}) - s_\alpha (T_\alpha - T_\beta) \right], \quad (56)$$

$$\mu_{ix} - \mu_{i\beta} = (3/r_*) (\partial\sigma / \partial\rho_{ix}), \quad (57)$$

$$T_\alpha - T_\beta = (3/r_*) (\partial\sigma / \partial s_\alpha). \quad (58)$$

Here p is the pressure, ρ the volume density of the ($i = 1, 2, \dots, k$) different components in the system, s is the volume density of the entropy. The subscript α specifies, again, the parameters of the cluster, while β refers to the parameters of the ambient phase.

In order to determine the parameters of the critical clusters, one has to know the values of the surface tension (or the specific interfacial energy). In the simplest case [79,82,98,100], it can be expressed as a quadratic form in the differences of the state parameters of the ambient ($\{\varphi_{i\beta}\}$) and cluster ($\{\varphi_{ix}\}$) phases as

$$\sigma = \sum \sum \Xi_{ij} (\varphi_{ix} - \varphi_{i\beta}) (\varphi_{j\alpha} - \varphi_{j\beta}). \quad (59)$$

The values of the parameters Ξ_{ij} can be determined then from the knowledge of the specific interfacial energy for phase coexistence at planar interfaces.

As it turns out, the work of critical cluster formation can be written generally again in the well-known classical form

$$W_* = \frac{1}{3} \sigma A_*, \quad (60)$$

where A_* is the surface area of the critical cluster. Note however that the results for the numerical values for the work of critical cluster formation are different in both discussed classical and generalized Gibbs' approaches since the state parameters of the clusters differ in these two methods.

In general, the parameters of the critical clusters as obtained via the generalized Gibbs approach differ significantly from the parameters obtained following the classical Gibbs method. However, for phase equilibrium of macroscopic systems, the equilibrium conditions derived in the generalized Gibbs approach coincide with Gibbs' classical expressions (here the radius of the critical clusters tends to infinity and the classical Gibbs equilibrium conditions are obtained as a special case). Note that Gibbs' classical equilibrium conditions are retained in the above given generalized equations also as a limiting case when the derivatives of the interfacial specific energy with respect to the intensive state parameters of the cluster phase are set equal to zero.

Employing the generalized Gibbs' approach to the determination of critical cluster properties for a variety of phase-separating systems (segregation in solutions [80], condensation and boiling in one-component fluids [81], boiling in multi-component fluids [82]) it has been shown that the predictions concerning the properties of critical clusters and the work of critical cluster formation, derived in the generalized Gibbs' approach, are in agreement with van der Waals' and more advanced density functional methods of determination retaining, on the other hand, the simplicity in applications similarly to the classical Gibbs method as an additional advantage. For example, in Fig. 16 the composition of the critical clusters as obtained via the generalized Gibbs approach is shown by a dashed curve (curve 1). For small supersaturations, the results of all mentioned approaches agree, however, when

1688 the whole range of initial supersaturations is considered
1689 and especially for large supersaturations the results of the
1690 generalized Gibbs' approach are similar to the results
1691 obtained via square gradient density functional computa-
1692 tions and deviate significantly from the results of Gibbs'
1693 classical approach. Such kind of behavior is essential in
1694 order to guarantee the vanishing of the surface free energy
1695 and of the work of critical cluster formation near the clas-
1696 sical spinodal curve, two features commonly considered as
1697 essential for a correct description of nucleation and which
1698 are not described by the classical approach when the capil-
1699 larity approximation is utilized [88]. It can be shown fur-
1700 ther in a general way [99] that the classical Gibbs
1701 approach employing in addition the capillarity approxima-
1702 tion as a rule overestimates the work of critical cluster for-
1703 mation and, in general, significantly.

1704 Recently the generalized Gibbs' approach was further
1705 extended [91,101–104] to allow the description not only
1706 of nucleation but also of growth and dissolution processes
1707 taking into account changes of the bulk and surface state
1708 parameters of the clusters as a function of supersaturation
1709 and size. Hereby a criterion was advanced to allow one the
1710 quantitative determination of the changes in the bulk and
1711 surface properties of the clusters in the course of their
1712 growth. As a first application, this new theory of growth
1713 and dissolution processes was applied to the analysis of
1714 segregation in solutions. However, the method is generally
1715 applicable. In the framework of this approach, the change
1716 of a variety of thermodynamic and kinetic properties with
1717 cluster size has been determined for the first time such as
1718 the change of the surface tension, the driving force of clus-
1719 ter growth, the dependence of the effective diffusion coeffi-
1720 cients on cluster size, etc. As it turns out the respective
1721 thermodynamic and kinetic parameters may change signif-
1722 icantly in dependence on cluster size. In this way, the esti-
1723 mates of these parameters obtained from nucleation data
1724 may not be appropriate for the description of growth pro-
1725 cesses of clusters of macroscopic sizes and vice versa. This
1726 result gives a new key to the solution of the problems posed
1727 by Granasy and James [105] that growth rates computed
1728 with values of kinetic coefficients obtained from nucleation
1729 data may lead to deviations between theory and experiment
1730 reaching several orders of magnitude. Even peculiarities in
1731 the evolution of the cluster size distributions – like the
1732 development of bimodal distributions in intermediate
1733 states of the nucleation-growth process and unexpected
1734 properties – may be explained straightforwardly based on
1735 these concepts [102,104,106,107]. Thus, in a correct theo-
1736 retical treatment not only deviations of the composition
1737 of the critical nuclei from those of the respective macro-
1738 scopic phases, but also variations in the composition of
1739 the sub- and supercritical crystals have to be and can be
1740 accounted for.

1741 The extension of these concepts in application to crystal-
1742 lization is in progress. Here, in addition to changes in com-
1743 position and density also possible differences in the
1744 structure of the critical clusters (and their mutual interde-

1745 pendence with concentration fluctuations [12,88,108,109]),
1746 as compared with the state of the crystalline macro-phase,
1747 and its possible change in the course of the growth of the
1748 supercritical crystallites have to be taken into consideration
1749 (cf., e.g., [110–112]).

1750 5.4.4. Discussion

1751 Let us first briefly summarize the results of the preceding
1752 subsection: In order to develop a consistent theoretical
1753 method of determination of the properties of the critical
1754 clusters, we have generalized Gibbs' theory starting with
1755 the thermodynamic description of non-equilibrium states
1756 and including in this way into the theoretical schema the
1757 possibility of description of clusters of sub- and supercriti-
1758 cal sizes in the ambient phase. In order to realize such task,
1759 Gibbs' fundamental equation for the superficial thermody-
1760 namic state parameters was generalized to allow one, in
1761 particular, an incorporation into the theory of the depen-
1762 dence of the interfacial or surface tension both on the state
1763 parameters of the ambient and the newly evolving cluster
1764 phases, respectively. Such essential additional step in the
1765 generalization of Gibbs' classical approach was not done
1766 in earlier own work [99] and also not in the two (to the
1767 knowledge of the authors) existing alternative generaliza-
1768 tions of Gibbs' theory to non-equilibrium states (see
1769 [113]). By this reason, in latter mentioned approaches
1770 [99,113] the equilibrium conditions retain the same form
1771 as in the classical Gibbs' approach.

1772 Following the generalized Gibbs' approach, it is possible
1773 to determine the properties of the critical clusters in a new
1774 way. We arrive at relations, which are, in general, different
1775 as compared with the predictions of the classical Gibbs
1776 approach. The respective results are – for model systems
1777 – in agreement with density functional computations and
1778 results of computer simulations. Moreover, since we have
1779 formulated a consistent description of clusters in thermo-
1780 dynamically non-equilibrium states, regular methods can
1781 be and are developed to determine also the properties of
1782 clusters of sub- and supercritical sizes in dependence on
1783 supersaturation and their sizes. In this way, a new tool
1784 for the description of nucleation-growth processes, in gen-
1785 eral, and crystallization processes in glass-forming liquids,
1786 in particular, has been developed allowing one to interpret
1787 a variety of experimental findings from a new point of view
1788 [91,102–104,111].

1789 As an alternative non-classical method of theoretical
1790 treatment of crystallization going back already to van der
1791 Waals [83,84], the van der Waals and Cahn–Hilliard square
1792 gradient density functional approach is employed presently
1793 intensively for the interpretation of nucleation in crystalli-
1794 zation processes [77,87–89,114]. These studies are supple-
1795 mented by the analysis of nucleation-growth processes
1796 based on so-called phase field models, a dynamic extension
1797 of the van der Waals and Cahn–Hilliard approach
1798 [78,87,115–118], allowing one the determination of the evo-
1799 lution of the order-parameter fields with time. These types
1800 of analyses are confronted, however, with one principal

1801 problem, which has to be taken into consideration – as it
 1802 seems to us – more carefully in future. This problem is
 1803 the prediction – in the framework of mentioned van der
 1804 Waals and Cahn–Hilliard type approaches – of spinodal
 1805 curves in melt-crystallization.

1806 More than three decades ago, Skripov and Baidakov
 1807 [119], based on the analysis of experimental and computer
 1808 simulation data – advanced the conjecture about the non-
 1809 existence of a spinodal curve in one-component melt crys-
 1810 tallization processes (or widely equivalent to them poly-
 1811 morphic transformations where liquid and crystal phases
 1812 have the same composition). It was emphasized that this
 1813 statement is in agreement with the point of view of the
 1814 non-existence of a critical point in liquid–solid phase equi-
 1815 libriums and of a necessarily discontinuous transition
 1816 between liquid and crystal [120]. A further detailed proof
 1817 of this statement in a period of about 30 years resulted in
 1818 a confirmation of its validity [74,121]. An additional sup-
 1819 port of such point of view can be obtained from the anal-
 1820 ysis of experimental data on crystallization processes of
 1821 liquids, in general, and glass-forming melts, in particular.
 1822 Such analysis does not give any indication on the existence
 1823 of spinodal curves in crystallization processes of the con-
 1824 sidered type [12]. The latter conclusion is supported, for
 1825 example, by Oxtoby [87,88] and Granasy and James [77].

1826 However, density functional theories of crystallization
 1827 predict in a variety of cases the existence of spinodal
 1828 curves. Since such kind of behavior is not found by exper-
 1829 iments, parameters are chosen that transfer the spinodal
 1830 into parameter regions, where – due to the high viscosity
 1831 – phase formation processes cannot occur [77,87,122,123].
 1832 A spinodal type behavior is also predicted in some cases
 1833 by Granasy’s so-called diffuse interface theory and even
 1834 close to the glass transition temperature [124]. Provided –
 1835 as we believe – the conjecture of Skripov and Baidakov is
 1836 correct, the prediction of a spinodal in the mentioned the-
 1837 ories leads to some serious doubts into their applicability to
 1838 melt crystallization, at least, in the present form. A theory
 1839 cannot be correct if it predicts – not as an exception but as
 1840 a rule – phenomena, which are absolutely not observed in
 1841 nature. By the above discussed reasons, a further detailed
 1842 analysis of the basic ideas and limitations of density func-
 1843 tional approaches in application to melt crystallization
 1844 seems to be absolutely essential.

1845 Completing the discussion on the limitations of the clas-
 1846 sical Gibbs approach to the description of the properties of
 1847 critical clusters, we would like to add a few comments on
 1848 the so-called ‘nucleation theorem’ [125–128] employed fre-
 1849 quently in order to determine the properties of critical clus-
 1850 ters based on nucleation rate data [88,94,96,129,130]. In an
 1851 approximate form and for one-component systems, the
 1852 content of this theorem can be formulated as [125]

$$1853 \quad dW_*/d\Delta\mu \approx -n_*, \quad (61)$$

1856 i.e., derivatives of the work of critical cluster formation (or
 1857 the steady-state nucleation rate) with respect to the state

1858 parameters of the ambient phase allow one to determine
 1859 the parameters of the critical clusters. Relations of this type
 1860 – derived in the framework of Gibbs’ classical theory and
 1861 employing the capillarity approximation – have been
 1862 known for a long time. The increased interest in dependen-
 1863 cies of such type resulted from the statements by Kashchiev
 1864 [125] that the nucleation theorem is valid independent of
 1865 the method employed for the thermodynamic description
 1866 and valid for any kind of phase transformation and size
 1867 of the critical clusters considered. However, the indepen-
 1868 dence of the mentioned relation on the way of description
 1869 of the clusters is questionable already on general argumen-
 1870 tations. For example, Einstein noted in a conversation with
 1871 Heisenberg on the foundations of quantum mechanics that
 1872 *it is the theory which determines what can be measured*. In a
 1873 detailed analysis of the results of Ref. [125] it has been
 1874 shown recently in detail [127,128] that all above mentioned
 1875 statements concerning Eq. (61) are not correct.

1876 In an extension of the analysis of Ref. [125], Oxtoby and
 1877 Kashchiev developed similar relations in application to
 1878 multi-component systems [126]. In this analysis, Gibbs’
 1879 classical theory of thermodynamically heterogeneous sys-
 1880 tems was employed without introducing any additional
 1881 assumptions like the capillarity approximation, i.e., the
 1882 assumption that the surface tension of critical clusters is
 1883 equal to the respective value for an equilibrium coexistence
 1884 of both phases at planar interfaces. Consequently, the men-
 1885 tioned generalizations of the nucleation theorem are of the
 1886 same level of validity in application to experiment as the
 1887 classical Gibbs approach. They can describe the parameters
 1888 of the real critical clusters correctly only as far as Gibbs’
 1889 classical method is adequate to the considered particular
 1890 situation. Having in mind the above discussed limitations
 1891 of Gibbs’ classical approach in the description of the
 1892 parameters of critical clusters, mentioned generalizations
 1893 of the nucleation theorem do not supply us, in general, with
 1894 a description of the real critical clusters but merely with a
 1895 description of Gibbs’ model clusters resulting in the same
 1896 value of the work of critical cluster formation as for the
 1897 real critical clusters. Consequently, also the correctly
 1898 derived – in the framework of the classical Gibbs’ approach
 1899 – versions of the nucleation theorem do not describe, in
 1900 general, the parameters of the real critical clusters.

1901 Since the generalized Gibbs approach allows one a
 1902 determination of the parameters of the critical clusters, that
 1903 is, for model systems, in agreement with density functional
 1904 computations and computer simulation studies, it is of
 1905 interest to prove whether dependencies similar to the
 1906 ‘nucleation theorem’ can be formulated also in this gener-
 1907 alization of the classical Gibbs approach. The respective
 1908 work is in progress.

1909 Finally, we would like to note that there exist also
 1910 approaches connecting the deviations of the experimental
 1911 data on crystallization and growth with the effect of static
 1912 disorder in the melts [131] or the existence of so-called
 1913 floppy and rigid modes in glasses [132–134].

1914 5.5. Compositional changes of the crystal nuclei at
1915 nucleation-growth process: some experimental findings

1916 The formation of solid solutions is a common phenom-
1917 enon in silicate systems. By this reason, it is important to
1918 keep in mind that the critical nuclei can be a proper solid
1919 solution with thermodynamic properties, which may differ
1920 considerably from those of the finally evolving macroscopic
1921 phase. Thus, we can expect that contradictions between
1922 experimental results and theoretical predictions concerning
1923 nucleation rates and growth kinetics in such systems would
1924 be considerably diminished even neglecting for some time
1925 possible deviations in the critical nuclei structure as com-
1926 pared with the evolving macro-phase.

1927 The following reasons could generally lead to a difference
1928 in the bulk properties of the critical and near-critical crystal-
1929 lites as compared with the respective newly evolving macro-
1930 scopic phase and to a reduction of the thermodynamic
1931 driving force: (a) It is reasonable to assume that near-critical
1932 nuclei are less ordered than the material in the corresponding
1933 bulk phase and it is possible to show that, in this case,
1934 $\Delta G_V < \Delta G_\infty$ holds [69]. (b) According to the model of ideal
1935 associated solutions [135,136], a glass-forming melt can be
1936 considered as a solution of oxide components and salt-like
1937 (stoichiometric) phases. Then, critical cluster formation
1938 could be represented as a segregation process in a multi-com-
1939 ponent solution. As shown in Ref. [97], in this case, the driv-
1940 ing force may be smaller than for the macroscopic phase. (c)
1941 The deviation of the critical nuclei composition from that of
1942 the evolving macro-phase (e.g., owing to the formation of
1943 metastable phases or solid solutions) has also to reduce the
1944 thermodynamic driving force, as compared with that for
1945 the stable macro-phase. This effect, i.e., the deviation of
1946 the critical nuclei composition from those of the evolving
1947 macro-phase and the parent stoichiometric glass was
1948 recently observed [137] and is discussed in detail below.

1949 Within certain limits, addition, removal or replacement
1950 of different components can continuously change the com-
1951 position of a given crystallographic system. Hence, gener-
1952 ally speaking, compositional variations of critical nuclei
1953 of a new phase and, consequently, variations of their prop-
1954 erties as compared with those of the corresponding macro-
1955 phase could be expected. Indeed such deviations were
1956 observed in both stoichiometric $\text{Na}_2\text{O} \cdot 2\text{CaO} \cdot 3\text{SiO}_2$ glass
1957 and glasses belonging to the solid solution (s/s) region
1958 between $\text{Na}_2\text{O} \cdot 2\text{CaO} \cdot 3\text{SiO}_2$ ($\text{N}_1\text{C}_2\text{S}_3$) and $\text{Na}_2\text{O} \cdot \text{CaO} \cdot 2\text{SiO}_2$ ($\text{N}_1\text{C}_1\text{S}_2$) [137]. Ref. [137] shows that the formation
1959 of stoichiometric crystals occurs via nucleation of s/s whose
1960 composition continuously approaches the stoichiometric
1961 one and arrives at that in the final stage of crystallization.
1962 Figs. 17 and 18 show the evolution of crystal and glassy
1963 matrix compositions and the corresponding change of the
1964 lattice parameter, respectively. An extrapolation of the
1965 change of crystal composition to zero time (or zero volume
1966 fraction, $\alpha = 0$, of the crystallized phase) gives a strong
1967 indication that the critical clusters are also enriched in
1968 sodium.
1969

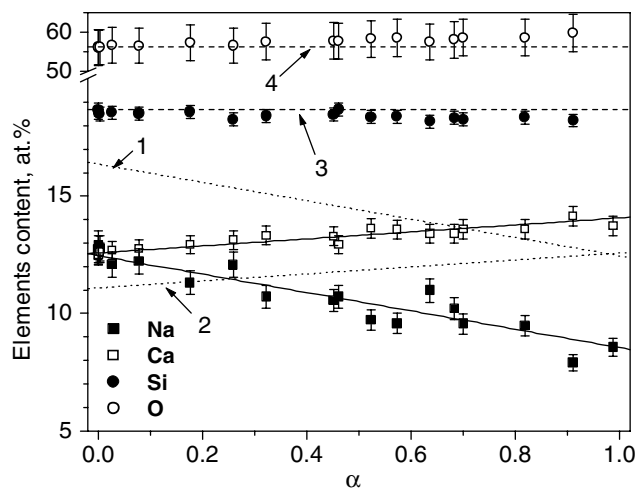


Fig. 17. Composition of the glassy matrix, measured by EDS (points), and of crystals calculated from the parent glass composition, $\text{N}_1\text{C}_2\text{S}_3$ (dotted lines 1 and 2 – Na and Ca, respectively) versus volume fraction crystallized at $T = 650^\circ\text{C}$. Solid lines fit the experimental data. Dashed lines 3 (Si) and 4 (O) refer to the parent glass composition [137].

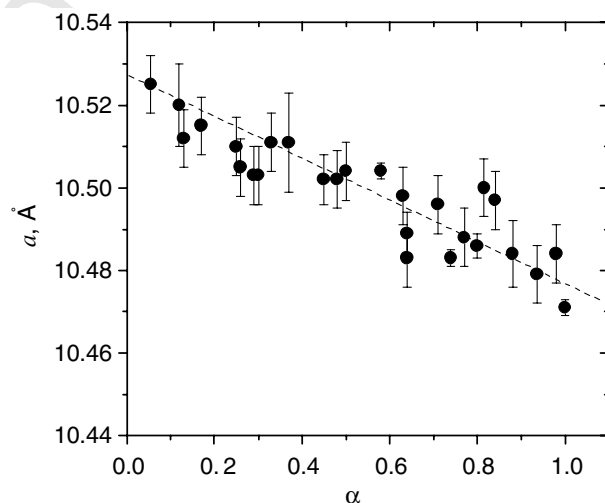


Fig. 18. Lattice parameter of the hexagonal crystal cell of the solid solutions against volume fraction of crystalline phase in stoichiometric $\text{N}_1\text{C}_2\text{S}_3$ glass heat-treated at 650°C [137].

1970 The exhaustion of sodium in the glassy matrix during
1971 crystallization leads to an inhibition of nucleation and crystal
1972 growth. According to an analysis of the overall crystal-
1973 lization kinetics using crystal growth data [137], the
1974 nucleation process is terminated if about 20% of the volume
1975 is crystallized. Fig. 19(a) and (b) shows the volume fraction
1976 of crystals and the size of the largest crystals as a function of
1977 heat treatment time at $T = 650^\circ\text{C}$ for a glass of stoichiomet-
1978 ric composition $\text{N}_1\text{C}_2\text{S}_3$. Nucleation takes place up to
1979 $t \sim 150$ min ($\ln(t) = 5$): $n \approx 4$, $m \approx 1$, $k = n - 3m \approx 1$
1980 ($n = k + 3m$) (see Eq. (24)). This conclusion is confirmed
1981 by a $N(t)$ -plot obtained by the ‘development’ method (see
1982 Fig. 19(c)). But, at $\ln(t) > 5$ crystallization proceeds only
1983 by crystal growth with $m \approx 0.33$, $n \approx 1$, $k \approx 0$ ($n = 3m$).

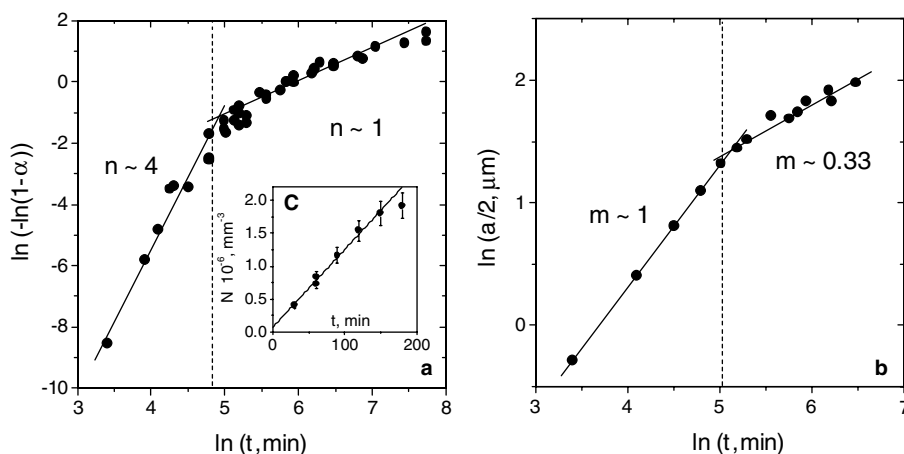


Fig. 19. Volume fraction of crystals (a), size of largest crystals (b), and number of crystals (c) as a function of heat treatment time at $T = 650\text{ }^{\circ}\text{C}$ for stoichiometric glass $\text{N}_1\text{C}_2\text{S}_3$ [137].

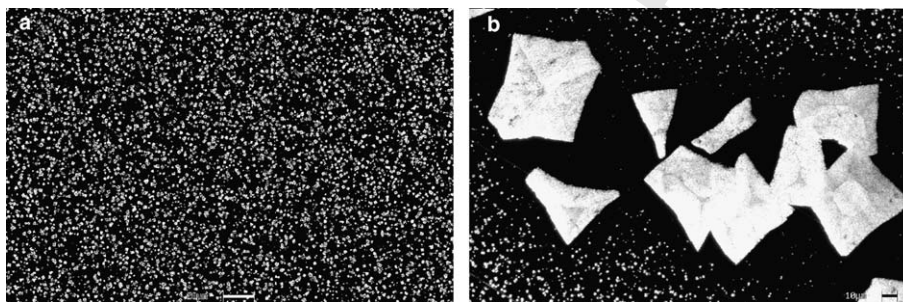


Fig. 20. SEM micrographs of $\text{N}_1\text{C}_2\text{S}_3$ glass subjected to single (a) and double (b) stage heat treatments: (a) $T = 590\text{ }^{\circ}\text{C}$, $t = 1560\text{ min}$; (b) $T_1 = 720\text{ }^{\circ}\text{C}$, $t_1 = 20\text{ min}$ and $T = 590\text{ }^{\circ}\text{C}$, $t = 1560\text{ min}$. The bars have a length of (a) $20\text{ }\mu\text{m}$ and (b) $10\text{ }\mu\text{m}$.

1984 Na-depleted diffusion fields around the growing crystals
 1985 can be visualized by a second heat treatment at a tempera-
 1986 ture corresponding to reasonable values of nucleation
 1987 and growth rates. A comparison of the samples subjected
 1988 to single-stage (cf. Fig. 20(a)) and double-stage (cf.
 1989 Fig. 20(b)) heat treatments reveals that pre-existing crystals
 1990 (formed in first heat treatment) diminish the number of
 1991 crystals nucleated in the subsequent treatment. Refs.
 1992 [48,138] show that the nucleation rate decreases with
 1993 decreasing sodium content in the glass. Hence, it is appar-
 1994 ent that the areas observed around the large crystals refer
 1995 to diffusion fields. A similar transformation path was
 1996 observed for glasses of compositions between $\text{N}_1\text{C}_2\text{S}_3$ and
 1997 $\text{N}_1\text{C}_1\text{S}_2$, with the only difference that fully crystallized
 1998 glasses are s/s with compositions of the parent glasses.

1999 According to the results presented in Fig. 21, the differ-
 2000 ence between the compositions of the critical nuclei and the
 2001 parent glass diminishes as the latter approaches the bound-
 2002 ary of s/s formation. The deviation of the nuclei composi-
 2003 tion from stoichiometry (glass $\text{N}_1\text{C}_2\text{S}_3$) or from the initial
 2004 glass compositions (glasses of the s/s region) diminishes
 2005 the thermodynamic driving force for crystallization, ΔG_V ,
 2006 and increases the thermodynamic barrier for nucleation.
 2007 Moreover, this deviation also may lead to an increase of
 2008 the kinetic barrier. Nevertheless, nucleation of crystals with

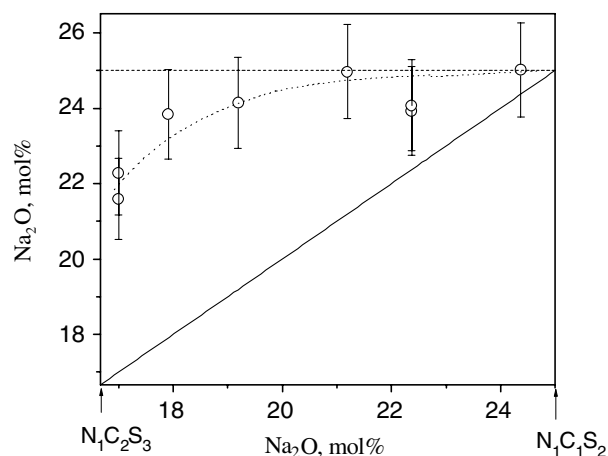


Fig. 21. Sodium oxide content in the critical nuclei versus composition of the parent glass. The solid line represents the case when the compositions of the critical nuclei and the parent glasses are the same.

2009 changed compositions (as compared with those of the par-
 2010 ent glasses) actually takes place. Hence, the decrease in
 2011 ΔG_V must be compensated by a decrease in surface energy
 2012 in Eq. (4). However, the determination of the variation of
 2013 the surface energy with composition is not a trivial problem
 2014 and warrants further study.

2015 Deviations of the composition of the smallest crystals
 2016 (50 nm) from that of the ambient glass have also been
 2017 observed for surface crystallization of μ -cordierite in a
 2018 glass of cordierite composition. But the composition of
 2019 the largest μ -cordierite crystals ($>1 \mu\text{m}$) was equal to that
 2020 of the parent glass [139]. Variations of the crystal composi-
 2021 tions during phase transformation were also found in
 2022 CaO–Al₂O₃–SiO₂ glasses [140]. A direct experimental
 2023 proof of changes of crystal composition with size in crystal-
 2024 lization of Ni(P)-particles in hypoeutectic Ni–P amorphous
 2025 alloys was recently reported in Refs. [106,107].

2026 All mentioned results give a further experimental confir-
 2027 mation of the thesis of a considerable variation of the prop-
 2028 erties of the clusters in the course of their evolution
 2029 corroborating the predictions of the generalized Gibbs'
 2030 approach.

2031 5.6. Independent estimate of the time-lag for nucleation 2032 from nucleation and growth kinetics

2033 It was correctly claimed in Ref. [141] that another prob-
 2034 lem may occur in the treatment of nucleation-growth pro-
 2035 cess in glasses. For a glass with a composition close to
 2036 lithium disilicate, it was shown in Ref. [141] that the induc-
 2037 tion time for crystal growth, t_{gr} , estimated (as illustrated by
 2038 Fig. 22) from a $R \sim t$ plot, where R is the size of the largest
 2039 crystal experimentally observed, and t the time elapsed
 2040 from the beginning of the nucleation-growth process,
 2041 strongly exceeds the induction period for nucleation
 2042 ($t_{\text{ind}} = \frac{6}{\pi^2} \tau$, see Eq. (11)). Latter value was estimated from
 2043 an $N \sim t$ plot obtained by the 'development' method. How-
 2044 ever, if crystal nucleation and growth rates refer to the for-
 2045 mation of the same phase, t_{gr} and t_{ind} are expected to be
 2046 similar [21]. In other words, it is reasonable to assume that
 2047 after an elapsed time t_{gr} the first supercritical nuclei have

2048 formed, which then deterministically grow up to sizes visi-
 2049 ble under an optical microscope.

2050 The discrepancy in induction times reported in Ref.
 2051 [141] has also been observed for lithium silicate glasses con-
 2052 taining 32.6–38.4 mol% Li₂O [142] belonging to the compo-
 2053 sition range where solid solution crystals precipitate via
 2054 homogeneous nucleation [143,144]. An example of $N \sim t$
 2055 and $R \sim t$ plots for lithium silicate glass with 35.1 mol%
 2056 Li₂O at $T = 460 \text{ }^\circ\text{C}$ is shown in Fig. 22, while Fig. 23 shows
 2057 the time parameters t_{ind} and t_{gr} estimated at different tem-
 2058 peratures for lithium silicate glasses with 33.5 and
 2059 32.6 mol% Li₂O. Since the $N \sim t$ curve was obtained by
 2060 the 'development' method (see Section 3.2), t_{ind} is overesti-
 2061 mated as compared with the correct value corresponding to
 2062 the nucleation temperature. (In Ref. [145] measurements of
 2063 nucleation and growth rates and corresponding time-lags
 2064 in lithium disilicate glass were undertaken using single-
 2065 stage heat treatments at a relatively high temperature,
 2066 $500 \text{ }^\circ\text{C} > T_{\text{max}} = 455 \text{ }^\circ\text{C}$. The estimated (extrapolated)
 2067 nucleation time-lag was considerably higher than that
 2068 obtained by the 'development' method. We now think that
 2069 this result was probably due to insufficient stereological
 2070 corrections of the crystal number density of the samples
 2071 subjected to single-stage treatments; see Section 3.4.) Thus,
 2072 the $t_{\text{gr}}/t_{\text{ind}}$ ratios experimentally obtained in the cited refer-
 2073 ences are only a lower bound for the difference between the
 2074 real induction periods. To correct the value of t_{gr} to partly
 2075 resolve the above discussed problem, an attempt was
 2076 undertaken in Ref. [141] to account for the effect of a size
 2077 dependent growth rate. However, the discrepancy between
 2078 induction times independently estimated from nucleation
 2079 and growth experiments remained too high. By this reason,
 2080 it was suggested that initially nucleation of metastable

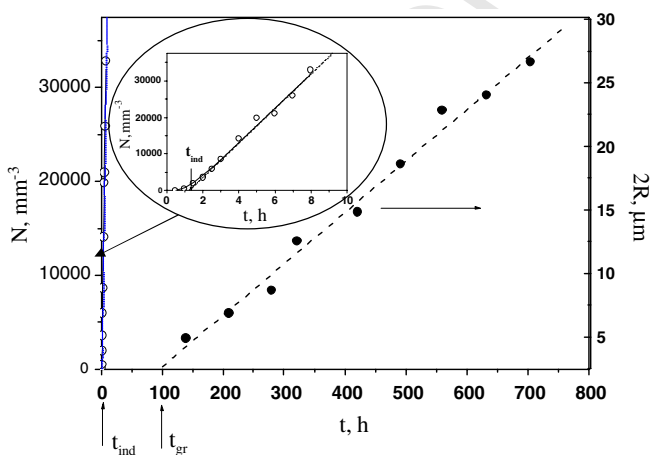


Fig. 22. Number density of crystals, N , and size of the largest crystals, $2R$, versus time of heat treatment at $T = 460 \text{ }^\circ\text{C}$ for a lithium silicate glass with 35.1 mol% Li₂O. The inset shows the $N \sim t$ data on a larger scale. The solid line was plotted with Eq. (10) and the dashed line is a linear fit of the $2R(t)$ -data [142].

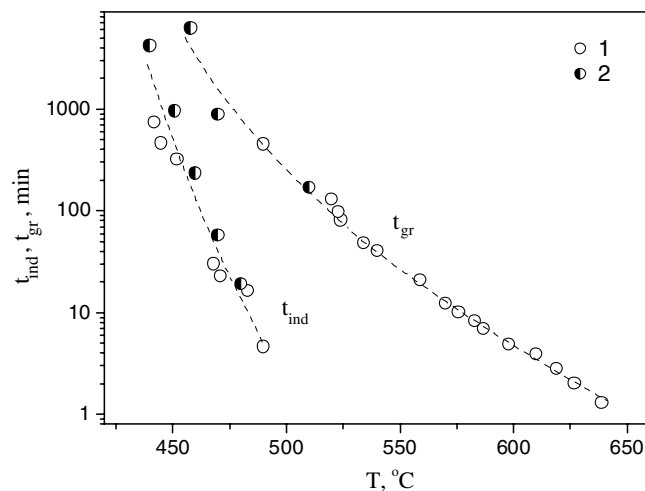


Fig. 23. Induction periods for crystal nucleation, t_{ind} , and for crystal growth, t_{gr} , versus temperature for lithium silicate glasses with 32.6 mol% (curve 2) Li₂O [142] and 33.5 mol% (curve 1) Li₂O [141]. t_{ind} were taken from N versus t plots obtained by the 'development method' (they are thus overestimated, see text) while t_{gr} were estimated from single-stage experiments at each temperature.

phase crystals take place, which grow more slowly than the macroscopic crystals of the stable phase.

Weinberg [146] questioned the conclusions of Ref. [141] with the argument that the induction time for growth can not be uniquely determined because it depends on the cluster size for which the measurements are performed. He also stated that the induction time for growth becomes unbounded even for measurements performed at large cluster sizes. Strictly speaking those arguments are correct, but since the growth rate tends to time-independent values fairly rapidly with increasing R (see, e.g., Eq. (39) or Eq. (62) and Fig. 24), the induction time also tends to a practically finite value when the measurements are extended to large (optical microscopy scale) crystal sizes. Consequently, we believe that the comparison of induction times independently obtained by nucleation and growth experiments can be a useful tool, and, in principle, allows one to draw conclusions similar to those of Ref. [141].

Nevertheless, the results and analysis of induction times for growth deserve some comments. The analysis carried out in Ref. [141] was based on the solution of macroscopic growth equations starting with an initial cluster radius equal to the critical cluster size. With such initial condition, the induction time for growth tends to infinity independently of any particular growth mechanism, since $U(r_*) = 0$, and the numerical integration employed in Ref. [141] could not resolve this problem. In other words, the macroscopic growth equation is not valid for $R = r_*$ and cannot be employed to describe the change of the nuclei size close to the critical one. Recall that according to the Zeldovich–Frenkel equation, in the vicinity of the critical cluster size the ‘motion’ of the clusters in cluster size space is mainly governed by diffusion-like processes in cluster size space under the action of the concentration gradient with respect to the cluster size distribution function, and thus it is not governed by the thermodynamic driving force, as it is the case in deterministic growth. In addition,

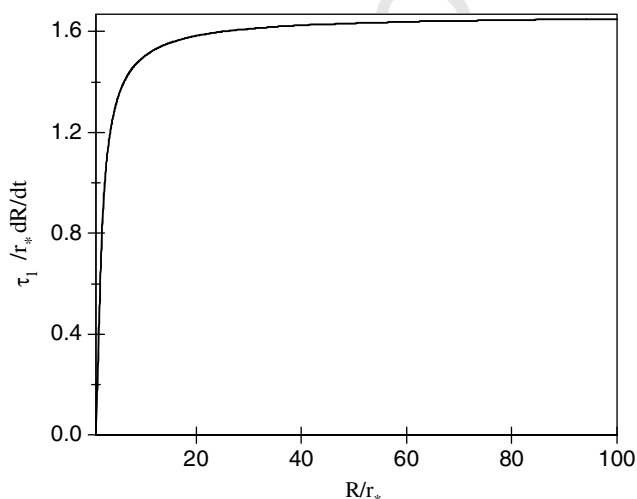


Fig. 24. Crystal growth rate (dR/dt) in (r_*/τ_1) -units versus reduced crystal size according to Eq. (62).

the discrepancy observed in Ref. [141] could also be explained in different ways, and not only via the assumption of formation of metastable phases.

To reconsider the above mentioned problem from a different perspective, we employed an analytical solution of the Fokker–Planck or Frenkel–Zeldovich equation describing nucleation-growth process (cf. Ref. [147]). According to this analysis, for nuclei with sizes larger than two critical sizes, $R > 2r_*$, the following relation holds:

$$\hat{\tau} = \frac{3}{5} \left[\hat{R} + \ln(\hat{R} - 1) + \frac{2}{3} \right]. \quad (62)$$

In Eq. (62) the following dimensionless variables are used:

$$\hat{R} \equiv \frac{R}{r_*}, \quad \hat{\tau} \equiv \frac{t}{\tau_1}. \quad (63)$$

Here τ_1 is the period of time needed to establish a steady-state cluster size distribution in a range of cluster sizes slightly exceeding the critical size, i.e., it is practically equal to the time required to establish a steady-state nucleation rate for clusters of critical sizes. Recall that, according to Eq. (9) or (10), to practically establish a steady-state nucleation rate a time period about 5τ is required (see Fig. 6(b)). Hence the following relation between τ_1 and τ exists

$$\tau_1 \cong 5\tau. \quad (64)$$

It should be emphasized that Eq. (62) was derived with the following (strong) assumptions commonly employed in CNT:

- (i) The bulk state of the clusters is independent on their sizes and is identical to that of the newly evolving macroscopic phase;
- (ii) The mechanism of cluster growth does not depend on cluster size, and growth is kinetically limited.

The term ‘kinetically limited’ refers to the ballistic growth mechanism, where the growth process is only limited by diffusion across the interface, and does not depend on bulk diffusion, as it is the case, for instance, for significant compositional differences between the liquid phase and growing crystal.

The experimental $R(t)$ data were fitted to Eq. (62) using τ_1 and r_* as fit parameters [142]. Fig. 25 shows the result of such calculations. In this way, in order to arrive at the $R(t)$ -dependence we did not use any macroscopic growth equation, but relied instead on an analytical solution of the Frenkel–Zeldovich equation, which gives a correct description of the evolution of the cluster ensemble. In addition, in our approach, we do not determine an induction time for growth, but instead determine the time-lag for nucleation by fitting experimental growth data to the nonlinear Eq. (62). Hence, even if Weinberg’s comments [146] about the impossibility of defining t_{gr} from $R(t)$ curves are strictly correct, they do not affect our analysis.

The value of τ_1 exceeds the corresponding nucleation induction time, 5τ , estimated from the $N \sim t$ curve, by

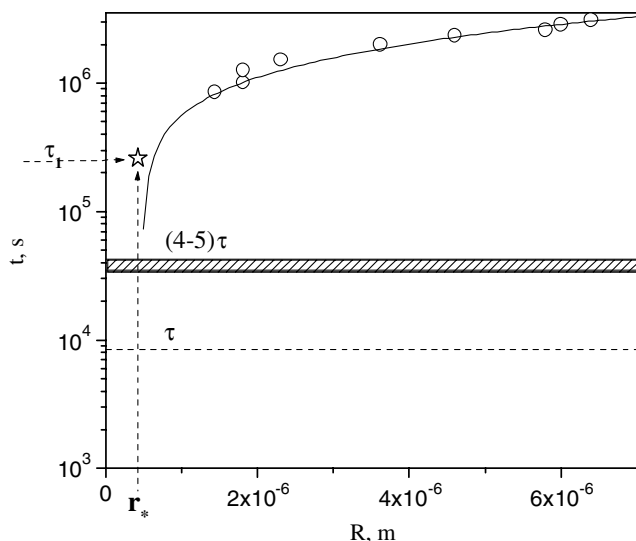


Fig. 25. Time necessary for a crystal to achieve a size R in a lithium silicate glass with 32.6 mol% Li_2O at 460 °C. The full curve was plotted by Eq. (62) using τ_1 and r_* as fit parameters. The coordinates of the open star show the fit parameters τ_1 and r_* . The circles refer to the experimental data. The dashed horizontal line shows the value of the time-lag for nucleation τ estimated by a fit of the $N \sim t$ data to Eq. (10). The crosshatched band corresponds to the time when the nucleation rate achieves 95–99% of its steady-state value [142].

2174 about one order of magnitude (see Fig. 25). However, pro-
 2175 vided the conditions (i) and (ii) are fulfilled, one expects
 2176 that τ_1 must be equal to about 5τ , see Eq. (64), since both
 2177 τ_1 and τ refer to nucleation kinetics. This discrepancy leads
 2178 to the following conclusion: *at least one or both of the*
 2179 *assumptions underlying the derivation of Eq. (62) are not*
 2180 *valid.*

2181 In order to explain the present results, one should recall
 2182 the assumptions made in the derivation of the above equa-
 2183 tions. In particular, one can assume that the compositions
 2184 of near-critical clusters deviate from those of the macro-
 2185 scopic crystals to which the crystal size measurements refer.
 2186 Since in the advanced stages of crystallization the compo-
 2187 sition of the macro-crystals coincides with those of the
 2188 ambient melt, this assumption leads to the conclusion that
 2189 growth of near-critical nuclei is limited by diffusion and is
 2190 thus not kinetically determined. Moreover, as shown in the
 2191 analysis of a model system [102], the size dependence of the
 2192 cluster composition results in a cluster size dependence of a
 2193 variety of thermodynamic and kinetic parameters (driving
 2194 force, surface tension, effective diffusion coefficients, and
 2195 growth rates). These deviations are not taken into account
 2196 in the derivation of Eq. (62).

2197 Consequently, the mentioned deviations can be inter-
 2198 preted as an additional indication that the classical
 2199 approach to the description of nucleation-growth processes
 2200 is insufficient for an interpretation of experimental results
 2201 on crystallization in lithium disilicate glasses. One of the
 2202 possible solutions is the assumption of a size (and eventu-
 2203 ally structure) dependent composition of the crystallites.
 2204 For completeness we should also to mention an alternative

2205 approach [148,149] connecting the possible deviations with
 2206 possible (cluster-size dependent) solute depletion and vol-
 2207 ume diffusion in nucleation. Taking into account the results
 2208 of the generalized Gibbs' approach, density functional
 2209 studies and computer simulation methods of the properties
 2210 of critical clusters, the first interpretation of the deviations
 2211 between the time-lag established in two independent ways
 2212 (being the result of the change of both cluster properties
 2213 and growth kinetics in dependence on their sizes) seems
 2214 to us to be a more convincing explanation.

2215 The questions under which conditions and in what way
 2216 nuclei change their properties and the growth mechanism
 2217 are not trivial to answer, especially if these changes occur
 2218 in the early stages of crystallization. However, the transfor-
 2219 mation must finally lead to the formation of a stable mac-
 2220 rophase with well-defined properties. One of the possible
 2221 and often assumed ways to account for such effects – the
 2222 formation of metastable phases – will be discussed in Sec-
 2223 tion 5.7 However, metastable phase formation is not the
 2224 only possible but a very particular explanation for such
 2225 kind of behavior (see, e.g., Section 5.5). The analysis of
 2226 already mentioned model system (segregation in regular
 2227 solutions [102]) shows that clusters may continuously
 2228 change their properties with their sizes and do not have
 2229 the properties of some fictive metastable phase. Such expla-
 2230 nation for the observed discrepancy is more general and
 2231 could be ascribed to the formation of different transient
 2232 phases more or less continuously changing their properties
 2233 in dependence on cluster size.

2234 5.7. On the possible role of metastable phases in 2235 nucleation

2236 As mentioned in Sections 5.3 and 5.5 the precipitation of
 2237 metastable phases in the early stages of nucleation may be
 2238 one of the reasons for the deviation of the critical nuclei
 2239 properties (e.g., composition) from that of the evolving
 2240 (stable) macro-phase. The formation of metastable phases
 2241 is consistent with the original formulation of Ostwald's
 2242 *Rule of Stages* according to that, 'if the supersaturated
 2243 state has been spontaneously removed then, instead of a
 2244 solid phase, which under the given conditions is thermody-
 2245 namically stable, a less stable phase will be formed' [150].
 2246 Note that Ostwald restricted his formulation to the possi-
 2247 ble result of the transformation not specifying the bulk
 2248 state of the critical clusters as done in the generalization
 2249 of this rule as given above (see Section 5.4). Implicitly it
 2250 is assumed in his formulation – and also in its theoretical
 2251 foundation as developed first by Stranski and Totomanov
 2252 [151] – that the critical clusters have properties equivalent
 2253 to the properties of one of the finite number of phases
 2254 which can exist in a macroscopic form, at least, in a meta-
 2255 stable state at the given conditions.

2256 Ostwald's rule is corroborated by the following thermo-
 2257 dynamic considerations. Employing the Skapski–Turnbull
 2258 equation, Eq. (31), to estimate the crystal/liquid interfacial
 2259 energy, one can show that the thermodynamic barrier for

2260 nucleation is proportional to the melting enthalpy. Hence,
 2261 higher nucleation rates of metastable phases than those of
 2262 the stable phase could be expected due to its lower melting
 2263 enthalpy and correspondingly lower thermodynamic barrier.
 2264 But a higher nucleation rate of a metastable phase
 2265 must be accompanied by a lower growth rate, since the latter
 2266 is proportional to the thermodynamic driving force.
 2267 This is especially true if the composition of the metastable
 2268 phase is similar to that of the parent glass.

2269 Once crystallites of a metastable phase form, they may
 2270 favor nucleation of crystallites of the stable phase if its formation
 2271 is followed by transformation into aggregates of the
 2272 more stable phase as discussed in Ref. [152]. Thus, metastable
 2273 crystals can, in principle, catalyze in one or the other
 2274 way nucleation processes of the stable phase. Some authors
 2275 suggested that such crystallization path occurs in $\text{Li}_2\text{O}\cdot 2\text{-}$
 2276 SiO_2 (LS_2) glass, which has been used for many years as
 2277 a model system to study homogeneous nucleation (see,
 2278 e.g., [153,154]). An article by Deubener et al. [141] (discussed
 2279 in Section 5.6) reawakened the interest in this problem
 2280 and stimulated an intensive search for metastable
 2281 phase formation in LS_2 -glass [155–157], mainly by transmission
 2282 electron microscopy (TEM) and X-ray diffraction (XRD)
 2283 methods. In addition to stable lithium disilicate and
 2284 metastable metasilicate crystals, other, so far unknown,
 2285 phases were found. However, the observations of different
 2286 authors were often in contradiction to each other. But,
 2287 in general, the probability of observing such new phases
 2288 in LS_2 glass increases with a decrease in time and temperature
 2289 of heat treatment [158]. Due to low nucleation rates and
 2290 correspondingly low crystal number densities, and extremely
 2291 small areas observed by TEM, the statistics of such measurements
 2292 are quite poor. Moreover, the electron beam can degrade
 2293 the crystals under study in a short time. As an example,
 2294 however, the results of Ref. [159] show that at $T = 454^\circ\text{C}$
 2295 (close to the nucleation rate maximum), only $\text{Li}_2\text{O}\cdot 2\text{SiO}_2$
 2296 (LS_2) and $\text{Li}_2\text{O}\cdot \text{SiO}_2$ (LS) crystals were detected in
 2297 the early stages of crystallization (less than 1% crystallized
 2298 fraction), but LS crystals were not detected in the most
 2299 advanced stages (5–10% crystallized fraction). It should
 2300 be emphasized that, according to the data collected in a
 2301 time interval 0–100 h at 454°C , the LS crystals sizes
 2302 practically do not change, while the LS_2 crystals
 2303 significantly grow (see Fig. 26). This result agrees with
 2304 calculations according to which the thermodynamic driving
 2305 force for LS crystallization in lithium disilicate glass
 2306 is lower than for LS_2 crystals [160], because a higher
 2307 thermodynamic driving force also results in higher growth
 2308 rates. Since there was no evidence of heterogeneous nucleation
 2309 of lithium disilicate on lithium metasilicate crystals,
 2310 it was concluded that LS nucleates concurrently with
 2311 the stable phase LS_2 and disappears with time. Recall that
 2312 lithium disilicate has a wide range of solid solutions (s/s)
 2313 formation [143,144]; hence, one can suppose that the
 2314 critical nuclei are also s/s. Here it should be noted that
 2315 the technique employed in Ref. [159] did not allow them
 2316 to distinguish stoichiometric compounds from solid solutions.

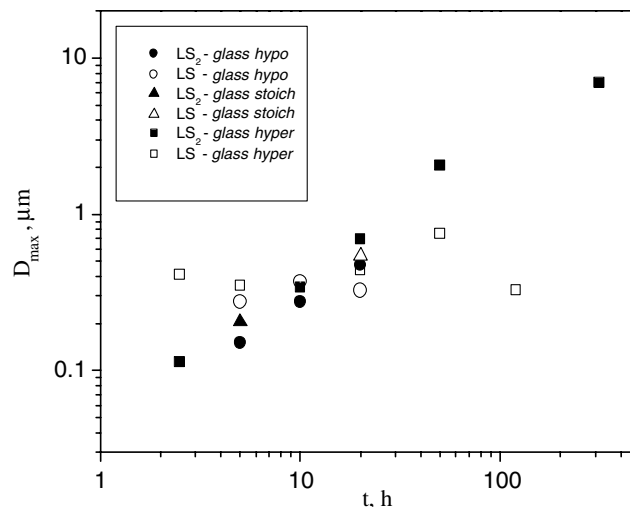


Fig. 26. Maximum dimension (D_{\max}) of the largest crystals observed by TEM in samples of *hypo*, *stoich*, and *hyper* lithium disilicate glasses versus heat treatment time at 454°C [159]. Solid and opened points refer to LS_2 and LS crystals, respectively.

The assumption of s/s nucleation does not contradict the results presented above, but allows one to consider changes of composition of the evolving nuclei with size, such as those demonstrated in Section 5.5 for soda-lime-silica glasses and assumed in Section 5.6. Thus, in some cases, it is possible that the role of metastable phases in nucleation could be simply a continuous variation of nuclei composition (and properties) during the phase transformation. However, there is another factor that has not been taken into consideration so far, but may be of considerable influence. That is the possible effect of elastic stress on nucleation in glass-forming melts. This effect will be analyzed in the next section.

5.8. Effect of elastic stresses on the thermodynamic barrier for nucleation

As it follows from Section 5.1, the thermodynamic barrier for nucleation, W_* , can be calculated in the framework of CNT by a fit of experimental data employing Eq. (34). For such computations, no additional assumptions are needed apart from the validity of CNT. In addition, one has to make some choice concerning the value of the surface energy in the pre-exponential term. However, this choice only weakly affects the final results.

According to Eq. (4), the work of critical cluster formation, W_* , monotonically decreases with decreasing temperature. Nevertheless, the value of $W_*(T/T_n)$, calculated from nucleation data for lithium disilicate glass at temperatures close to T_g shows an anomalous increase with decreasing temperature (cf. Fig. 27). A similar behavior of W_* was observed in other systems, e.g., for wollastonite glass [162]. The above mentioned deviations of the $W_*(T)$ -dependence from the expected (according to CNT) may be caused by elastic stresses. Since, in most cases of interest, the crystal densities differ from those of the corresponding

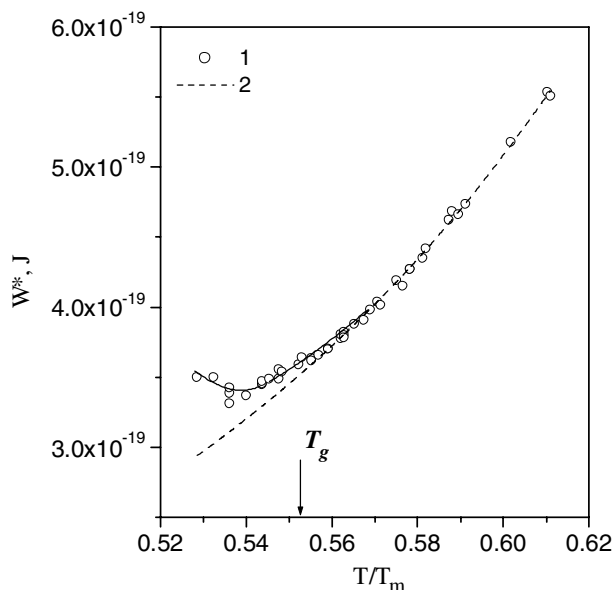


Fig. 27. Thermodynamic barrier for nucleation in $\text{Li}_2\text{O}\cdot 2\text{SiO}_2$ -glass (curve 1) estimated from a fit of experimental $I_{st}(T)$ and $t_{ind}(T)$ to Eq. (32), and (curve 2) calculated with Eq. (4) [161].

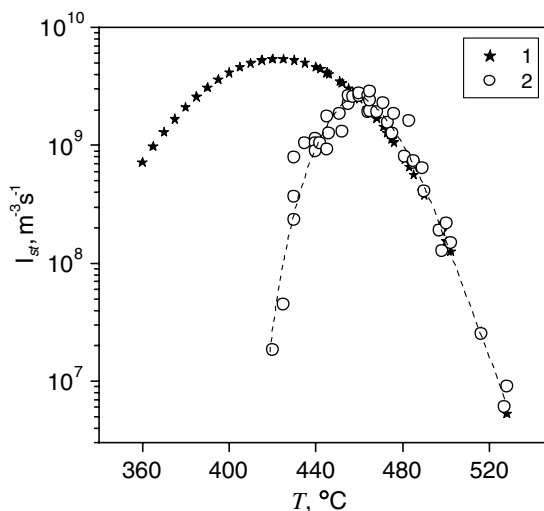


Fig. 28. Temperature dependence of the steady-state nucleation rates in lithium disilicate glass [161]. (Curve 1) I_{st} calculated with Eq. (34) for the case when elastic stresses do not play any role; (Curve 2) experimental values of I_{st} . The dashed line is just to guide the eyes.

2351 glasses, glass crystallization is accompanied by volume
 2352 changes. Such changes may result in stress development
 2353 which, in turn, diminishes the thermodynamic driving force
 2354 for the phase transformation by a term connected with the
 2355 elastic strain energy. This energy can partly or even fully
 2356 [12,14,163,164] suppress the nucleation-growth process.
 2357 This effect may be the origin not only of the anomalous
 2358 behavior of the work of critical cluster formation, $W_*(T)$,
 2359 but also of a number of well-known additional experimen-
 2360 tal facts, e.g., the preference of surface to volume nucle-
 2361 ation [12,163,164], or the existence of a correlation
 2362 according to which glasses having densities much lower
 2363 than those of the corresponding crystals usually reveal only
 2364 surface crystallization [165].

2365 A theory of nucleation in viscoelastic bodies has been
 2366 developed recently [166,167] which takes into account both
 2367 stress development and relaxation in phase formation in
 2368 glass-forming melts (an analysis of the effect of elastic stres-
 2369 ses on crystal growth – based on the same theoretical pre-
 2370 mises – is given in Ref. [168]). It was concluded that the
 2371 effect of elastic stresses on nucleation can be remarkable
 2372 if the time of stress development (estimated as time-lag
 2373 for nucleation) is smaller than the characteristic time of
 2374 stress relaxation, which is governed by viscous flow. Such
 2375 a situation is possible at temperatures lower than the so-
 2376 called decoupling temperature $T_d \sim 1.2T_g$, when the
 2377 Stokes–Einstein equation may no longer be valid, i.e.,
 2378 when the nucleation kinetics is not governed by viscous
 2379 flow. A detailed analysis, performed for lithium disilicate
 2380 glass, shows that elastic stresses may decrease the steady-
 2381 state nucleation rate by up to two orders of magnitude
 2382 [169]. In this analysis, the work of critical cluster formation
 2383 in the absence of elastic stresses was determined following
 2384 classical nucleation theory.

2385 Recently an attempt was made to estimate the elastic
 2386 stress energy directly using the deviation of $W_*(T)$ -curves
 2387 from the theoretical one [161] for the same lithium disilicate
 2388 glass. The obtained values of elastic strain energy were
 2389 comparable in magnitude with those calculated using the
 2390 elastic constants of glass and crystals. It should be noted
 2391 that in the extrapolation of the $W_*(T)$ -dependence from
 2392 relatively high temperatures, at which elastic stress effects
 2393 can be neglected, to low temperatures, where the minimum
 2394 of experimental W_* -values is observed, both thermody-
 2395 namic driving force and crystal/melt surface energy were
 2396 considered as fit parameters. The fitting procedure pro-
 2397 duced, in accordance with the conclusions of Section 5.2,
 2398 values of effective surface energy that decrease with
 2399 decreasing temperature. Moreover, the thermodynamic
 2400 driving force turned out to be considerably less than that
 2401 for the respective macroscopic phase.

2402 Fig. 28 shows experimental steady-state nucleation rates
 2403 versus temperature together with the theoretical curve cal-
 2404 culated by neglecting elastic stresses, employing values for
 2405 the driving force and surface tension obtained via above
 2406 discussed fitting procedure. At low temperatures, the calcu-
 2407 lated I_{st} -values considerably exceed the experimental data
 2408 giving an indirect evidence of the essential role of elastic
 2409 stresses in nucleation.

6. Concluding remarks

2410
 2411 We presented an overview of experimental results on
 2412 crystal nucleation in silicate glasses and their theoretical
 2413 interpretation in the framework of CNT. Different modifi-
 2414 cations and alternative theoretical approaches of CNT do
 2415 exist and the importance of the correct determination of
 2416 the properties of critical clusters and, in particular, of
 2417 the work for their formation has been known since the

2418 formulation of the basic concepts of CNT. However, fol- 2475
2419 lowing Gibbs' ideas in the description of thermodynami- 2476
2420 cally heterogeneous systems, in the search for the 2477
2421 solution of this problem the properties of the critical clus- 2478
2422 ters have been commonly identified with the properties of 2479
2423 the newly evolving macroscopic phases. Exclusively under 2480
2424 such assumption, the supersaturation (or driving force) 2481
2425 can be considered – at constant pressure – as a function 2482
2426 only of temperature. As a consequence, in most attempts 2483
2427 to reconcile theoretical and experimental results attention 2484
2428 was predominantly directed to the determination of the 2485
2429 size-dependence of the specific interfacial energy. In con- 2486
2430 trast, it follows from the present review that the main prob- 2487
2431 lem regarding the application of CNT for a quantitative 2488
2432 description of nucleation kinetics in glass-forming liquids 2489
2433 consists primarily in the adequate description of the bulk 2490
2434 properties of the critical nuclei. Of course, a deviation of 2491
2435 the bulk properties of the critical clusters as compared with 2492
2436 the newly evolving macroscopic phases also leads to mod- 2493
2437 ifications of the specific interfacial energy. However, the 2494
2438 resulting variation of the specific interfacial energy – due 2495
2439 to changes in the bulk properties of the critical clusters as 2496
2440 compared with the newly evolving macroscopic phase – is 2497
2441 only a secondary factor that must be, of course, also ade- 2498
2442 quately incorporated into the theory. Therefore, the circle 2499
2443 of problems one has to solve for the theoretical description 2500
2444 of nucleation is enlarged. On the other hand, a new meth- 2501
2445 odology – the generalized Gibbs approach – that allows 2502
2446 one to overcome the mentioned problems, which cannot 2503
2447 be resolved following the classical concepts of Gibbs, has 2504
2448 been recently developed. 2505

2449 Direct experimental methods usually employed to study 2506
2450 micron-sized or larger crystals cannot be used for nuclei of 2507
2451 critical sizes, which are only of a few nanometers in the 2508
2452 temperature range of interest. This is one of the reasons 2509
2453 why one typically follows Gibbs' description of heteroge- 2510
2454 neous systems and assigns the thermodynamic properties 2511
2455 (particularly the thermodynamic driving force for crystalli- 2512
2456 zation) of the macro-phases to the critical nuclei, thus 2513
2457 assuming that the critical nuclei and the evolving stable 2514
2458 macro-phase can be characterized by similar bulk state 2515
2459 parameters. However, since the thermodynamic barrier 2516
2460 for nucleation includes both the thermodynamic driving 2517
2461 force and the nucleus-melt surface energy, a maximum 2518
2462 thermodynamic driving force (corresponding to the stable 2519
2463 phase) is not a necessary condition to attain the lowest 2520
2464 value of the thermodynamic barrier and, correspondingly, 2521
2465 the highest value of the nucleation rate. Moreover, the 2522
2466 thermodynamic properties of the critical nuclei can be 2523
2467 affected by elastic stresses arising from differences between 2524
2468 the densities of the nucleus and the melt. Hence, one can 2525
2469 suppose that, in some cases, the deviation of the composi- 2526
2470 tion of the nuclei from those of the stable phase may be 2527
2471 accompanied by an approach of the nuclei density to that 2528
2472 of the melt. In such cases, the effect of elastic stresses is 2529
2473 reduced and, correspondingly, a decrease in the thermody- 2530
2474 namic barrier for formation of such nuclei (as compared

with the respective value for the stable phase) could be 2475
expected. Thus, elastic stress effects can considerably com- 2476
plicate the thermodynamics of nucleation and extend the 2477
variety of possible structures and compositions of the crit- 2478
ical nuclei. 2479

Since, with rare exceptions, direct measurements of the 2480
characteristic properties of critical nuclei are inaccessible, 2481
it is rather difficult or impossible to attribute the measured 2482
nucleation rates to defined crystal phases. It seems that 2483
such situation will not change in the near future. Moreover, 2484
taking into account density functional studies, computer 2485
simulations and theoretical analyses connected with the 2486
generalization of Ostwald's rule of stages, it is even ques- 2487
tionable whether the critical clusters have structures and 2488
compositions resembling those of the possible macroscopic 2489
phases that may evolve in the system under consideration. 2490
As shown here, there is some remarkable evidence – partly 2491
presented in this review – for the existence of considerable 2492
differences between the properties of near-critical nuclei 2493
and those of the respective stable macroscopic phases. 2494

Glasses of stoichiometric compositions have been used 2495
as model systems in a variety of studies of crystal nucle- 2496
ation. Such choice was made hoping that it should be possi- 2497
ble to treat such systems as one-component systems. 2498
However, it now became clear that a stoichiometric glass 2499
composition, equal to the composition of the evolving crys- 2500
talline phase, does not guarantee that the nuclei have the 2501
same composition. Therefore, systematic investigations of 2502
nucleation rates versus glass compositions are of great 2503
interest allowing us to understand the true nature of nucle- 2504
ation in glasses. The great value of such analysis is rein- 2505
forced if the crystal growth rates are also measured in the 2506
same temperature range. In this way, additional informa- 2507
tion can be accumulated allowing one to reveal both the 2508
crystal nucleation and growth mechanisms operating in 2509
the systems under study. 2510

On the other hand, further development of the classical 2511
theories of nucleation and growth – aimed to describe not 2512
only critical nuclei formation, but also its subsequent 2513
growth, including the possible evolution of their composi- 2514
tion – may allow us to develop a more adequate description 2515
of phase transformation kinetics. Here we drew attention 2516
to a new approach to the description both of nucleation 2517
and growth – *the generalized Gibbs' approach* – which has 2518
been developed in recent years and already demonstrated 2519
its power in the analysis of phase formation in different sys- 2520
tems. Existing different alternative theories and modifica- 2521
tions of CNT and their further developments will show 2522
which of them will be most successful in treating nucle- 2523
ation-growth phenomena in crystallization. However, in 2524
order to be successful in the description of experimental 2525
data on nucleation and growth, any of the proposed theo- 2526
ries – and this is one of the main conclusions of the present 2527
review – must be able to appropriately describe the depen- 2528
dence of the properties of the critical clusters on the state of 2529
the ambient glass-forming melt and the change of the state 2530
of the crystallites with their sizes both in dissolution and 2531

2532 growth processes. We believe the analysis of the size-depen-
 2533 dence of the cluster properties and their theoretical inter-
 2534 pretation may lead to new exciting developments in the
 2535 field of crystal nucleation of glasses, with a variety of
 2536 new applications. Thus, despite the fact that numerous
 2537 analyses of crystallization kinetics and mechanisms of sili-
 2538 cate and other glasses have been performed for decades,
 2539 they are expected to remain a highly interesting subject
 2540 for both fundamental and applied research on nucleation
 2541 and phase transformations in general.

2542 **Acknowledgements**

2543 The authors would like to express their deep gratitude to
 2544 Professor Ivan Gutzow (Sofia, Bulgaria) for helpful discus-
 2545 sions and critical comments. Financial support by Fapesp,
 2546 Capes and CNPq (Brazil) is fully appreciated.

2547 **Appendix A**

2548 The experimental values of the thermodynamic driving
 2549 force for crystallization given by Eq. (5) is bounded by a
 2550 linear approximation (Eq. (6)), commonly denoted as
 2551 Turnbull's formula, and by the approximation of Hoffman
 2552 (Eq. (7)), see Fig. A1(b), (d), and (f). Eq. (6) directly fol-

lows from Eq. (5) in the case of $\Delta C_p = 0$. The Hoffman
 equation assumes $\Delta C_p = \text{constant}$ and some additional
 simplifications. There are other approximations that pre-
 dict values of ΔG_V located inside the range given by Eqs.
 (6) and (7). Some of them, taken from Ref. [13], are

$$\Delta G_V = \frac{\Delta H_V \Delta T}{T_m} \left[\frac{7T}{T_m + 6T} \right], \quad (\text{A.1})$$

$$\Delta G_V = \frac{\Delta H_V \Delta T}{T_m} - \gamma \Delta S_m \left[\Delta T - T \ln \left(\frac{T_m}{T} \right) \right], \quad (\text{A.2})$$

$$\Delta G_V = \frac{\Delta H_V \Delta T}{T_m} \frac{2T}{T_m + T}. \quad (\text{A.3})$$

Fig. A1(b), (d), (f), and (h) shows the values of ΔG_V versus
 temperature calculated with Eqs. (6), (A.1), (A.2), (A.3),
 and (7). The value of γ in Eq. (A.2) was chosen equal to
 0.8. Experimental data on ΔG_V are also shown for $\text{Li}_2\text{O} \cdot 2\text{SiO}_2$,
 $\text{Na}_2\text{O} \cdot 2\text{CaO} \cdot 3\text{SiO}_2$ and $2\text{Na}_2\text{O} \cdot 1\text{CaO} \cdot 3\text{SiO}_2$ glasses.
 Different approximations for the thermodynamic driving
 force were used to plot the nucleation rates as shown in
 Fig. 23(a), (c), (e), and (g). The intercepts and slopes of
 the linear fits at $T > T_g$ were employed to estimate I_o^{exp}
 and σ_{cm}^* . These parameters are listed in Table A1.

According to Table A1 the discrepancy between experi-
 mental and theoretical values of I_o is always drastic and
 becomes even stronger when the $\Delta G_V(T)$ -function becomes

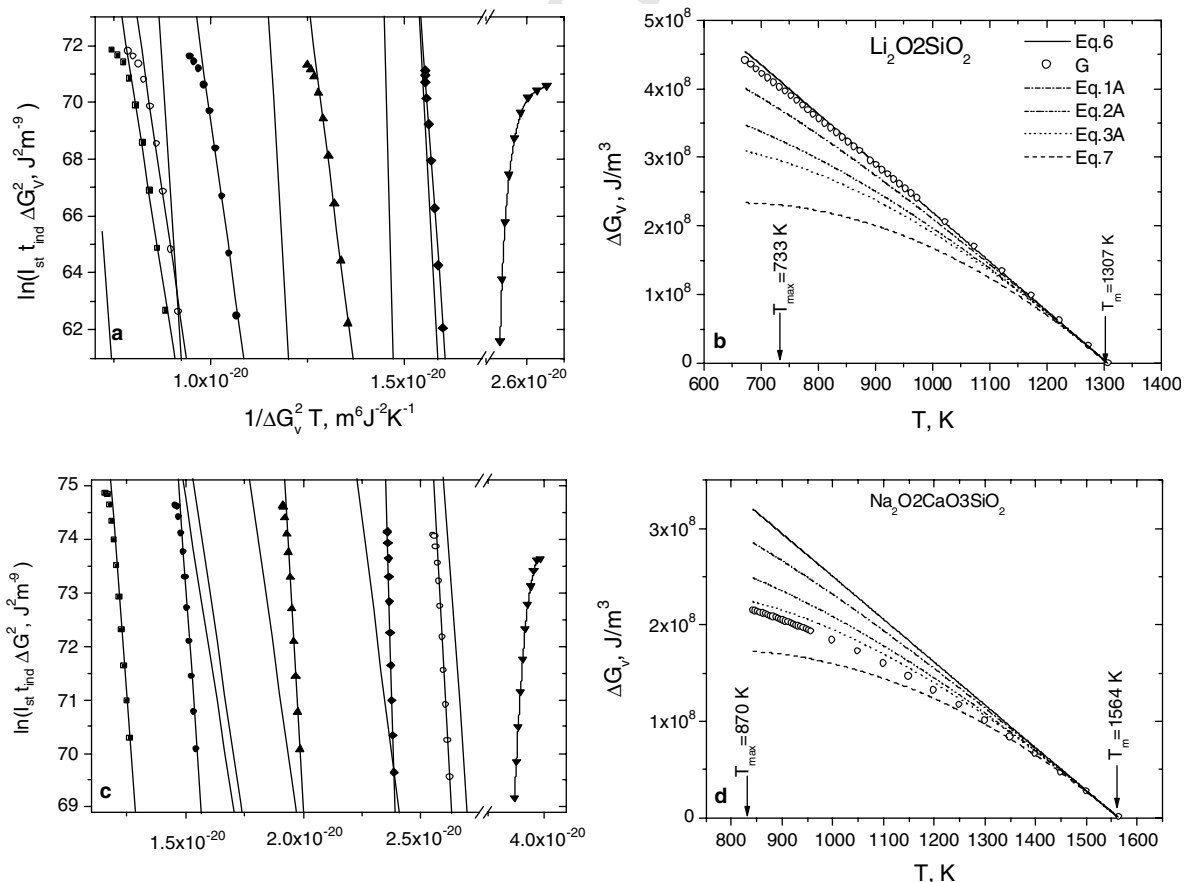


Fig. A1. Analysis of nucleation data with different expressions for the thermodynamic driving force. (b,d,f,h): thermodynamic driving force versus temperature; (a,c,e): $\ln(I_{st} t_{ind} \Delta G_V^2)$; (g): $\ln(I_{st} \eta)$ versus $1/\Delta G_V^2 T$.

Table A1

Ratio of experimental and theoretical pre-exponential terms, and surface energy for different glasses [40] calculated by fitting nucleation data to CNT employing experimental and approximate values of the thermodynamic driving force

	Li ₂ O·2SiO ₂		Na ₂ O·2CaO·3SiO ₂		2Na ₂ O·CaO·3SiO ₂		BaO·2SiO ₂ ^a	
	σ_{cm}^*	$\log\left(\frac{I_0^{\text{exp}}}{I_0^{\text{theo}}}\right)$	σ_{cm}^*	$\log\left(\frac{I_0^{\text{exp}}}{I_0^{\text{theo}}}\right)$	σ_{cm}^*	$\log\left(\frac{I_0^{\text{exp}}}{I_0^{\text{theo}}}\right)$	σ_{cm}^*	$\log\left(\frac{I_0^{\text{exp}}}{I_0^{\text{theo}}}\right)$
Eq. (6)	0.19	15	0.17	18	0.15	27	0.13	8
Eq. (A.1)	0.20	27	0.18	30	0.16	46	0.13	14
Eq. (A.2)	0.20	45	0.19	51	0.17	79	0.13	23
Eq. (A.3)	0.25	113	0.22	156			0.14	43
Experiment	0.20	19	0.19	72	0.17	139		

The specific interfacial energy is given in J m⁻².

^a Viscosity was used to calculate I_0^{exp} and σ_{cm}^* .

2574 weaker, while σ_{cm}^* depends only weakly on the choice of a
2575 particular expression for the thermodynamic driving force.

2576 References

- 2577 [1] J.W.P. Schmelzer, in: J.W.P. Schmelzer, G. Röpke, V.B. Priezhev
2578 (Eds.), Nucleation Theory and Applications, Joint Institute for
2579 Nuclear Research Publishing Department, Dubna, Russia, 1999, p.
2580 1.
2581 [2] J.M.F. Navaro, El Vidrio, CSIC, Madrid, Spain, 1991.
2582 [3] W. Höland, G. Beall, Glass-ceramic technology, American Ceramic
2583 Society, 2002.
2584 [4] J.W. Gibbs, The Collected Works, Thermodynamics, vol. 1,
2585 Longmans & Green, New York, 1928.
2586 [5] R. Kaischew, I.N. Stranski, Z. Phys. Chem. B 26 (1934) 317.
2587 [6] M. Volmer, A. Weber, Z. Phys. Chem. 119 (1926) 277.
2588 [7] R. Becker, W. Döring, Ann. Phys. 24 (1935) 719;
2589 R. Becker, W. Döring, Ann. Phys. 32 (1938) 128.
2590 [8] M. Volmer, Kinetik der Phasenbildung, Steinkopf, Dresden, 1939.
2591 [9] J. Frenkel, Kinetic Theory of Liquids, Oxford University Press,
2592 Oxford, 1946.
2593 [10] D. Turnbull, J.C. Fisher, J. Chem. Phys. 17 (1949) 71.
2594 [11] H. Reiss, J. Chem. Phys. 18 (1950) 840.
2595 [12] I. Gutzow, J. Schmelzer, The Vitreous State: Thermodynamics,
2596 Structure, Rheology and Crystallization, Springer, Berlin, 1995.
2597 [13] K.F. Kelton, Solid State Phys. 45 (1991) 75.
2598 [14] J.W. Christian, The Theory of Transformations in Metals and
2599 Alloys. Part I, Pergamon Press, Oxford, 1981.
2600 [15] F.C. Collins, Z. Electrochem. 59 (1955) 404.
2601 [16] D. Kashchiev, Surf. Sci. 14 (1969) 209.
2602 [17] V.N. Filipovich, V.M. Fokin, N.S. Yuritsyn, A.M. Kalinina,
2603 Thermochim. Acta 280&281 (1996) 205.
2604 [18] G. Tammann, Z. Phys. Chem. 25 (1898) 441.
2605 [19] M. Ito, T. Sakaino, T. Moriya, Bull. Tokyo Inst. Technol. 88 (1968)
2606 127.
2607 [20] V.N. Filipovich, A.M. Kalinina, Izv. Akad. Nauk USSR, Neorgan.
2608 Mat. 4 (1968) 1532 (in Russian).
2609 [21] I. Gutzow, Contemp. Phys. 21 (1980) 121, 243.
2610 [22] S. Toschev, I. Gutzow, Phys. Status Solidi 24 (1967) 349.
2611 [23] U. Köster, Mater. Sci. Eng. 97 (1988) 183.
2612 [24] V.M. Fokin, N.S. Yuritsyn, V.N. Filipovich, A.M. Kalinina, J. Non-
2613 Cryst. Solids 219 (1997) 37.
2614 [25] E.D. Zanotto, P.F. James, J. Non-Cryst. Solids 124 (1990) 86.
2615 [26] E.D. Zanotto, J. Mater. Res. 13 (1998) 2045.
2616 [27] S. Toschev, in: P. Hartman (Ed.), North-Holland Publishing
2617 Company, Amsterdam, 1973, p. 1.
2618 [28] V.P. Skripov, V.P. Koverda, Spontaneous Crystallization of Super-
2619 cooled Liquids, Nauka, Moscow, 1984 (in Russian).
2620 [29] A.N. Kolmogorov, Izv. Akad. Nauk USSR, Ser. Mathem. 3 (1937)
2621 355 (in Russian).
2622 [30] W.A. Johnson, R.F. Mehl, Trans. AIME 135 (1939) 416.

- [31] M. Avrami, J. Chem. Phys. 7 (1939) 1103. 2623
[32] V.N. Filipovich, A.M. Kalinina, V.M. Fokin, E.K. Shishchikina, D.D. 2624
Dmitriev, Fiz. Khim. Stekla 9 (1983) 58 [English trans.: Soviet J. 2625
Glass Phys. Chem. 9 (1983) 45]. 2626
[33] E.D. Zanotto, A.C. Galhardi, J. Non-Cryst. Solids 103 (1982) 73. 2627
[34] A.A. Cabral, V.M. Fokin, E.D. Zanotto, J. Non-Cryst. Solids 330 2628
(2003) 174. 2629
[35] V.M. Fokin, A.M. Kalinina, V.N. Filipovich, J. Cryst. Growth 52 2630
(1980) 115. 2631
[36] A.M. Kalinina, V.M. Fokin, V.N. Filipovich, J. Non-Cryst. Solids 2632
38&39 (1980) 723. 2633
[37] U. Schiffrer, W. Pannhorst, Glastechn. Ber. 60 (1987) 211. 2634
[38] A.M. Kalinina, V.M. Fokin, V.N. Filipovich, Fiz. Khim. Stekla 2 2635
(1976) 298 [English trans.: Soviet J. Glass Phys. Chem. 2 (1976) 294]. 2636
[39] I. Gutzow, S. Toschev, M. Marinov, E. Popov, Kristall Technik 3 2637
(1968) 337. 2638
[40] E.D. Zanotto, V.M. Fokin, Phil. Trans. R Soc. Lond. A 361 (2002) 2639
591. 2640
[41] V.M. Fokin, A.M. Kalinina, V.N. Filipovich, Fiz. Khim. Stekla 3 2641
(1977) 122 [English trans.: Soviet J. Glass Phys. Chem. 3 (1977) 113]. 2642
[42] S.C. Glotzer, J. Non-Cryst. Solids 274 (2000) 342. 2643
[43] V.M. Fokin, A.M. Kalinina, V.N. Filipovich, Fiz. Khim. Stekla 3 2644
(1977) 129 [English trans.: Soviet J. Glass Phys. Chem. 3 (1977) 119]. 2645
[44] Z. Kozisek, Cryst. Res. Technol. 23 (1988) 1315. 2646
[45] K.F. Kelton, A.L. Greer, Phys. Rev. B 38 (1988) 10089. 2647
[46] A.L. Greer, K.F. Kelton, J. Am. Ceram. Soc. 74 (1991) 1015. 2648
[47] J. Deubener, in: Proc. XIX Int. Cong. on Glass, vol. 2, Extended 2649
Abstracts, Soc. Glass Technology, Edinburgh, 2001, p. 66. 2650
[48] O.V. Potapov, V.M. Fokin, V.L. Ugolkov, L.Y. Suslova, V.N. 2651
Filipovich, Glass Phys. Chem. 26 (2000) 39. 2652
[49] D. Turnbull, J. Chem. Phys. 18 (1950) 769. 2653
[50] A.S. Skapski, Acta Metall. 4 (1956) 576. 2654
[51] A.M. Kalinina, V.N. Filipovich, V.M. Fokin, G.A. Sycheva, in: 2655
Proc. XIV Int. Cong. on Glass, vol. 1, New Delhi, 1986, p. 366. 2656
[52] O.V. Potapov, V.M. Fokin, V.N. Filipovich, J. Non-Cryst. Solids 2657
247 (1999) 74. 2658
[53] R. Müller, E.D. Zanotto, V.M. Fokin, J. Non-Cryst. Solids 274 2659
(2000) 208. 2660
[54] G. Tammann, Z. Elektrochemie 10 (1904) 532. 2661
[55] P.F. James, in: M.H. Lewis (Ed.), Glasses and Glass-Ceramics, 2662
Chapman and Hall, London, 1989, p. 59. 2663
[56] E.D. Zanotto, J. Non-Cryst. Solids 89 (1987) 361. 2664
[57] J. Deubener, J. Non-Cryst. Solids 274 (2000) 195. 2665
[58] V.M. Fokin, E.D. Zanotto, J.W.P. Schmelzer, J. Non-Cryst. Solids 2666
321 (2003) 52. 2667
[59] M.H. Lewis, J. Metacalf-Johanson, P.S. Bell, J. Am. Ceram. Soc. 62 2668
(1979) 278. 2669
[60] D. Turnbull, in: J.A. Prins (Ed.), Physics of Non-Crystalline Solids, 2670
North Holland Publishing Company, Amsterdam, 1965, p. 41. 2671
[61] G. Tammann, Der Glaszustand, Leopold Voss Verlag, Leipzig, 2672
1933. 2673

- 2674 [62] G.L. Mikhnevich, J.F. Browko, *Phys. Sowjetunion* 13 (1938) 113.
- 2675 [63] P.F. James, in: J.H. Simmons, D.R. Uhlmann, G.H. Beall (Eds.),
- 2676 *Advances in Ceramics*, vol. 4, American Ceramic Society, Colum-
- 2677 bus, Ohio, 1982, p. 1.
- 2678 [64] M.C. Weinberg, E.D. Zanotto, *J. Non-Cryst. Solids* 108 (1989) 99.
- 2679 [65] Y. Miyazawa, G.M. Pound, *J. Cryst. Growth* 23 (1974) 45.
- 2680 [66] D. Turnbull, *J. Chem. Phys.* 20 (1952) 411.
- 2681 [67] L. Shartsis, S. Spinner, *J. Res. Nat. Bur. Stand.* 46 (1951) 385.
- 2682 [68] A.A. Appen, K.A. Schishov, S.S. Kaylova, *Silikattechnik* 4 (1953)
- 2683 104.
- 2684 [69] V.M. Fokin, E.D. Zanotto, J.W.P. Schmelzer, *J. Non-Cryst. Solids*
- 2685 278 (2000) 24.
- 2686 [70] J. Stefan, *Ann. Phys.* 29 (1886) 655.
- 2687 [71] V.M. Fokin, E.D. Zanotto, *J. Non-Cryst. Solids* 265 (2000) 105.
- 2688 [72] I. Gutzow, D. Kashchiev, I. Avramov, *J. Non-Cryst. Solids* 73
- 2689 (1985) 477.
- 2690 [73] A.I. Rusanov, *Phasengleichgewichte und Grenzflächenerscheinun-*
- 2691 *gen*, Akademie-Verlag, Berlin, 1978.
- 2692 [74] V.P. Skripov, M.Z. Faizulin, in: J.W.P. Schmelzer (Ed.), *Nucleation*
- 2693 *Theory and Applications*, Wiley-VCH, Berlin-Weinheim, 2005, p. 4.
- 2694 [75] F. Spaepen, *Solid State Phys.* 47 (1994) 1.
- 2695 [76] V.N. Filipovich, T.A. Zhukovskaya, *Fiz. Khim. Stekla* 14 (1988) 300
- 2696 (in Russian).
- 2697 [77] L. Granasy, P. James, *J. Non-Cryst. Solids* 253 (1999) 210.
- 2698 [78] L. Granasy, T. Börzsony, T. Pusztai, *J. Cryst. Growth* 237 (2002)
- 2699 1813.
- 2700 [79] J.W.P. Schmelzer, G.Sh. Boltachev, V.G. Baidakov, in: J.W.P.
- 2701 Schmelzer (Ed.), *Nucleation Theory and Applications*, Wiley-VCH,
- 2702 Berlin-Weinheim, 2005, p. 418.
- 2703 [80] V.G. Baidakov, G.Sh. Boltachev, J.W.P. Schmelzer, *J. Colloid*
- 2704 *Interface Sci.* 231 (2000) 312.
- 2705 [81] V.G. Baidakov, J.W.P. Schmelzer, *J. Phys. Chem. B* 105 (2001)
- 2706 11595.
- 2707 [82] J.W. P Schmelzer, V.G. Baidakov, G.Sh. Boltachev, *J. Chem. Phys.*
- 2708 119 (2003) 6166.
- 2709 [83] J.D. van der Waals, Ph. Kohnstamm, *Lehrbuch der Thermodyn-*
- 2710 *amik*, Johann-Ambrosius-Barth Verlag, Leipzig und Amsterdam,
- 2711 1908.
- 2712 [84] J.D. van der Waals, *Z. Phys. Chem.* 13 (1893) 657 (in German) [J.S.
- 2713 Rowlinson, Translation of J.D. van der Waals': *The thermodynamic*
- 2714 *theory of capillarity under the hypothesis of a continuous variation*
- 2715 *of density*, *J. Stat. Phys.* 20 (1979) 197].
- 2716 [85] J.W. Cahn, J.E. Hilliard, *J. Chem. Phys.* 28 (1959) 258;
- 2717 J.W. Cahn, J.E. Hilliard, *J. Chem. Phys.* 31 (1959) 688.
- 2718 [86] D.W. Oxtoby, R. Evans, *J. Chem. Phys.* 89 (1988) 7521.
- 2719 [87] C.K. Bagdassarian, D.W. Oxtoby, *J. Chem. Phys.* 100 (1994) 2139.
- 2720 [88] D.W. Oxtoby, *Acc. Chem. Res.* 31 (1998) 91.
- 2721 [89] L. Granasy, *J. Mol. Struct.* 485&486 (1999) 523.
- 2722 [90] L. Granasy, T. Pusztai, P. James, *J. Chem. Phys.* 117 (2002) 6157.
- 2723 [91] J.W.P. Schmelzer, A.S. Abyzov, J. Möller, *J. Chem. Phys.* 121 (2004)
- 2724 6900.
- 2725 [92] B.N. Hale, in: M. Kasahara, M. Kulmala (Eds.), 16th Int. Conf. on
- 2726 *Nucleation and Atmospheric Aerosols*, Kyoto, Japan, August 2004,
- 2727 compact disk.
- 2728 [93] P.R. ten Wolde, D. Frenkel, *J. Chem. Phys.* 109 (1998) 9919.
- 2729 [94] V.K. Shen, P.G. Debenedetti, *J. Chem. Phys.* 111 (1999) 3581.
- 2730 [95] K. Laasonen, S. Wonzak, R. Strey, A. Laaksonen, *J. Chem. Phys.*
- 2731 113 (2000) 9741.
- 2732 [96] B. Chen, J.I. Siepmann, K.J. Oh, M.L. Klein, *J. Chem. Phys.* 115
- 2733 (2000) 10903.
- 2734 [97] J.W.P. Schmelzer, J. Schmelzer Jr., I. Gutzow, *J. Chem. Phys.* 112
- 2735 (2000) 3820.
- 2736 [98] J.W.P. Schmelzer, in: J.W.P. Schmelzer (Ed.), *Nucleation Theory*
- 2737 *and Applications*, Wiley-VCH, Berlin-Weinheim, 2005, p. 447.
- 2738 [99] H. Ulbricht, J.W.P. Schmelzer, R. Mahnke, F. Schweitzer, *Ther-*
- 2739 *modynamics of Finite Systems and the Kinetics of First-Order Phase*
- 2740 *Transitions*, Teubner, Leipzig, 1988.
- [100] J.W.P. Schmelzer, V.G. Baidakov, *J. Chem. Phys.*, submitted for
- publication.
- [101] J.W.P. Schmelzer, *Phys. Chem. Glasses* 45 (2004) 116.
- [102] J.W.P. Schmelzer, A.R. Gokhman, V.M. Fokin, *J. Colloid Interface*
- Sci.* 272 (2004) 109.
- [103] J.W.P. Schmelzer, in: XX Int. Cong. on Glass, Kyoto, 2004,
- compact disk.
- [104] J.W.P. Schmelzer, A.S. Abyzov, in: J.W.P. Schmelzer, G. Röpke,
- V.B. Priezhev (Eds.), *Nucleation Theory and Applications*, Joint
- Institute for Nuclear Research Publishing Department, Dubna,
- Russia, 2006, p. 4.
- [105] L. Granasy, P.F. James, *J. Chem. Phys.* 113 (2000) 9810.
- [106] D. Tatchev, G. Goerigk, E. Valova, J. Dille, R. Kranold, S.
- Armyanov, J.-L. Delplancke, *Appl. Crystallogr.* 38 (2005) 787.
- [107] D. Tatchev, A. Hoell, R. Kranold, S. Armyanov, *Physica B* 369
- (2005) 8.
- [108] P.J. Desre, E. Cini, B. Vinet, *J. Non-Cryst. Solids* 288 (2001) 210.
- [109] W. Pan, A.B. Kolomeisky, P.G. Vekilov, *J. Chem. Phys.* 122 (2005)
- 174905.
- [110] G. Medeiros-Ribeiro, A.M. Bratkovski, T.I. Kamins, D.A.A.
- Ohlberg, R.S. Williams, *Science* 286 (1998) 353.
- [111] F.M. Ross, R.M. Tromp, M.C. Reuter, *Science* 286 (1999) 1931.
- [112] A. Rastelli, M. Kummer, H. van Käse, *Phys. Rev. Lett.* 87 (2001)
- 256101.
- [113] P.G. Debenedetti, H. Reiss, *J. Chem. Phys.* 108 (1998) 5498, and
- references cited therein.
- [114] D.W. Oxtoby, *Nature* 347 (1990) 725.
- [115] L. Granasy, T. Börzsony, T. Pusztai, *Phys. Rev. Lett.* 20 (2002)
- 206105.
- [116] L. Granasy, T. Pusztai, J.A. Warren, *J. Phys.: Cond. Matter.* 16
- (2004) R1205.
- [117] T. Pusztai, G. Bortel, L. Granasy, *Europhys. Lett.* 71 (2005) 131.
- [118] T. Pusztai, G. Bortel, L. Granasy, *Mater. Sci. Eng. A* 413&414
- (2005) 412.
- [119] V.P. Skripov, V.G. Baidakov, *High Temp. Thermal Phys.* 10 (1972)
- 1226 (in Russian).
- [120] L.D. Landau, I.M. Lifschitz, *Statistische Physik*, Akademie-Verlag,
- Berlin, 1976.
- [121] V.P. Skripov, M.Z. Faizullin, *Solid-Liquid-Gas Phase Transitions*
- and Thermodynamic Similarity*, Wiley-VCH, Berlin-Weinheim,
- 2006.
- [122] L. Granasy, T. Wang, P. James, *J. Chem. Phys.* 108 (1998) 7317.
- [123] L. Granasy, D.W. Oxtoby, *J. Chem. Phys.* 112 (2000) 2410.
- [124] L. Granasy, T. Pusztai, *J. Chem. Phys.* 117 (2002) 10121.
- [125] D. Kashchiev, *J. Chem. Phys.* 76 (1984) 5098.
- [126] D.W. Oxtoby, D. Kashchiev, *J. Chem. Phys.* 100 (1994) 7665.
- [127] J.W.P. Schmelzer, *J. Colloid Interface Sci.* 242 (2001) 354.
- [128] J.W.P. Schmelzer, *Russ. J. Phys. Chem.* 77 (2003) 143.
- [129] Y. Viisanen, R. Strey, H. Reiss, *J. Chem. Phys.* 99 (1993) 4680.
- [130] Y. Viisanen, R. Strey, *J. Chem. Phys.* 105 (1996) 8293.
- [131] V.G. Karpov, D.W. Oxtoby, *Phys. Rev.* 54 (1996) 9734.
- [132] M.F. Thorpe, *J. Non-Cryst. Solids* 57 (1983) 355.
- [133] M.F. Thorpe, M.I. Mitkova (Eds.), *Amorphous insulators and*
- semiconductors*, NATO ASI, Kluwer, Dordrecht, 1997.
- [134] I. Avramov, R. Keding, C. Rüssel, R. Kranold, *J. Non-Cryst. Solids*
- 278 (2001) 13.
- [135] B.A. Shakhmatkin, N.M. Vedishcheva, *J. Non-Cryst. Solids* 171
- (1994) 1.
- [136] B.A. Shakhmatkin, N.M. Vedishcheva, M.M. Shultz, A.C. Wright,
- J. Non-Cryst. Solids* 177 (1994) 249.
- [137] V.M. Fokin, O.V. Potapov, E.D. Zanotto, F.M. Spiandorello, V.L.
- Ugolkov, B.Z. Pevzner, *J. Non-Cryst. Solids* 331 (2003) 240.
- [138] E.N. Soboleva, N.S. Yuritsyn, V.L. Ugolkov, *Glass Phys. Chem.* 30
- (2004) 481.
- [139] G. Völksch, T. Kittel, F. Siegelin, H.-J. Kleebe, in: XIX Int. Cong.
- on Glass, Edinburgh, 2001.
- [140] M. Roskosz, M.J. Toplis, P. Besson, P. Richet, *J. Non-Cryst. Solids*
- 351 (2005) 1266.
- 2741
2742
2743
2744
2745
2746
2747
2748
2749
2750
2751
2752
2753
2754
2755
2756
2757
2758
2759
2760
2761
2762
2763
2764
2765
2766
2767
2768
2769
2770
2771
2772
2773
2774
2775
2776
2777
2778
2779
2780
2781
2782
2783
2784
2785
2786
2787
2788
2789
2790
2791
2792
2793
2794
2795
2796
2797
2798
2799
2800
2801
2802
2803
2804
2805
2806
2807
2808

- 2809 [141] J. Deubener, R. Brückner, M. Sternitzke, *J. Non-Cryst. Solids* 163 (1993) 1. 2836
- 2810 [142] N.S. Yuritsyn, J.W.P. Schmelzer, V.M. Fokin, E.D. Zanotto, In preparation. 2837
- 2811 [143] A.R. West, F.P. Glasser, in: L.L. Hench, S.W. Freiman (Eds.), *Advances in Nucleation and Crystallization in Glasses*, American Ceramic Society, Columbus, Ohio, 1971, p. 151. 2838
- 2812 [144] I. Hasdemir, R. Brückner, J. Deubener, *Phys. Chem. Glasses* 39 (1998) 253. 2839
- 2813 [145] E.D. Zanotto, M.L.G. Leite, *J. Non-Cryst. Solids* 202 (1996) 145. 2840
- 2814 [146] M.C. Weinberg, *J. Non-Cryst. Solids* 170 (1994) 300. 2841
- 2815 [147] V.V. Slezov, J.W.P. Schmelzer, in: J.W.P. Schmelzer, G. Röpke, V.B. Priezhev (Eds.), *Nucleation Theory and Applications*, Joint Institute for Nuclear Research Publishing Department, Dubna, Russia, 1999, p. 6. 2842
- 2816 [148] K.S. Russell, *Acta Metall.* 16 (1968) 761. 2843
- 2817 [149] K.F. Kelton, *Acta Mater.* 48 (2000) 1967. 2844
- 2818 [150] W. Ostwald, *Z. Phys. Chem.* 22 (1897) 289. 2845
- 2819 [151] I. Stranski, D. Totomanov, *Z. Phys. Chem. A* 163 (1933) 399. 2846
- 2820 [152] A.S. Milev, I.S. Gutzow, *Bulg. Chem. Commun.* 29 (1996/1997) 597. 2847
- 2821 [153] A.M. Kalinina, V.N. Filipovich, V.A. Kolesova, I.A. Bondar, in: E.A. Porai-Koshits (Ed.), *The Structure of Glass*, vol. 3, Consultants Bureau, New York, 1964, p. 53. 2848
- 2822 [154] D.L. Kinser, L.L. Hench, *J. Am. Ceram. Soc.* 12 (1971) 58. 2849
- 2823 [155] P.C. Soares Jr., Initial stages of crystallization in lithium disilicate glass revisited, MSc thesis, Universidade Federal de São Carlos, Brazil, 1997 (in Portuguese). 2850
- 2824 [156] Y. Iqbal, W.E. Lee, D. Holland, P.F. James, *J. Non-Cryst. Solids* 224 (1998) 1. 2851
- 2825 [157] L.I. Burger, P. Lucas, M.C. Weinberg, P.C. Soares Jr., E.D. Zanotto, *J. Non-Cryst. Solids* 274 (2000) 188. 2852
- 2826 [158] J. Deubener, *Homogene Volumenkeimbildung in Silicatschmelzen: Theorie und Experiment*, Habilitationsschrift, Berlin, 2001. 2853
- 2827 [159] P.C. Soares Jr., E.D. Zanotto, V.M. Fokin, H.J. Jain, *J. Non-Cryst. Solids* 331 (2003) 217. 2854
- 2828 [160] B.A. Shakhmatkin, N.M. Vedishcheva, Private communication, 2001. 2855
- 2829 [161] V.M. Fokin, E.D. Zanotto, J.W.P. Schmelzer, O.V. Potapov, *J. Non-Cryst. Solids* 351 (2005) 1491. 2856
- 2830 [162] L. Granasy, T. Pusztai, P.F. James, *J. Chem. Phys.* 117 (2002) 6157. 2857
- 2831 [163] J.W.P. Schmelzer, R. Pascova, J. Möller, I. Gutzow, *J. Non-Cryst. Solids* 162 (1993) 26. 2858
- 2832 [164] J.W.P. Schmelzer, J. Möller, I. Gutzow, R. Pascova, R. Müller, W. Pannhorst, *J. Non-Cryst. Solids* 183 (1995) 215. 2859
- 2833 [165] E.D. Zanotto, E.J. Müller, *J. Non-Cryst. Solids* 130 (1991) 220. 2860
- 2834 [166] J.W.P. Schmelzer, R. Müller, J. Möller, I.S. Gutzow, *Phys. Chem. Glasses* 43C (2002) 291. 2861
- 2835 [167] J.W.P. Schmelzer, R. Müller, J. Möller, I.S. Gutzow, *J. Non-Cryst. Solids* 315 (2003) 144. 2862
- 2836 [168] J.W.P. Schmelzer, E.D. Zanotto, I. Avramov, V.M. Fokin, *J. Non-Cryst. Solids*, in press. 2863
- 2837 [169] J.W.P. Schmelzer, O.V. Potapov, V.M. Fokin, R. Müller, S. Reinsch, *J. Non-Cryst. Solids* 333 (2004) 150. 2864